

**Fluxoid Quantization Effects in  
Superconducting  $\text{La}_{1.84}\text{Sr}_{0.16}\text{CuO}_4$   
Nanoloops**

**Ilya Sochnikov**

Department of Physics

Ph.D. Thesis

Submitted to the Senate of Bar-Ilan University

Ramat-Gan, Israel

May, 2011



This work was carried out under the supervision of  
Prof. Yosef Yeshurun and Prof. Avner Shaulov,  
Department of Physics, Bar-Ilan University.



## **Acknowledgements**

*I do not have adequate words to express my appreciation to **Profs. Yosef Yeshurun** and **Avner Shaulov** for their wisdom, patience, willingness to help, and all the other positive traits that I learned, in addition to the academic skills that I acquired from them.*

*I deeply thank **Dr. Ivan Božović** for believing in my abilities and agreeing to start the collaborative projects with me. Visiting him at Brookhaven National Laboratory was a significant step which significantly accelerated my educational career and personal development.*

*I express my appreciation to **Prof. Eli Zeldov** and **Dr. Yuri Myasoedov** for the time that they spent with me while I worked in the Superconductivity Lab at Weizmann Institute.*

*I would like to thank **Profs. Boris Shapiro** and **Baruch Rosenstein** for their enthusiasm during numerous consultations.*

*I am deeply grateful to **Prof. Lior Klein** for his unconditional support, advice, and interest in my work.*

*I would like to thank **Prof. Aviad Friedman** for guiding me to focus my research in order to optimize performance.*

*I appreciated all the discussions that I had with **Prof. Efrat Shimshoni**.*

*It was my pleasure to interact and engage in many exciting discussions with **Dr. Amos Sharoni**.*

*I want to express my deep gratitude to all the members of our group at the Bar-Ilan Institute of Superconductivity for their help, appreciation, and friendship: **Drs. Alex Friedman, Shuki Wolfus, Faina Kopansky, Prof. Michael Baziljevich**, and to the research students **Daniel Levi, Omri Sharon, Hadar Pinhas, and Yasha Nickulshin**.*

*I truly thank my friends and former members of the group **Dr. Beena Kalisky, Gregory Lukovsky, and Revital Kopeliansky** for 'being always there' and helping me in the right moments of my life.*

*I thank the engineering and technical personnel: **Eli Perel, Menachem Katz, and Danny Halabi** for their continuous support.*

*I thank **Drs. Oshri Pelleg, Adrian Gozar, Anthony Bollinger, and Gennady Logvenov** at BNL for having the opportunity to work with them. I deeply appreciate their friendship.*

*I thank my friends and colleagues from other groups at Bar-Ilan University for helping me in everyday work: **Dr. Ora (Liora) Bitton, Dr. Isaschar Genish, Dr. Eli Sloutskin, Eyal Dvash, Yishai Shperber, Netanel Naftalis, Snir Seri, and Vladislav Murashenko.***

*I would like to thank the secretaries of the Department of Physics: **Rachel Rotberg and Sarah Bialkovitz.** I thank the current and the former heads of the Department: **Profs. Richard Berkovits, Dennis Rapaport, Haim Taitelbaum,** and the advisor **Prof. Leonid Feigel.** You all created a home atmosphere in the department.*

*I deeply appreciate the support of the members of Bar-Ilan Institute for Nanotechnology and Advanced Materials: the head of the institute, **Prof. Arie Zaban, Drs. Orit Chasid, Efrat Bodner, Yossi Abulafia, and Moshe Feldberg.***

*This work could not be completed without the love and support of my parents, **Alexei and Tatiana,** and my older brother, **Pavel.***

*I'm grateful to my wife, **Rinat,** for turning this period of time into the happiest years of my life.*

*I would like to thank the funding organizations and institutions that generously supported me during my research activity:*

- ⇒ ***Bar-Ilan University – President's Scholarship***
- ⇒ ***The Israeli Ministry of Science and Technology – Eshkol Scholarship***
- ⇒ ***The Department of Physics at Bar-Ilan University – Award for Research Excellence***
- ⇒ ***The Faculty of Exact Sciences, Bar-Ilan University – David Barkovski Award***
- ⇒ ***The Bar-Ilan Institute for Nanotechnology and Advanced Materials – Excellence Scholarship and Publications Awards***
- ⇒ ***The Deutsche Forschungsgemeinschaft – support through the Deutsch Israelische Projektkooperation (grant no. 563363)***
- ⇒ ***The Bar-Ilan Institute of Superconductivity – research support***



# TABLE OF CONTENTS

<b>ABSTRACT .....</b>	<b>I</b>
<b>1 INTRODUCTION .....</b>	<b>1</b>
1.1 FLUXOID QUANTIZATION AND EARLY EXPERIMENTAL OBSERVATIONS OF MAGNETORESISTANCE OSCILLATIONS IN MULTIPLY CONNECTED LOW TEMPERATURE SUPERCONDUCTORS.....	1
1.2 EXPERIMENTAL OBSERVATION OF MAGNETORESISTANCE OSCILLATIONS IN HIGH-TEMPERATURE SUPERCONDUCTORS .....	5
1.3 THEORETICAL PREDICTIONS FOR HALF FLUX QUANTUM AND TWO FLUX QUANTA PERIODICITIES ...	8
1.4 BEREZINSKII-KOSTERLITZ-THOULESS TRANSITION .....	10
<b>2 EXPERIMENTAL.....</b>	<b>11</b>
2.1 FABRICATION OF $\text{LA}_{2-x}\text{SR}_x\text{CUO}_4$ FILMS - MOLECULAR BEAM EPITAXY (MBE).....	12
2.2 NANO-PATTERNING .....	14
2.3 MAGNETO-TRANSPORT MEASUREMENTS.....	17
<b>3 RESULTS.....</b>	<b>19</b>
3.1 SINGLE-LOOP LIKE ENERGY OSCILLATIONS AND STAIRCASE VORTEX OCCUPATION IN SUPERCONDUCTING DOUBLE NETWORKS.....	21
3.2 UNCORRELATED BEHAVIOR OF FLUXOIDS IN SUPERCONDUCTING DOUBLE NETWORKS .....	41
3.3 LARGE OSCILLATIONS OF THE MAGNETORESISTANCE IN NANO-PATTERNED HIGH-TEMPERATURE SUPERCONDUCTING FILMS: EXPERIMENTAL RESULTS AND THEORETICAL MODEL .....	49
3.4 CONTRIBUTION OF THERMALLY EXCITED VORTICES AND ANTIVORTICES TO THE MAGNETORESISTANCE OF $\text{LA}_{1.84}\text{SR}_{0.16}\text{CUO}_4$ NANOLOOPS: POSSIBILITY OF BEREZINSKII- KOSTERLITZ-THOULESS TRANSITION .....	55
<b>4 SUMMARY AND CONCLUSIONS.....</b>	<b>65</b>
<b>APPENDIX: PUBLICATIONS, PRESENTATIONS, AND AWARDS .....</b>	<b>67</b>
<b>REFERENCES.....</b>	<b>71</b>



LIST OF FIGURES

**Figure 1.** Population of fluxons (a), supercurrent (b), and kinetic energy of the supercurrent (c) in a superconducting loop (left schematic drawing), as a function of magnetic flux piercing the loop, expressed in units of the flux quantum. .... 3

**Figure 2.** Left panel: Resistance of the tin cylinder as a function of magnetic flux. Right panel: Schematic plot of resistance versus temperature: interpretation of changes in the critical temperature reflected as changes in the resistance [7-9]. ..... 4

**Figure 3.** Left panel: Amplitude of the oscillations in the 'critical temperature', as a function of temperature measured in the YBCO square network, shown in the inset (the scale bar is 20  $\mu\text{m}$ ). Right panel: oscillations in the 'critical temperature' derived from the measured magnetoresistance oscillations in the YBCO network, as a function of the magnetic field [27]. ..... 5

**Figure 4.** (a) An example of a single ring of YBCO measured by Carillo *et al.*; (b) oscillations in the magnetoresistance measured at 70 K in YBCO single ring; (c) oscillations in the critical temperature derived from the magnetoresistance; (d) Fourier transform showing the multiple 'frequencies' of the oscillations in the magnetoresistance [29]...... 6

**Figure 5.** Energy and persistent current in a small loop of a hypothetical superconductor with zeros in the energy gap, as a function of the magnetic flux threading the loop [36]...... 9

**Figure 6.** Left panel shows a typical scanning electron microscope (SEM) image of a simple square network with a unit cell size of 150 nm. Right panel shows a typical SEM image of a double network consisting of two interlacing networks of large loops of 500 nm, and small loops of 150 nm. .... 11

**Figure 7.** Molecular Beam Epitaxy chamber at BNL (Adapted from the Brookhaven Oxide MBE group website.). ..... 12

**Figure 8.** CRESTEC CABLE 9000 high resolution Electron Beam Lithography system at Bar-Ilan Institute of Nanotechnology and Advanced Materials (Adapted from CRESTEC website.)..... 14

**Figure 9.** Main nanopatterning steps: (1) spin-coating of the sample with a PMMA resist; (2) electron beam writing in the CRESTEC CABL 9000 system; (3) cross-linked pattern in the layer of PMMA; (4) PMMA mask on top of the superconducting film after development; (5) pattern transfer with Ar ion milling; (6) resulting pattern of the network in the superconducting film..... 16

**Figure 10.** Quantum Design Physical Property Measurement System (PPMS®) installed at the Bar-Ilan Institute of Nanotechnology and Advanced Materials (Adapted from the Quantum Design website.) ..... 17

## ABSTRACT

This work describes a study of fluxoid quantization effects in a novel type of superconducting network, consisting of two interlaced sub-networks of small and large loops. The motivation for designing such a network was to create an array of decoupled small loops that behave like isolated single loops. We fabricated such 'double' networks from atomically smooth Molecular Beam Epitaxially grown  $\text{La}_{1.84}\text{Sr}_{0.16}\text{CuO}_4$  films. High resolution electron-beam lithography was used to prepare a pattern of thousands of loops made of  $\sim 30$  nanometer-wide wires with a loop side of down to 75 nm, the smallest high-temperature superconducting loops prepared to date.

Our theoretical study, based on computer simulations and mean-field calculations, showed different behavior for the sub-networks of the large and small loops in the double network. In particular, while the occupation of the large loops by fluxons grows linearly with the external magnetic field, the occupation of the small loops grows in steps, similar to the occupation of a single loop. Furthermore, the calculations showed that the field dependent energy of the sub-network of small loops is similar to that of an isolated single loop. We observed features characterizing single loops also experimentally, in measurements of the magnetoresistance of  $\text{La}_{1.84}\text{Sr}_{0.16}\text{CuO}_4$  double networks.

The magnetoresistance measurements revealed periodic oscillations with a periodicity corresponding to magnetic flux quanta,  $\Phi_0 = hc/2e$  ( $h$  is the Planck constant,  $c$  is the speed of light in a vacuum and  $e$  is the electron's charge), as in the Little-Parks effect. However, the amplitude of the oscillations was found to be larger by almost two orders of magnitude than the amplitude expected from the Little-Parks effect. Moreover, the temperature dependence of the oscillations' amplitude was at variance with the Little-Parks predictions. We, therefore, proposed a new model for these oscillations.

The essence of our model is that the resistance results from thermally activated hopping of vortices across the loops, and the oscillations of the resistance are caused by periodic changes in the activation energy required for a vortex hopping. The periodic changes in the activation energy result from

the interaction of vortices with fluxoid currents in the loop, which are periodic functions of the magnetic field. We found an excellent agreement between the experimental results and the theoretical predictions of our dynamic model for both the oscillations' amplitude and its temperature dependence.

To explain the monotonically increasing background on which the magnetoresistance oscillations are superimposed, we extended the dynamic model to include the interaction of vortices and antivortices with the external field. A good fit between the theoretical predictions and the measured background was found, revealing the existence of both vortices and antivortices with comparable probabilities near the transition temperature. This finding is consistent with the occurrence of Berezinskii-Kosterlitz-Thouless transition in  $\text{La}_{1.84}\text{Sr}_{0.16}\text{CuO}_4$  films.

Double networks comprising nano-loops of high- $T_c$  superconducting materials, can serve as an effective tool in the search for the recently predicted  $\Phi_0/2 = hc/4e$  and  $2\Phi_0 = hc/e$  flux periodicities in both striped superconductors and in superconductors with  $d$ -wave symmetry of the wave function of Cooper pairs, respectively. These networks offer large magnetoresistance oscillations and a large signal to noise ratio. Efforts to discover such periodicities should continue by extending this work to higher and lower doping across the entire phase diagram, in  $\text{La}_{2-x}\text{Sr}_x\text{CuO}_4$  and  $\text{La}_{2-x}\text{Ba}_x\text{CuO}_4$  nanoloops.

# 1 INTRODUCTION

## 1.1 FLUXOID QUANTIZATION AND EARLY EXPERIMENTAL OBSERVATIONS OF MAGNETORESISTANCE OSCILLATIONS IN MULTIPLY CONNECTED LOW TEMPERATURE SUPERCONDUCTORS

Fritz London introduced the concept of *fluxoid* in multiply connected superconductors as a sum of total magnetic flux,  $\Phi$ , through the superconductor and an integral of the supercurrent,  $\vec{J}$ , around an opening (a hole) in the superconductor [1]:

$$\Phi' = \Phi + \left(\frac{4\pi}{c}\right) \oint \lambda^2 \vec{J} \cdot d\vec{s}, \quad (1)$$

where  $c$  is the speed of light,  $\lambda$  is the magnetic field penetration depth [1,2] and  $d\vec{s}$  is the infinitesimal element of a path around the opening in the superconductor. London showed that the fluxoid may have only discrete values, and is quantized in units of superconducting flux quantum,  $\Phi_0$ :

$$\Phi' = n\Phi_0 = n \frac{hc}{2e} \quad (2)$$

where  $n$  is integer,  $h$  is the Planck constant,  $c$  is the speed of light and  $2e$  is the charge of a pair of electrons (Cooper pair).

In transport measurements, the resistance is typically detected near the critical temperature of a superconductor. Therefore, the screening of the external magnetic field is very weak, and the total flux  $\Phi$  through the superconductor approximately equals the externally applied magnetic flux  $\Phi_a$ . Using this assumption, with Eq. (1) and (2), we may express the supercurrent surrounding a hole in a ring-shaped superconductor (see Figure 1) as

$$J = \frac{c\Phi_0}{4\pi\lambda^2 L} \left(n - \frac{\Phi_a}{\Phi_0}\right), \quad (3)$$

where  $L = 2\pi r$  is the loop circumference, and  $r$  is the loops radius. The integer number,  $n$ , called the winding number, counts *fluxons* inside the

superconducting loop. This term is used to describe the magnetic quasi-particles associated with a circulating current, and a flux enclosed by this current.

Due to the induced supercurrent, the energy of the superconducting loops will acquire a shift proportional to the kinetic energy of the circulating Cooper pairs, which is proportional to the square of the supercurrent

$$E_k = \frac{4\pi\lambda^2}{c^2} J^2 . \quad (4)$$

At the lowest energy level, the number of fluxons changes in a stepwise form as shown in Figure 1a. According to Eq. (3), the current will change periodically with the magnetic flux (see Figure 1b). And, as defined in Eq. (4), the energy proportional to the squared current has magnetic flux dependence in the form of multiple parabolas replicated with periodicity of  $\Phi_0$  (see Figure 1c).

In the square network of loops, the fluxoid quantization (Eq. (1)) has to be satisfied for every loop: in each cell there may be a different number of vortices,  $n$ , and a different current in every side of every loop. Solving the set of fluxoid equations together with the requirement for minimal energy, shows [3-6] that the number of vortices in the network grows linearly with the field – completely different from the stepwise population of a single loop.

*We show in this work that in contrast to the square network, in the specially designed double network consisting of two interlaced sub-networks of small and large loops (introduced in Section 2), the small loops are occupied by fluxons in steps, closely resembling the behavior a single loop.*

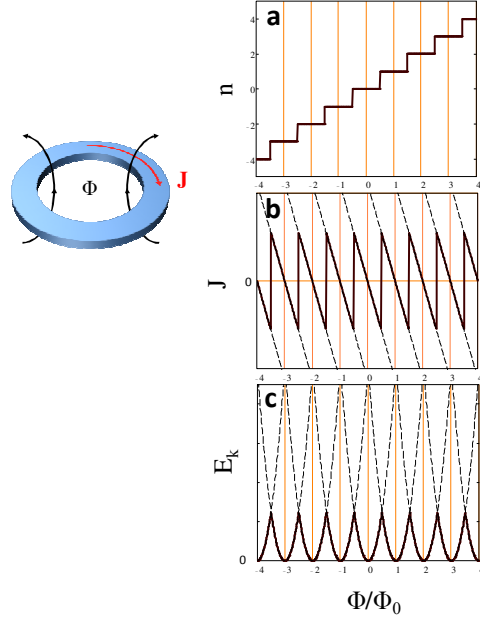


**Figure 1.** Population of fluxons (a), supercurrent (b), and kinetic energy of the supercurrent (c) in a superconducting loop (left schematic drawing), as a function of magnetic flux piercing the loop, expressed in units of the flux quantum.

The additional energy,  $E_k$ , of the fluxoid currents defined in Eq. (4) will suppress periodically the critical temperature,  $T_c$ , of a superconducting. This effect was first observed experimentally by Little and Parks [7-9]. They demonstrated that a thin-walled superconducting tin cylinder pierced by a magnetic flux shows magnetoresistance oscillations with the period equal to the superconducting flux quantum  $\Phi_0 = hc/2e$  (see the left panel of Figure 2). Little and Parks associated the resistance oscillations  $\Delta R(H)$  with periodic changes  $\Delta T_c$  (see the right panel of Figure 2) in the superconducting transition temperature  $T_c$ ,  $\Delta R = \Delta T_c (dR/dT)$ . The amplitude of the oscillations,  $\Delta T_c$ , scales with  $(\xi_0/r)^2$ , where  $\xi_0$  is the zero-temperature coherence length, and  $r$  is the radius of the cylinder.

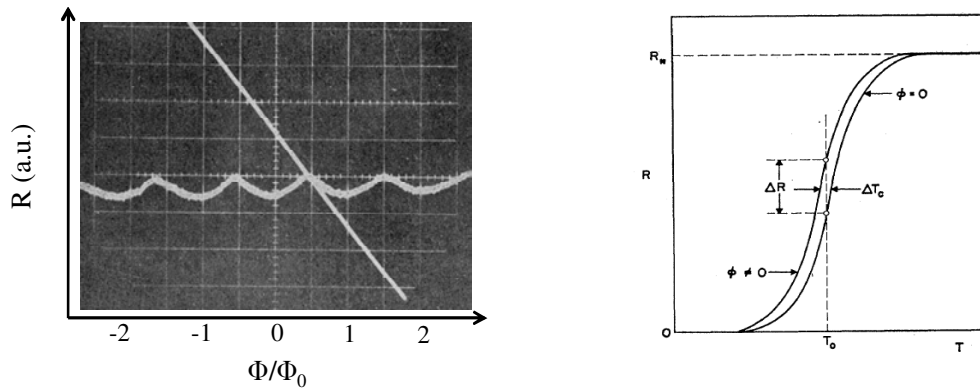


**Figure 2.** Left panel: Resistance of the tin cylinder as a function of magnetic flux. Right panel: Schematic plot of resistance versus temperature: interpretation of changes in the critical temperature reflected as changes in the resistance [7-9].

Fluxoid quantization effects were studied in many works on microscopic and mesoscopic multiply connected structures made of conventional superconductors: oscillatory behavior was observed in resistance and magnetization of single loops [10-19], different types of networks [3-5,20,21], arrays of Josephson junctions (see for example ref. [22-24]), and more complex structures [25,26]. A review of all the works is far beyond the scope of this thesis. Yet, as we show in the next section, only a few works describe fluxoid quantization effects in loops made of high temperature superconductors [27-29].

## 1.2 EXPERIMENTAL OBSERVATION OF MAGNETORESISTANCE OSCILLATIONS IN HIGH-TEMPERATURE SUPERCONDUCTORS

In 1990, Gammel *et al.* [27] reported magnetoresistance oscillations in a network of  $\sim 2 \mu\text{m}$  square loops made of  $\text{YBa}_2\text{Cu}_3\text{O}_{7-\delta}$  (see image of the network in Figure 3, left panel) and attributed these oscillations to the oscillations in the critical temperature, i.e. the Little-Parks effect. However, *the amplitude* of the oscillations and its *temperature dependence* in their experiment could not be accounted for. As  $\xi_0$  in high- $T_c$  superconductors is relatively small (several nm),  $\Delta T_c \propto T_c (\xi_0 / r)^2$  is expected to be in the sub mK range even for micron-size high temperature superconducting loops. The Little-Parks magnetoresistance oscillations,  $\Delta R = \Delta T_c (dR/dT)$ , in high- $T_c$  superconductors is, therefore, expected to be very small. Gammel *et al.* observed much larger oscillations, as demonstrated in the right panel of in Figure 3. In addition  $\Delta T_c$  depends on  $T$ , as shown in the left panel of Figure 3. This finding is also inconsistent with the expected constant amplitude of the changes in the critical temperature in the Little-Parks effect. The large amplitude and the temperature dependence of  $\Delta T_c$  remain open questions.

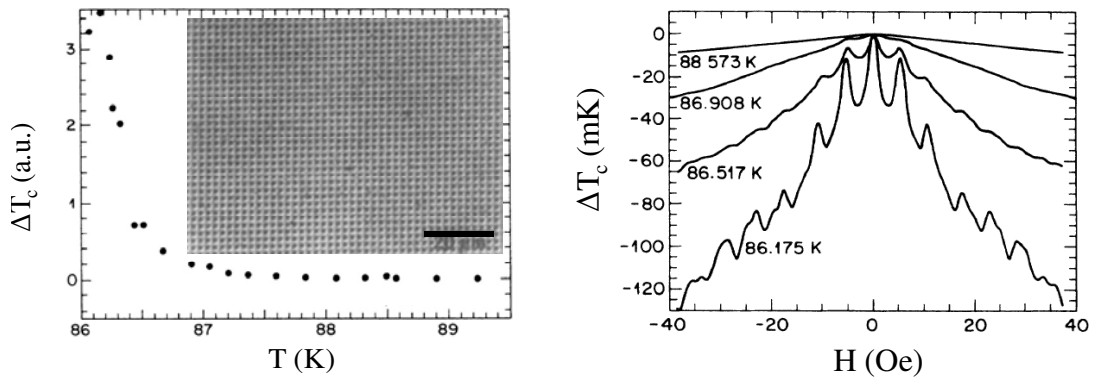


**Figure 3.** Left panel: Amplitude of the oscillations in the 'critical temperature', as a function of temperature measured in the YBCO square network, shown in the inset (the scale bar is  $20 \mu\text{m}$ ). Right panel: oscillations in the 'critical temperature' derived from the measured magnetoresistance oscillations in the YBCO network, as a function of the magnetic field [27].

The configuration of the square network in the work of Gammel *et al.* exhibits an intrinsic disadvantage due to the fact that the squares share sides. This configuration results in interactions between the loops [3-5,20,21], which may complicate the analysis of the results. This problem may be solved by fabricating single rings, as was recently demonstrated by Carillo *et al.* [29]. They performed magneto-transport measurements on submicron YBCO high temperature superconducting single loops with an outer diameter of about 1  $\mu\text{m}$  (Figure 4a). The observed oscillations (Figure 4b) have an amplitude larger than expected from the Little-Park effect (Figure 4c). However, the frequency was difficult to define due to multiple frequencies present in the oscillations (Figure 4d). The authors explained the large amplitude and multi-frequency oscillations in terms of non-uniform vorticity: supercurrent density varies in a radial direction forming concentric domains with a separation of  $\sim 30$  nm within the ring arms.

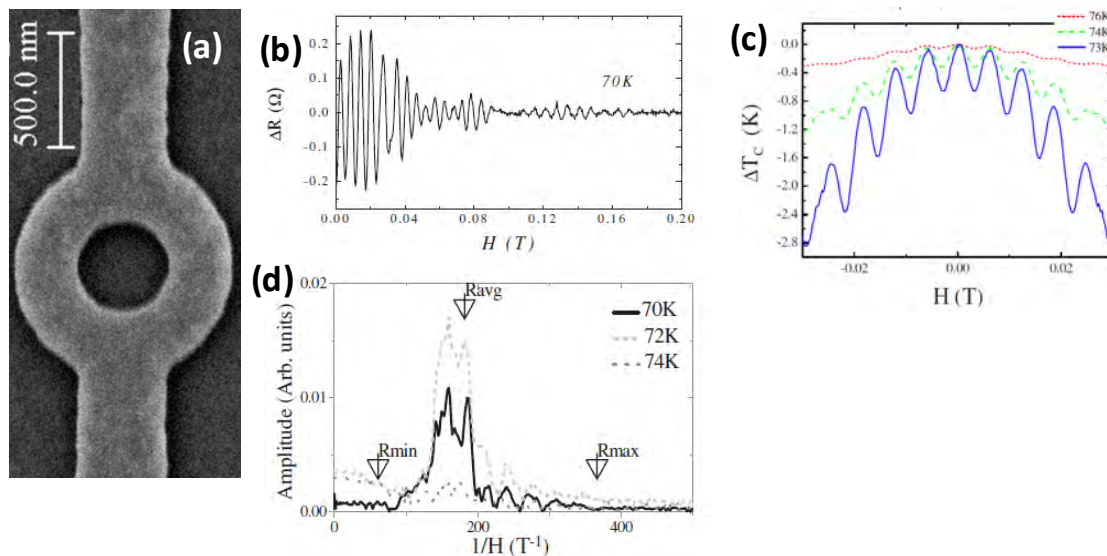


**Figure 4.** (a) An example of a single ring of YBCO measured by Carillo *et al.*; (b) oscillations in the magnetoresistance measured at 70 K in YBCO single ring; (c) oscillations in the critical temperature derived from the magnetoresistance; (d) Fourier transform showing the multiple 'frequencies' of the oscillations in the magnetoresistance [29].

Although a single loop configuration used in the above experiment has advantages over a square network, such as simplicity in the analysis, the

single loop configuration presents significant disadvantages: in a single ring, the signal-to-noise ratio is typically low; variations from loop to loop may introduce a need for the statistical measurement of a large number of single loops, which may be impractical. Therefore, in some cases the single loop geometry may not be the optimal choice.

In this work, we exploit the advantages of the two approaches, networks and single loops, by fabricating a specially designed double network, overcoming the disadvantages of each of the two approaches: in this network, the loops behave similarly to an ensemble of independent loops, making the system simple to analyze; measuring many loops in the network averages over a sample inhomogeneity and significantly increases the signal-to-noise ratio.

The open questions, mentioned above in the context of the work by Gammel *et al.*, partially motivated the current study. We show here that both *the amplitude* and the *temperature dependence* can be accounted for in a dynamic model. This model takes into account the hopping of Abrikosov vortices/anti-vortices into or out of loops, while taking into account the interaction of these Abrikosov vortices with fluxoid currents circulating around loop.

The periodicity of the oscillations is an additional characteristic of the behavior of superconducting loops that is important for the analysis of wave function symmetry and mechanisms of superconductivity. Several recent theoretical works have predicted unusual, exotic fluxoid periodicities in high temperature superconducting nanoloops, as described in the following section.

### 1.3 THEORETICAL PREDICTIONS FOR HALF FLUX QUANTUM AND TWO FLUX QUANTA PERIODICITIES

The nature of the pairing mechanism and the symmetry of the order parameter are among the most important, yet unresolved issues in the field of unconventional superconductivity [30,31]. The explanation of intriguing phenomena such as a gap opening in the excitation spectra of electrons at temperatures above the superconducting transition in these materials are closely connected to these fundamental questions [32]. These issues were mainly addressed in cuprates materials, but the newly discovered iron based superconductors demonstrate that the nature of superconductivity at elevated temperatures is probably even more complex [33]. The experimental studies of superconducting properties are affected in many cases by artifacts arising from experimental limitations such as surface quality, contact resistance, edge roughness, and crystal quality. The magnetic fluxoid quantization in multiply connected superconducting structures is robust, unaffected by such artifacts.

Several groups predicted recently that an 'exotic' flux periodicity with a period of  $2\Phi_0 = hc/e$  will emerge in nano-scale loops of superconductors with d-wave symmetry and other unconventional superconductors with nodes (zeros) in the energy gap [34-38]. These works show that at a magnetic flux around  $\Phi_0 \cdot (2m+1)$ ,  $m$  is integer, there is a paramagnetic quasi-particle-like contribution to the circulating current in a loop. This contribution enhances the magnetic field, resulting in an energy gain and reconstruction of the superconducting condensate. Consequently, the total energy and other physical properties of the loop will possess periodicity of  $2\Phi_0$  with a magnetic flux. As seen Figure 5, the persistent current slope is larger at fluxes around  $\Phi_0 \cdot (2m+1)$  than at fluxes around  $\Phi_0 \cdot (2m)$ . Parabolas of the energy which is roughly proportional to the square of the persistent current are elevated at values of  $\Phi_0 \cdot (2m+1)$  (compare to the classical calculations shown in Section 1.1, Figure 1). However, the  $2\Phi_0$  periodicity is only a small component on top of the dominant  $\Phi_0$  periodicity. The size of a loop must be

small for the effect to be clearly observed. *In this work, we have been able to fabricate and measure flux periodicity in the loops of  $\sim 35$  nm in radius.*

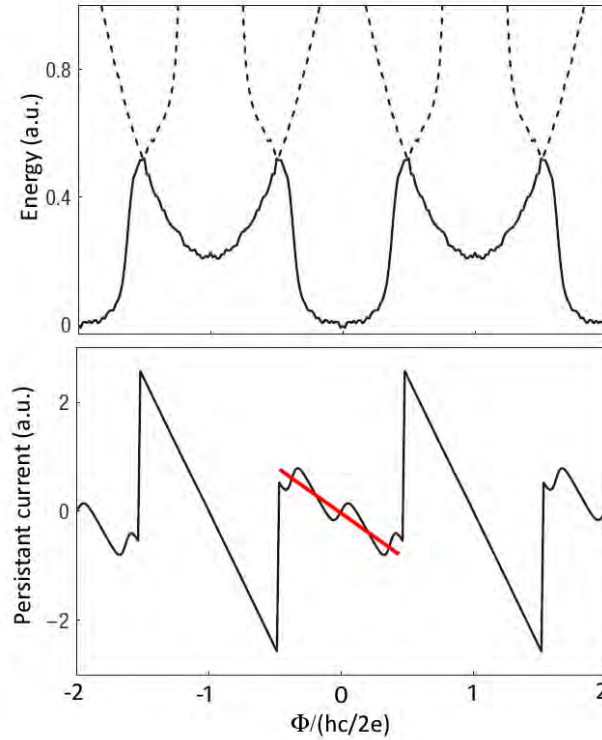


**Figure 5.** Energy and persistent current in a small loop of a hypothetical superconductor with zeros in the energy gap, as a function of the magnetic flux threading the loop [36].

Another theoretical prediction was made for flux periodicity of  $\Phi_0/2 = hc/4e$ , in superconductors that exhibit striped form the order parameter [39]. This work predicts that in loops formed from a striped superconductor [40], the movement of Cooper pairs is dramatically suppressed, due to the perpendicular orientation of stripes between the layers of the superconductor. However, dislocations in the striped structure may permit transfer of the charge  $4e$ , leading to  $hc/4e = \Phi_0/2$  periodicity. *In this work, we analyze the magnetoresistance of the nanoloops to search for  $hc/4e$  and  $hc/e$  periodicities.*

Another fundamental issue in the field of high temperature superconductivity is the mechanism responsible for the transition to the

normal state. One of the possible scenarios is the Berezinskii-Kosterlitz-Thouless (BKT) transition, that is addressed in the following section.

#### 1.4 BEREZINSKII-KOSTERLITZ-THOULESS TRANSITION

The Berezinskii-Kosterlitz-Thouless (BKT) transition [41-43] is one of the possible scenarios of the phase transition from the superconducting state to the normal state in two-dimensional superconductors (thin film) [44,45]. In this scenario, pairs of Abrikosov vortices and antivortices are created in the superconductor [2]. At low temperatures, vortex and antivortex bind in a pair by an electromagnetic attractive force. At these low temperatures, the external current cannot move a pair as the net Lorentz force applied on the pair is zero. Therefore, no energy dissipation and zero resistance are observed at these temperatures. However, at some higher temperatures, the thermal energy,  $k_B T$ , becomes higher than the binding energy of the pairs leading to the *unbinding* of a vortex and an antivortex. At these temperatures, the external current can move the vortex in one direction, and the antivortex in an opposite direction, leading to energy dissipation detected as a resistance. According to this picture, the critical temperature,  $T_{BKT}$ , is the onset temperature of the resistance of the superconductor.

The study of the BKT transition was the topic of a large number of works in thin superconducting films. However, controversial experimental data and its interpretation can be found in the literature, in particular in measurements of the layered cuprates, which may be considered as a system of quasi two-dimensional layers [46-50].

The BKT mechanism is predicted for 2D systems. In this work, we study the relevance of the BKT model to nanowires forming networks in thin films of  $\text{La}_{1.84}\text{Sr}_{0.16}\text{CuO}_4$  high-temperature superconductors. We argue that in order to explain the field dependence of the magnetoresistance we have to account for both vortices and antivortices spontaneously created in the wires. The presence of the vortices and antivortices in the nanowires is consistent with the assumptions of the BKT transition.

## 2 EXPERIMENTAL

We pattern networks of nanoloops in high quality  $\text{La}_{1.84}\text{Sr}_{0.16}\text{CuO}_4$  films grown by Molecular Beam Epitaxy. First, we create a mask of a network in the layer of an electron beam resist using a high resolution electron beam writer. We then etch the uncovered areas of the film with Ar-ion milling. The entire structure, including the network and the contacts, is made of a single piece of  $\text{La}_{1.84}\text{Sr}_{0.16}\text{CuO}_4$  to avoid high contact resistance. The network resistance is then measured using a four-contact method in the cryogenic system for transport measurement.

In this work, we introduce two types of superconducting networks: a conventional square network (see Figure 6, left panel); and the newly designed double network made by placing small loops in every vertex of a square network (see Figure 6, right panel). Unlike the square network, the small loops in the double network do not share sides and are therefore decoupled. In a later chapter (Section 3.1), we confirm theoretically the decoupling nature of the network. This network combines the advantages of both a single loop and of a square network (high signal to noise ratio, higher critical current, and averaging over sample inhomogeneities).

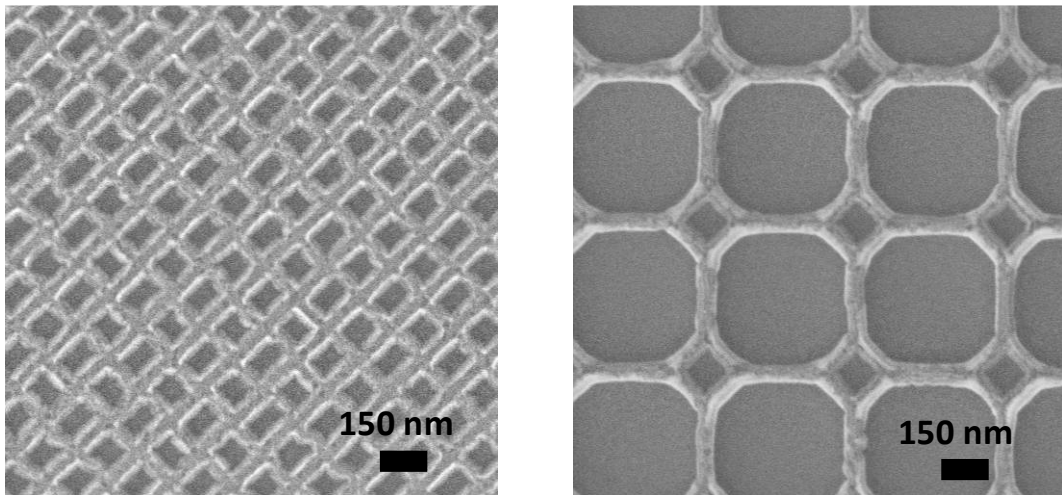


**Figure 6.** Left panel shows a typical scanning electron microscope (SEM) image of a simple square network with a unit cell size of 150 nm. Right panel shows a typical SEM image of a double network consisting of two interlacing networks of large loops of 500 nm, and small loops of 150 nm.

## 2.1 FABRICATION OF $\text{La}_{2-x}\text{Sr}_x\text{CuO}_4$ FILMS - MOLECULAR BEAM EPITAXY (MBE)

The high quality  $\text{La}_{1.84}\text{Sr}_{0.16}\text{CuO}_4$  films used in this study were grown at Brookhaven National Laboratory (BNL), in the group of Ivan Božović, using a Molecular Beam Epitaxy (MBE) machine. MBE film deposition is performed in ultra high vacuum ( $<10^{-8}$  Pa). The slow deposition rate allows the films to grow one atomic layer after another in a controllable way. Ultra-pure elements (La, Sr, Cu) are heated in separate cells until they begin to slowly evaporate (after melting or by sublimation). The gaseous elements then condense on the wafer, where they produce a layer of the desired compound.

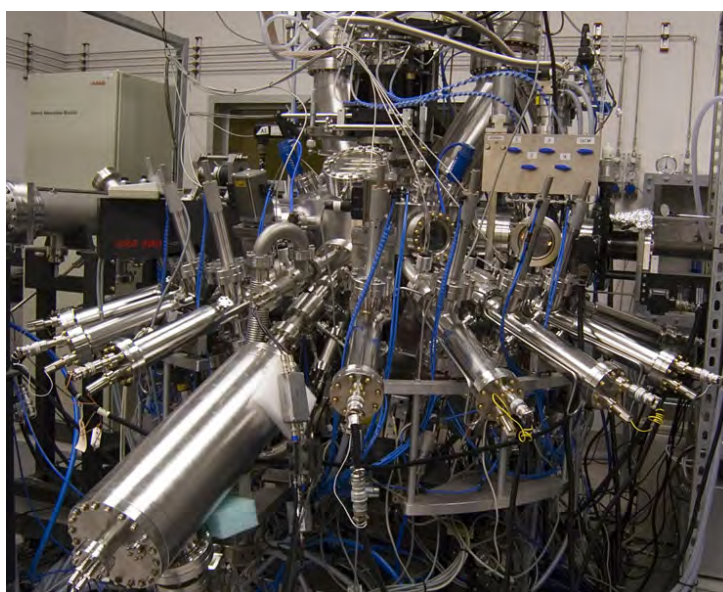


**Figure 7.** Molecular Beam Epitaxy chamber at BNL (Adapted from the Brookhaven Oxide MBE group website.).

The main tool at BNL is a unique multi-chamber Molecular Beam Epitaxy (MBE) system (Figure 7) for the synthesis of complex oxides with atomic-layer precision. The MBE growth chamber consists of the following parts: (i) ultra-high vacuum chamber with two 1,000 l/s turbo-molecular pumps and 24 differential 70 l/s pumps; (ii) sample transfer mechanism to introduce samples from the air into the MBE chamber without venting the MBE; the main chamber includes an introduction chamber, a transfer chamber, and vacuum controls; (iii) a sample manipulator with 6 degrees of freedom, motorized and computer-controlled; the manipulator carries a sample heater with 4 individually controlled quartz lamps capable of heating the substrate to 750°C;

(iv) pure ozone generation, collection, and a delivery system; (v) sixteen evaporation sources with individual pumping stations, gate valves, and fast-acting shutters; (vi) a unique 16-channel atomic absorption spectroscopy (AAS) system for monitoring source rates in real time; (vii) a quartz-crystal oscillator monitor (QCM), mounted on a separate manipulator with 3 translation degrees of freedom, motorized, and computer controlled; (viii) scanning reflection high-energy electron diffraction (RHEED); (ix) a time-of-flight ion scattering and recoil spectroscopy (TOF-ISARS) system for real-time chemical analysis of the film surface; (x) an automatic operation control system that operates vacuum valves, roughening and turbo-molecular pumps, all motorized motions, the pneumatic shutters, and power supplies for thermal evaporation sources, substrate heater lamps, and the ozone source.

The second major vacuum chamber is devoted to *in-situ* pre-lithographic processing, including ion-beam etching and electron-beam deposition of metallization and insulation layers. This chamber is equipped with an Ion Tech 2-inch ion source, a 5-source Thermionics electron-beam evaporator, and an Oxford Applied Research atomic oxygen source. This chamber is installed in the clean room, so that substrates can be prepared in a class-100 clean environment, and loaded into the system without surface contamination.

The growth and processing chambers are connected via a transfer chamber, which has load-locks on both ends, supplied with quartz lamps for fast outgassing of substrates when they are first introduced into the vacuum system. Loading can be accomplished within minutes. The transport chamber is also equipped with ion pumps and Ti-sublimation pumps, and has been tested to maintain vacuum down to  $10^{-11}$  Torr. The transport chamber can be used for storage of 18 substrate holders, 3" each.

For the determination of the crystallographic structure of films, the MBE group has a PANalytical Xpert Pro X-ray diffractometer (XRD). This instrument is a high-resolution (down to 5 arcsec) 4-circle goniometer which enables the study of in-plane and out-of-plane lattice constants, pole figures, rocking curves, and grazing-angle reflectance. We also used a Nanoscope-III Atomic Force Microscope (AFM) for surface characterization.

## 2.2 NANO-PATTERNING

A high resolution electron beam (e-beam) lithography system was exploited for nano-patterning the films. The e-beam system installed at the Bar-Ilan Institute of Nanotechnology and Advanced Materials is the CRESTEC-9500C (Figure 8). The electron beam lithography is based on 'writing' with a focused electron beam in a thin layer of a material sensitive to the accelerated electrons (electron beam resist). The main advantage of electron beam lithography is that it is a very effective way to go beyond the diffraction limit of light and make features of few tens of nanometers or even less. In some cases, the exposed parts of the resist become highly soluble and can be removed by liquid developers (positive tone resists). In other cases, the exposed parts of the resist become unsolvable and the un-exposed parts can be removed by developers (negative tone resists).

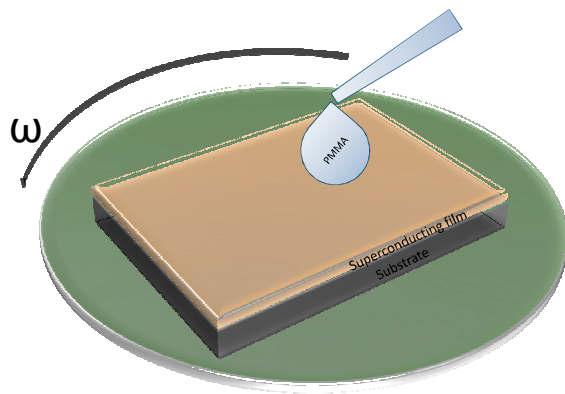


**Figure 8.** CRESTEC CABLE 9000 high resolution Electron Beam Lithography system at Bar-Ilan Institute of Nanotechnology and Advanced Materials (Adapted from CRESTEC website.).

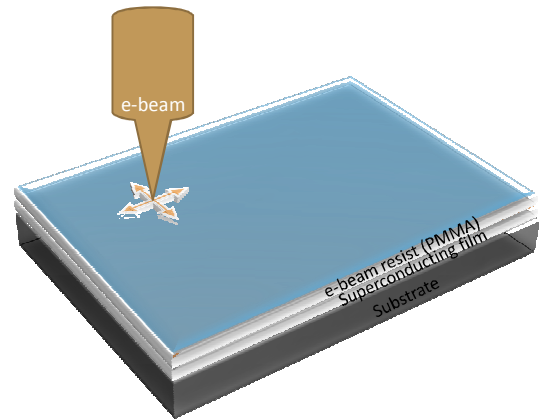
We used Poly(methyl methacrylate) (PMMA) as a negative tone resist. Although, in typical conditions PMMA functions as a positive resist, at increased exposure times PMMA may crosslink and become unsolvable in typical organic developers [51]. We observed that a cross-linked negative tone PMMA ensures a much higher contrast, resolution, and aspect ratio. In a layer of  $\sim 180$  nm, we could reach an aspect ratio (width/height) of up to 1/10 in features down to 16 nm. Generally in thinner layers of PMMA, one can reach a resolution below 10 nm. Cross-linked PMMA are also very stable

during ion milling, probably due to the enhanced stiffness of the crosslinked polymer.

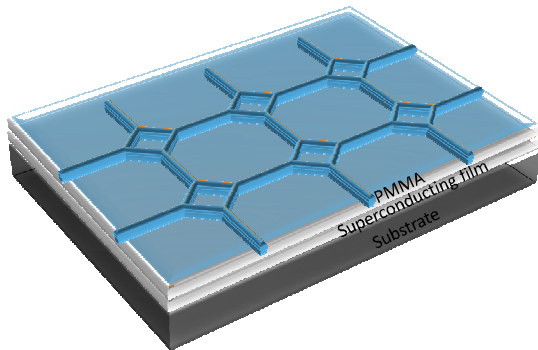
Nanopatterning steps are described schematically in Figure 9. A layer of poly(methyl methacrylate) (PMMA) resist was spun-off on top of a  $\text{La}_{1.84}\text{Sr}_{0.16}\text{CuO}_4$  film (step 1). We used PMMA with a molecular weight of 495,000 (Microchem PMMA 495 A11) diluted further with anisole (approximately 50:50 volume ratio) to produce a film of ~180 nm after spin-coating at the speed of 4,000 RPM. The sample with the resist layer was 'baked' on a hot plate for 1.5 min at 100 - 180 C°. Then the desired patterns of the networks were exposed using a CRESTEC Cable-9000C high resolution e-beam lithography system with an acceleration voltage of 50 KeV and typical beam current of 1 nA (step 2). We used relatively high doses of electron beam exposure to produce a negative tone image of the network in the layer of PMMA. The exposure time was about one to two orders of magnitude higher than the time for the positive regime of the PMMA resist (step 3). The standard developer, based on MIBK (methyl isobutyl ketone), was then used to remove parts of the resist near the negative unsolvable (cross-linked) parts of the PMMA (step 4). This 'negative' PMMA pattern served as a mask for transferring the pattern to the superconducting film by Ar-ion milling, with energies of 1.5 – 3.5 KeV, and currents of 20 – 120 uA (steps 5 and 6).



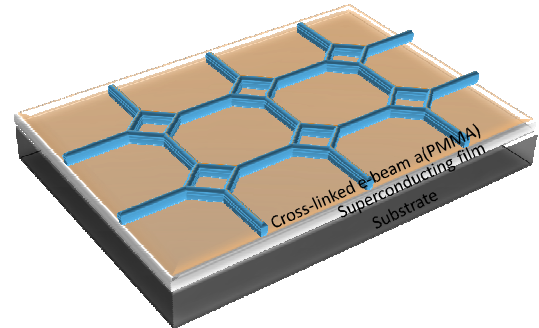
1. Spin-coating



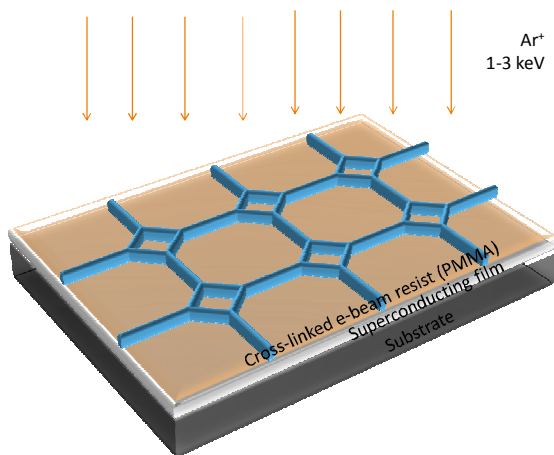
2. E-beam writing



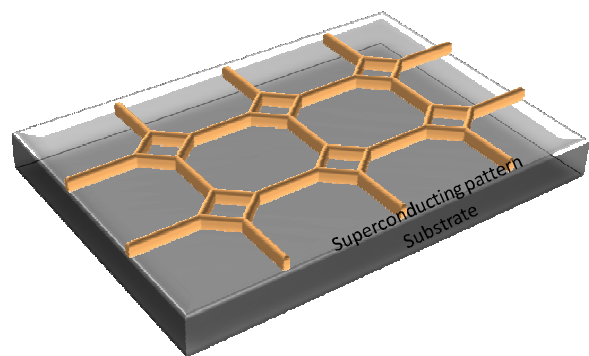
3. Cross-linked PMMA pattern



4. After development



5. Ar-ion milling



6. Final pattern

**Figure 9.** Main nanopatterning steps: (1) spin-coating of the sample with a PMMA resist; (2) electron beam writing in the CRESTEC CABL 9000 system; (3) cross-linked pattern in the layer of PMMA; (4) PMMA mask on top of the superconducting film after development; (5) pattern transfer with Ar ion milling; (6) resulting pattern of the network in the superconducting film.

### 2.3 MAGNETO-TRANSPORT MEASUREMENTS

The magnetoresistance of the superconducting networks was measured in a Quantum Design Physical Property Measurement System (PPMS®) (Figure 10). Sample environment controls include fields up to  $\pm 9$  Tesla and a temperature range of 1.9 - 400 K.



**Figure 10.** Quantum Design Physical Property Measurement System (PPMS®) installed at the Bar-Ilan Institute of Nanotechnology and Advanced Materials (Adapted from the Quantum Design website.).



### 3 RESULTS

The details of this work are described in the following papers:

- I. I. Sochnikov, A. Shaulov, Y. Yeshurun, G. Logvenov and I. Bozovic, "*Large oscillations of the magnetoresistance in nano-patterned high-temperature superconducting films*", *Nature Nanotechnology* **5**, 516 - 519 (2010).
- II. I. Sochnikov, A. Shaulov, Y. Yeshurun, G. Logvenov and I. Bozovic, "*Oscillatory magnetoresistance in nano-patterned superconducting  $La_{1.84}Sr_{0.16}CuO_4$  films*", *Physical Review B* **82**, 094513 (2010).
- III. I. Sochnikov, Y. Shokef, A. Shaulov, and Y. Yeshurun, "*Single-loop like energy oscillations and staircase vortex occupation in superconducting double networks*", submitted to *Physical Review B* (2011).
- IV. I. Sochnikov, I. Božović, A. Shaulov and Y. Yeshurun, "*Uncorrelated behavior of fluxoids in superconducting double networks*", unpublished.

As indicated in Section 2, our experiments focus on the specially designed double network (Figure 6, right panel) composed of two interlaced sub-networks of small and large loops. In Section 3.1 (paper III) we provide a detailed theoretical analysis and computer simulations of the screening current distribution, energy 'waveform' (i.e., energy vs. field) and vortex occupation in the large and small loops of the double network. We show that these two sub-networks exhibit remarkably different behavior. While the sub-network of large loops behaves similarly to a conventional square network, the behavior of the small loops resembles very closely the behavior of a single loop. Thus, for example, the vortex occupation of the large loops increases linearly with the field, whereas the small loops are occupied in steps. In addition, the form of the energy as a function of magnetic field in the double network is similar to the energy form of a single loop. These findings establish theoretically the sub-network of the small loops as an ensemble of decoupled loops.

To confirm experimentally these results, in Section 3.2 (papers IV) we compare magnetoresistance oscillations measured in a conventional square network with loop size of 150 nm, and a double network of 150 nm small and 500 nm large loops made of  $La_{1.84}Sr_{0.16}CuO_4$ . In the square network, we

observe oscillations with features indicative of collective behavior of the loops, e.g. finite slope  $dR/dH$  at  $H = 0$ , downward cusps and pronounced secondary dips at half integer values of  $\Phi/\Phi_0$ . In the double network, we observed dichotomic fluxoid quantization effects: The sub-network of the large loops behaves as regular periodic network, exhibiting correlated behavior of the fluxoids. In contrast, the sub-network of the small square loops exhibits a single-loop-like behavior. This experimental observation indicates uncorrelated arrangements of fluxoids in the sub-network of the small loops in the double network, confirming the theoretical predictions mentioned above.

In Sections 3.3 (paper I) we present magnetoresistance measurements in double networks of  $\text{La}_{1.84}\text{Sr}_{0.16}\text{CuO}_4$  with small loops as low as 75 nm. We observe magnetoresistance oscillations corresponding to the small loops with flux periodicity of  $hc/2e$ . It is tempting to interpret these oscillations as the Little-Parks effect, reflecting oscillations with the field in the transition temperature  $T_c$ . However, the amplitude of these oscillations is two orders of magnitude larger than the amplitude expected from the Little-Parks effect. We therefore proposed a new model for this large effect based on fluxoid dynamics. This model provides a good quantitative description of the oscillations amplitude and its temperature dependence. We also show that, due to the magnitude of the effect, the double network may serve as an effective tool in search of  $hc/e$  and  $hc/4e$  fluxoid periodicities in superconducting nanoloops.

In Section 3.4 (paper II) we further extend the fluxoid dynamics model to include the interaction between the external field and the magnetic moment of the vortices and antivortices. The extended model accounts quantitatively for the measured monotonic background on which the magnetoresistance oscillations are superimposed. Moreover, an analysis of the background within this model indicates that in the patterned film both vortices and antivortices are present. This finding is consistent with the superconducting phase transition scenario proposed by Berezinskii, Kosterlitz and Thouless [41-45].

### 3.1 SINGLE-LOOP LIKE ENERGY OSCILLATIONS AND STAIRCASE VORTEX OCCUPATION IN SUPERCONDUCTING DOUBLE NETWORKS



# Single-loop like energy oscillations and staircase vortex occupation in superconducting double networks

I. Sochnikov<sup>1</sup>, Y. Shokef<sup>2</sup>, A. Shaulov<sup>1</sup>, and Y. Yeshurun<sup>1</sup>

<sup>1</sup> *Department of Physics, Institute of Superconductivity and Institute of Nanotechnology and Advanced Materials, Bar-Ilan University, Ramat-Gan 52900, Israel*

<sup>2</sup> *Department of Materials and Interfaces, Weizmann Institute of Science, Rehovot 76100, Israel*

The magnetic-field dependence of the energy and vortex occupation is calculated for the recently realized superconducting double network consisting of two interlaced sub-networks of small and large loops. Two different approaches are employed, both based on the  $J^2$  model: Mean-field analysis that minimizes the network energy assuming random vortex configurations, and numerical simulations in which energy is minimized avoiding this assumption. In the mean-field analysis the vortex population in both sub-networks increases linearly with applied field. In contrast, the simulations show that while the population of the large loops increases linearly with field, the occupation of the small loops grows in steps, resembling the behavior of an ensemble of decoupled loops. This decoupling is also reflected in the waveform of the energy versus applied field. A modified mean-field analysis which introduces decoupling between the small loops yields results in excellent agreement with the simulations. These findings suggest that the behavior of a single loop is reflected in the double network, and thus constitute it as a favorable system for the experimental study of quantization effects in superconducting loops.

PACS numbers: 74.81.Fa; 74.78.Na; 74.25.Uv; 75.75.-c

## Introduction

In the early days of superconductivity London predicted that the fluxoid<sup>1</sup>, defined as the sum of the magnetic flux and a term involving the persistent current, is quantized in a multiply connected superconductor in units of  $\phi_0 = hc/2e$ . For a single superconducting loop, the fluxoid quantization, together with the requirement for energy minimization, dictates periodic changes in the screening current density  $J$  and step-wise occupation of the loop with flux quanta. The energy, being proportional to  $J^2$ , is also periodic with the magnetic field, giving rise to periodic changes in the critical

temperature,  $T_c$ , as demonstrated by Little and Parks<sup>2</sup>.

Similar to a single superconducting loop, two-dimensional periodic networks of superconducting loops also exhibit magnetoresistance oscillations with field periodicity  $\phi_0/A$ , where  $A$  corresponds to the area of each loop in the network<sup>3-11</sup>. Analyses of the current distribution and the energy vs. magnetic field in such networks are usually based on the  $J^2$ -model<sup>12-14</sup> assuming current conservation in each node and that the average field for the entire network is equal to the externally applied field<sup>15-17</sup>.

Recently, we fabricated a novel type of superconducting network<sup>18, 19</sup> made by connecting the vertexes of small square loops with relatively long wires, forming two interlaced sub-networks of small and large loops, see Figure 1a. The motivation for designing such a network was to create an array of decoupled small loops that behave like isolated loops. Here we analyze this unique network employing two theoretical approaches both based on the  $J^2$ -model, one is the mean-field approach that minimizes the network energy assuming random vortex configurations, and the second is based on numerical simulations in which energy is minimized avoiding this assumption. We first demonstrate these two approaches in the analysis of a *simple square lattice* (Figure 1b). Although in this case both methods yield similar results for the periodicity and the occupation rate, the numerical simulations show additional local minima at normalized fields  $0.5 + m$ , with integer  $m$ , corresponding to the checkerboard configuration studied previously<sup>3, 12, 14, 20</sup>. More dramatic differences between the two approaches are manifested in the analysis of the *double network* (Figure 1a). While in the naïve mean-field analysis the vortex population in both sub-lattices of small and large loops increases linearly with the applied field, the numerical simulations show that the occupation of the small loops grows in steps, resembling the behavior of an ensemble of nearly decoupled loops. However, we show that a modified mean-field analysis which includes decoupling between the small loops reproduces the staircase vortex occupation and the energy waveform obtained in the simulations. Finally, we point to the advantage of the numerical simulations in providing the

actual spatial distribution of the vortices in the double network, demonstrating visually the different occupation of the large and small loops at various magnetic fields. These results will guide future experimental efforts to measure vortex occupations in such complex networks.

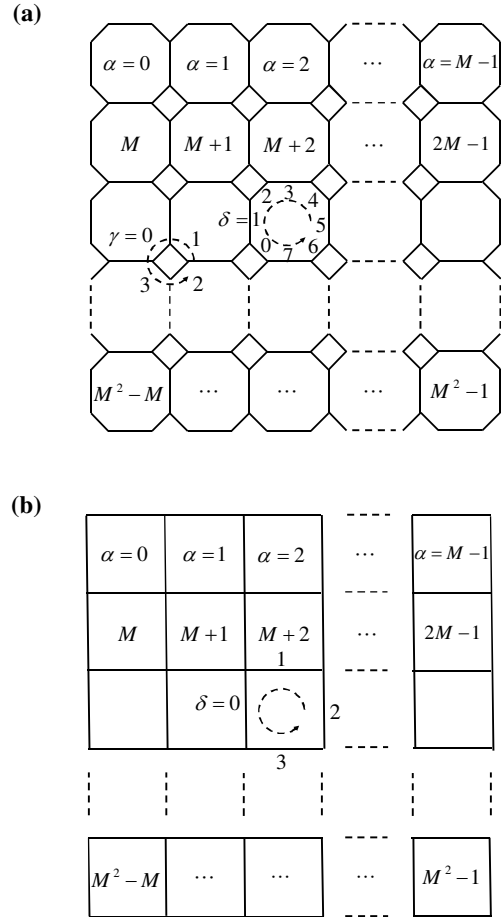


**Figure 1.** Schematic diagram of (a) the double network, and (b) the simple square network.

## Square network

We consider a network of  $M \times M$  square loops, each of side  $L$ , in an external magnetic field  $H$ , see Figure 1b. The fluxoid quantization<sup>1, 21</sup> requires that the integral over the currents around each loop is balanced by the flux quanta in the loop and the external magnetic flux. Thus,

$$\sum_{\delta} L J_{\delta\alpha} = N_{\alpha} \phi_0 - HL^2, \quad (5)$$

where  $\delta = 0, 1, 2, 3$  indexes the edges of the square loop  $\alpha = 0, 1, \dots, M^2 - 1$ , carrying a screening current  $J_{\delta\alpha}$ , and  $N_{\alpha}$  is the number of vortices in the loop  $\alpha$ .

The energy is given by the sum of  $J^2$  over all the network wires:

$$E = \sum_{\alpha=0}^{M^2-1} L (J_{0\alpha}^2 + J_{1\alpha}^2), \quad (6)$$

where two sides in each loop are considered and the summation over all loops ensures that each wire in the network is accounted for. Eqs. (5) and (6) are the basis for both the mean field and the numerical simulation approaches. In writing these equations we adopted the assumptions of the  $J^2$  model<sup>12-14</sup>, namely that the magnetic penetration length is much larger than the wires width and the screening currents are therefore very small. These currents produce magnetic fields which are perturbations on the applied field and are therefore neglected. This model also neglects the geometric inductance<sup>22, 23</sup> and the additional energy from the induced currents interacting with the applied field as compared to the kinetic energy. Notably, the model assumption on the screening length is well satisfied in our experiments<sup>18, 19</sup>.

### Mean field solution

We assume that a fraction  $F$  of the square loops have  $N+1$  vortices and the remaining  $1-F$  have  $N$ . Therefore, the total magnetic flux through the system is

$$N_T [F(N+1) + (1-F)N] \phi_0 = HN_T L^2, \quad (7)$$

where  $N_T = M^2$  is the number of loops in the lattice. Thus

$$N + F = \frac{HL^2}{\phi_0}. \quad (8)$$

Since  $F$  is a fraction and  $N$  is an integer, we may write

$$F = \left\{ \frac{HL^2}{\phi_0} \right\}, \quad N = \left| \frac{HL^2}{\phi_0} \right|, \quad (9)$$

where  $\{\bullet\}$  denotes the fractional part and  $|\bullet|$  the integer part.

We refer to a loop carrying  $(N+1)$  flux quanta as occupied and to one carrying only  $N$  quanta as vacant. Each edge in the network has two neighboring loops, and in the mean-field approximation the probability that both loops are occupied is  $F^2$ , that one is occupied and one is vacant  $2F(1-F)$ , and that both are vacant is  $(1-F)^2$ . Moreover, we will assume that these three types of edges carry currents  $J_{++}$ ,  $J_{+-}$ , and  $J_{--}$ , respectively. Hence, the average current in the system is

$$\langle J \rangle = F^2 J_{++} + 2F(1-F) J_{+-} + (1-F)^2 J_{--}. \quad (10)$$

Eq. (5) for the occupied and vacant loops takes the form,

$$4L[FJ_{++} + (1-F)J_{+-}] = (N+1)\phi_0 - HL^2 = (1-F)\phi_0. \quad (11)$$

$$4L[FJ_{+-} + (1-F)J_{--}] = N\phi_0 - HL^2 = -F\phi_0$$

In writing Eq. (11), we assumed that for each one of the four loops surrounding a given loop, there is a probability  $F$  to be occupied and probability  $1-F$  to be vacant. It is straightforward to verify from Eqs. (10) and (11) that the requirement

that the average current in the network  $\langle J \rangle = 0$  is automatically satisfied.

Eq. (6), for the energy, takes the form

$$E = 2N_T L [F^2 J_{++}^2 + 2F(1-F)J_{+-}^2 + (1-F)^2 J_{--}^2] \quad (12)$$

We are interested in the minimal energy for a given external field; therefore we seek the current distribution in the system that minimizes the energy given in Eq. (12). We use the constraints of Eq. (11) to express  $J_{++}$  and  $J_{--}$  in terms of  $J_{+-}$ , then substitute these in Eq. (12) and minimize with respect to  $J_{+-}$  by requiring  $\partial E / \partial J_{+-} = 0$ . After some algebra this yields

$$E = \frac{N_T \phi_0^2}{4L} F(1-F). \quad (13)$$

The solid line in Figure 2 shows the normalized energy per loop as a function of the normalized external field. Note that the energy waveform for the network is inverted and shifted by a quarter of a period relative to that of a single loop (see, e.g., Figure 4.5 in Ref. <sup>21</sup>). In addition, in contrast to an isolated loop in which the occupation grows in steps <sup>21</sup>, in the square network the occupation grows linearly with the field, see Eq. (8).

This solution is valid as long as the vortex distribution in the network is disordered, namely that there are no correlations between the occupations of neighboring loops. It is instructive to see how this breaks down for  $F = 1/2$ , where the minimum energy configuration is known to be that of a checkerboard arrangement of the vortices on the lattice. For such a configuration, all edges have an

occupied loop on one side and a vacant loop on the other <sup>24, 25</sup>. Eq. (11) should be modified to have only contributions from  $J_{+-}$  for both types of loops, which leads to  $J_{+-} = \phi_0 / (8L)$ . Similarly, Eq. (12) for the energy should be modified to include only a contribution from  $J_{+-}^2$ , eventually leading to  $E = N_T \phi_0^2 / (32L)$ , denoted by the bold circles in Figure 2, which is half of the mean-field value of  $N_T \phi_0^2 / (16L)$  obtained by substituting  $F = 1/2$  in Eq. (13). Also, note that for the checkerboard arrangement of vortices, Eq. (10) may no longer be used, yet the total current still vanishes. Here, the magnitude of the current on all edges is equal, but their directions alternate in space to achieve a net current in one direction around the occupied loops and in the opposite direction around the vacant loops.

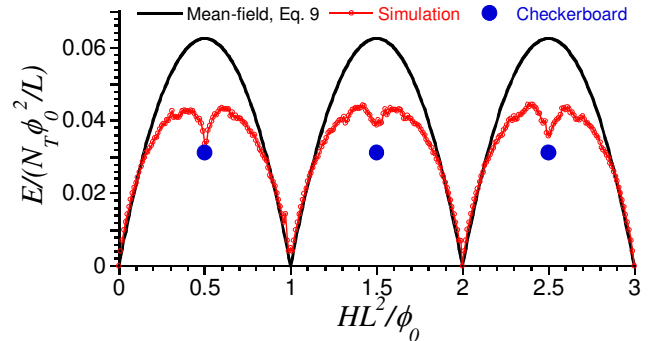


**Figure 2.** (Color online) Normalized energy per loop obtained from the mean-field analysis, Eq. (13), and from the simulations (solid line and open circles respectively) plotted versus the normalized field. The bold circles indicate the theoretical value of the energy corresponding to the checkerboard configuration of vortices in the square network,  $E = N_T \phi_0^2 / (32L)$ .

The numerical simulation, discussed in the next section, offers a more accurate

solution, not limited to disordered distributions of vortices in the network.

### **Numerical simulation**

For a given external field  $H$  we calculate the total number of vortices in the system as

$$N_v = N_T L^2 H / \phi_0. \quad (14)$$

We initially distribute these vortices randomly throughout the network. Then, we employ the following procedure to find the currents  $J_{\delta\alpha}$  through all edges such that the total energy of the network is minimized: We assign a circular current  $\tilde{J}_\beta$  to each loop  $\beta$  and express  $J_{\delta\alpha}$  in terms of  $\tilde{J}_\beta$ :

$$J_{\delta\alpha} = \sum_{\beta} K_{\alpha\beta}^{\delta} \tilde{J}_\beta, \quad (15)$$

where the four  $N_T \times N_T$  matrices  $\mathbf{K}^0, \mathbf{K}^1, \mathbf{K}^2$  and  $\mathbf{K}^3$  are evaluated in Appendix A, assuming current conservation at every node of the network<sup>26</sup> and periodic boundary conditions. Eq. (15) provides four sets of  $M^2$  linear equations. By substituting Eq. (15) into Eq. (5) one gets  $N_T$  linear equations with  $M^2$  variables  $\tilde{J}_\beta$

$$N_\alpha \phi_0 - HL^2 = \sum_{\delta\beta} LK_{\alpha\beta}^{\delta} \tilde{J}_\beta = \sum_{\beta} Y_{\alpha\beta} \tilde{J}_\beta, \quad (16)$$

where  $Y_{\alpha\beta} = \sum_{\delta} LK_{\alpha\beta}^{\delta}$  is an  $M^2 \times M^2$  matrix.

Having the population vector  $\mathbf{N}$  we evaluate the vector of the circular currents  $\tilde{\mathbf{J}}$  by inversion

$$\tilde{\mathbf{J}} = \mathbf{Y}^{-1}(\mathbf{N}\phi_0 - HL^2). \quad (17)$$

Knowledge of  $\tilde{\mathbf{J}}$  for a given spatial distribution of the vortices on the lattice allows calculation of the current matrix  $J_{\delta\alpha}$  using Eq. (15) and thus the total energy  $E$  using Eq. (6).

The minimum energy and the vortex configuration corresponding to it are found as follows: One cell is randomly chosen and the number of vortices in this cell is reduced by one and subsequently the number of vortices in one of the neighboring cells is incremented by one. We calculate the currents  $J_{\delta\alpha}$  and the energy for the new configuration. If the energy of this new configuration is lower than the energy of the previous state, then we accept the new one. Otherwise, the old state is preserved. This process is repeated for every cell in the network, completing one sweep of energy minimization. Such sweeps are repeated (typically 500-1000 times) until we reach a steady state. Results of the calculated energy for a  $10 \times 10$  network are shown in Figure 2 (open circles). Convergence of the calculations presented in Figure 2 was confirmed for several fields in a  $20 \times 20$  network.

Notably, although the periodicity of the energy *versus* field and the occupation rate are as in the mean field case, the simulation shows local minima at normalized fields  $1/2 + m$ , with integer  $m$ , corresponding to the checkerboard configuration<sup>3, 12, 14, 24, 25</sup>. Hints for additional minima at normalized magnetic fields of  $1/3$  and  $2/3$  may be observed in Figure 2 in agreement with e.g. reference 9. Additional possible minima are in the noise level. More dramatic differences between the two approaches of the mean-

field solution and numerical simulations are found in the case of the double network, as described below.

## Double network

We refer to the double network of Figure 1a, made up of a square lattice of side  $L$  and square loops of side  $\ell < L$  oriented at  $45^\circ$  with respect to this lattice and placed at every vertex of the large lattice. Each large loop has four short edges of length  $\ell$  and four long edges of length  $x = L - \sqrt{2}\ell$ . (We refer to these edges as long even though for  $x < \ell$ ,  $\sqrt{2}\ell < L < (1 + \sqrt{2})\ell$ ). The area of each small loop is  $\ell^2$  and the area of each large loop is  $L^2 - \ell^2$ .

### Mean-field solution

When this system is placed in an external magnetic field  $H$ , a fraction  $f$  of the small loops have  $n+1$  flux quanta through them, and a fraction  $1-f$  have  $n$ , and similarly, a fraction  $F$  of the large loops have  $N+1$  and a fraction  $1-F$  have  $N$ . These quantities are related to the external field since the total magnetic flux satisfies

$$N_T [f(n+1) + (1-f)n + F(N+1) + (1-F)N] \phi_0 = HN_T L^2 \quad (18)$$

The left-hand side is the result of counting the number of flux quanta according to the above definitions ( $N_T$  is the number of loops of each size), and the right-hand side is the external field multiplied by the total area of the system. This leads to

$$N + F + n + f = \frac{HL^2}{\phi_0}. \quad (19)$$

In deriving the mean-field solution for the double grid, we note that as for the simple square lattice, there are three types of long edges: those separating two occupied loops ( $++$ ), those separating an occupied loop and a vacant loop ( $+-$ ), and those separating two vacant loops ( $--$ ). We assume that the probabilities of finding each of these types are given by  $F^2$ ,  $2F(1-F)$ , and  $(1-F)^2$ , respectively. We assume these types of edges carry currents  $J_{++}$ ,  $J_{+-}$ , and  $J_{--}$ , respectively. Therefore, the requirement that the average current vanishes<sup>26</sup> reads

$$\langle J \rangle = F^2 J_{++} + 2F(1-F) J_{+-} + (1-F)^2 J_{--} = 0 \quad (20)$$

Each short edge separates a small loop and a large loop, therefore the types ( $+ \rightarrow$ ) and ( $\rightarrow +$ ) are not symmetric as for the long edges, and we need to deal with four types of edges: separating two occupied loops ( $++$ ), separating an occupied small loop and a vacant large loop ( $+ \rightarrow$ ), separating a vacant small loop and an occupied large loop ( $\rightarrow +$ ), and separating two vacant loops ( $--$ ). We assume currents  $j_{++}$ ,  $j_{+ \rightarrow}$ ,  $j_{\rightarrow +}$ , and  $j_{--}$  on them, and within the mean-field approximation, the probabilities of finding each of them are given by  $fF$ ,  $f(1-F)$ ,  $(1-f)F$ , and  $(1-f)(1-F)$ , respectively. The requirement that the average current on the short edges vanishes is

$$\langle j \rangle = fF j_{++} + f(1-F) j_{+ \rightarrow} + (1-f)F j_{\rightarrow +} + (1-f)(1-F) j_{--} = 0 \quad (21)$$

An occupied small loop has the following relation between the integral of the currents around it and the magnetic flux through it,

$$4\ell[Fj_{++} + (1-F)j_{+-}] = (n+1)\phi_0 - H\ell^2, \quad (22)$$

For a vacant small loop we similarly have

$$4\ell[Fj_{-+} + (1-F)j_{--}] = n\phi_0 - H\ell^2. \quad (23)$$

The currents on each of the edges are determined by the flux in the large loop on the other side of that edge, and we have used the mean-field assumption that the flux in adjacent loops is uncorrelated, thus the probabilities for having each of the neighboring large loops occupied or vacant are  $F$  and  $1-F$ , respectively.

Similarly, an occupied large loop has

$$\begin{aligned} &4\ell[fj_{++} + (1-f)j_{+-}] + \\ &+ 4x[FJ_{++} + (1-F)J_{+-}] =, \\ &= (N+1)\phi_0 - H(L^2 - \ell^2) \end{aligned} \quad (24)$$

and a vacant large loop has

$$\begin{aligned} &4\ell[fj_{++} + (1-f)j_{+-}] + \\ &+ 4x[FJ_{++} + (1-F)J_{+-}] =. \\ &= N\phi_0 - H(L^2 - \ell^2) \end{aligned} \quad (25)$$

Multiplying Eq. (22) by  $F$  and Eq. (23) by  $1-F$ , and adding, leads by the use of Eq. (21) to

$$\frac{n+f}{N+F} = \frac{\ell^2}{L^2 - \ell^2}. \quad (26)$$

It is easy to see that now Eq. (20) is satisfied as well. Together with Eq. (19), we obtain  $N+F = H(L^2 - \ell^2)/\phi_0$  and

$n+f = H\ell^2/\phi_0$ . Since  $N$  and  $n$  should be integer and  $f$  and  $F$  fractional, we obtain

$$\begin{aligned} F &= \left\{ \frac{H(L^2 - \ell^2)}{\phi_0} \right\}, N = \left\lfloor \frac{H(L^2 - \ell^2)}{\phi_0} \right\rfloor, \\ f &= \left\{ \frac{H\ell^2}{\phi_0} \right\}, n = \left\lfloor \frac{H\ell^2}{\phi_0} \right\rfloor, \end{aligned} \quad (27)$$

where  $\{\bullet\}$  denotes the fractional part and  $\lfloor \bullet \rfloor$  the integer part.

We are now left with four equations (22)-(25) connecting the seven unknown currents ( $J_{++}, J_{+-}, J_{-+}, j_{++}, j_{+-}, j_{-+}, j_{--}$ ). We use these four equations to express  $J_{++}, J_{--}, j_{++}, j_{--}$  in terms of  $J_{+-}, j_{+-}, j_{-+}$ . The energy, given by the sum of  $xJ^2$  over  $2N_T$  long edges and the sum of  $\ell j^2$  over  $4N_T$  short edges,

$$\begin{aligned} E &= 2N_T x [F^2 J_{++}^2 + 2F(1-F)J_{+-}^2 + \\ &+ (1-F)^2 J_{-+}^2] + \\ &+ 4N_T \ell [fFj_{++}^2 + f(1-F)j_{+-}^2 + \\ &+ (1-f)Fj_{-+}^2 + (1-f)(1-F)j_{--}^2] \end{aligned} \quad (28)$$

may now be expressed in terms of the parameters  $J_{+-}, j_{+-}, j_{-+}$ . We minimize  $E$  with respect to these parameters by demanding that  $\partial E/\partial J_{+-} = \partial E/\partial j_{+-} = \partial E/\partial j_{-+} = 0$ . After some algebra, this yields

$$E = \frac{N_T \phi_0^2}{4} \left[ \frac{F(1-F)}{x+\ell} + \frac{f(1-f)}{\ell} \right]. \quad (29)$$

Figure 3a and 3b show the mean-field calculations (Eq. (29)) of the normalized energy per unit cell of the double network and the occupation,  $N_v = N+F$  and  $n_v = n+f$ , of the large and the small loops, respectively, for  $L/\ell = 5$ . The short period oscillations shown in Figure 3a are associated with the

large loops. These oscillations are superimposed on oscillations of longer period associated with the small loops. Figure 3b shows that the mean field solution predicts that the occupation of both the large and small loops increases linearly with the field, behaving as in two separate square networks consisting of large and small loops. As described in the next section, the numerical simulations show that while the occupation of the large loops increases linearly with the applied field, the occupation of the small loops grows in steps, resembling the behavior of an ensemble of nearly decoupled loops.

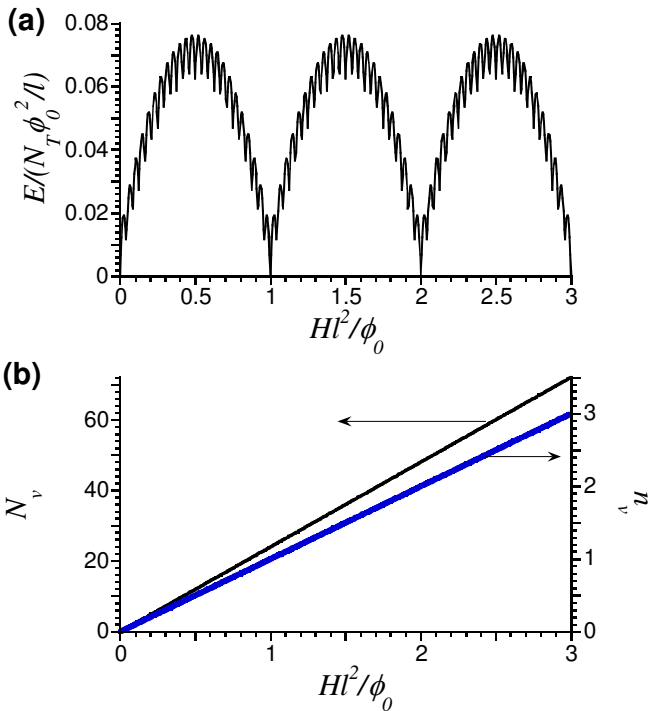


**Figure 3.** (Color online) (a) Mean-field calculations (Eq. (29)) of the normalized energy per unit cell of the double network and (b) the occupation,  $N_v = N + F$ , of the large and the small loops,  $n_v = n + f$ , for  $L/\ell = 5$ . Note that the ratio of the slopes of the two lines is 24, corresponding to the ratio between the areas of the large and small loops.

## Numerical simulations

For the *double network* (Figure 1a) the fluxoid quantization takes a form of two systems of discrete sums

$$\sum_{\delta} L_{\delta} J_{\delta\alpha} = N_{\alpha} \phi_0 - H(L^2 - \ell^2) \quad (30)$$

$$\sum_{\gamma} \ell j_{\gamma\alpha'} = n_{\alpha'} \phi_0 - H\ell^2$$

where  $J_{\delta\alpha}$  is the current through the side  $\delta = 0, 1, \dots, 7$  of the loop  $\alpha$  in the sub-network of the large loops and  $j_{\gamma\alpha'}$  is the current through the side  $\gamma = 0, 1, \dots, 3$  of the small loop  $\alpha'$  adjacent to the large loop  $\alpha$  (see Figure 1a).  $L_{\delta} = x$  for  $\delta = 1, 3, 5, 7$  and  $L_{\delta} = \ell$  for  $\delta = 0, 2, 4, 6$ . Thus, we have  $N_T$  linear equations for the population of vortices in the large loops and  $N_T$  equations for the vortices in the small loops. As for the simple network, we rather use the notation of circular currents:  $\tilde{J}$  for large loops and  $\tilde{j}$  for small loops. The total current in a specific wire is then expressed using these circular currents:

$$J_{\delta\alpha} = \sum_{\beta} A_{\alpha\beta}^{\delta} \tilde{J}_{\beta} + \sum_{\beta} B_{\alpha\beta}^{\delta} \tilde{j}_{\beta} \quad (31)$$

$$j_{\gamma\alpha} = \sum_{\beta} C_{\alpha\beta}^{\gamma} \tilde{J}_{\beta} + \sum_{\beta} D_{\alpha\beta}^{\gamma} \tilde{j}_{\beta}$$

where the  $N_T \times N_T$  matrices  $\mathbf{A}^{\delta}$ ,  $\mathbf{B}^{\delta}$ ,  $\mathbf{C}^{\gamma}$  and  $\mathbf{D}^{\gamma}$  are evaluated in Appendix B, assuming current conservation at every node of the network<sup>26</sup> and periodic boundary conditions. Substitution of the total currents from Eq. (31) to Eq. (30) leads to the quantization rule expressed in terms of the circular currents

$$\begin{aligned}
& \sum_{\delta\beta} L^\delta A_{\alpha\beta}^\delta \tilde{\mathbf{J}}_\beta + \sum_{\delta\beta'} L^\delta B_{\alpha\beta'}^\delta \tilde{\mathbf{J}}_{\beta'} = \quad (32) \\
& = \sum_{\beta} Y_{\alpha\beta}^{(0)} \tilde{\mathbf{J}}_\beta + \sum_{\beta'} Y_{\alpha\beta'}^{(1)} \tilde{\mathbf{J}}_{\beta'} = \\
& = N_\alpha \phi_0 - H(L^2 - \ell^2) \\
& \sum_{\gamma\beta} \ell C_{\alpha\beta}^\gamma \tilde{\mathbf{J}}_\beta + \sum_{\gamma\beta'} \ell D_{\alpha\beta'}^\gamma \tilde{\mathbf{J}}_{\beta'} = \\
& \sum_{\beta} Y_{\alpha\beta}^{(2)} \tilde{\mathbf{J}}_\beta + \sum_{\beta'} Y_{\alpha\beta'}^{(3)} \tilde{\mathbf{J}}_{\beta'} = n_\alpha \phi_0 - H\ell^2
\end{aligned}$$

Using vector form we can invert Eq. (32) and derive the vectors of circular currents  $\tilde{\mathbf{J}}$  and  $\tilde{\mathbf{j}}$

$$\begin{bmatrix} \tilde{\mathbf{J}} \\ \tilde{\mathbf{j}} \end{bmatrix} = \begin{bmatrix} \mathbf{Y}^{(0)} & \mathbf{Y}^{(1)} \\ \mathbf{Y}^{(2)} & \mathbf{Y}^{(3)} \end{bmatrix}^{-1} \begin{bmatrix} \mathbf{N}\phi_0 - H(L^2 - \ell^2) \\ \mathbf{n}\phi_0 - H\ell^2 \end{bmatrix}, \quad (33)$$

where  $\mathbf{Y}^{(0)}$ ,  $\mathbf{Y}^{(1)}$ ,  $\mathbf{Y}^{(2)}$  and  $\mathbf{Y}^{(3)}$  are  $N_T \times N_T$  sub-matrices,  $\mathbf{N}$  and  $\mathbf{n}$  is the number of vortices in the large and the small loops respectively written in vector form.

The energy of the network is expressed in terms of the currents in each wire:

$$E = \sum_{\delta=0,1,2,3,4,6} L_\delta J_{\delta\alpha}^2, \quad (34)$$

by summing over  $\alpha$  we ensure that each of the sides, including  $\delta = 5, 7$ , are accounted for.

As described in the previous section the algorithm is based on minimizing the energy associated with the kinetic energy of the screening currents induced in the superconducting network. For the double network the occupation is described by a vector of length  $2N_T$ , corresponding to  $N_T$  small and  $N_T$  large loops. For a given external field  $H$ , at the initial step the loops are randomly filled with  $N_T H L^2 / \phi_0$  vortices.

Using Eq. (31) and Eq. (33) we calculate the currents induced in the sides of the small and large loops. Knowledge of these currents allows the calculation of the energy of the network using Eq. (34).

The minimum energy of the double network and the vortex configuration corresponding to it are found following a similar procedure as described above. Namely, one cell, small or large, is randomly chosen and one vortex is moved from this cell to one of its nearest neighbors and the currents  $J_{\delta\alpha}$  and  $j_{\gamma\alpha}$  the energy for the new configuration are calculated. If the energy of this new configuration is lower than the energy of the previous state, then we accept the new one. Otherwise, the old state is preserved. We repeat this procedure for every cell in the network (i.e.  $2N_T$  times), completing one sweep of the energy minimization. Such sweeps are repeated (typically 500-1000 times). The symbols in Figure 4 present the results of these calculations for a network consisting of  $10 \times 10$  large and  $10 \times 10$  small loops for different values of the ratio  $L/\ell$ . Numerical convergence of the calculations were confirmed for several fields in a  $20 \times 20$  network of  $L/\ell = 5$ .

The squares in Figure 4a show the normalized energy of the double network for  $L/\ell = 10, 5$  and  $3$ . As in the mean-field solution, oscillations of short periods, corresponding to the large loops, are superimposed on the oscillations of large periods corresponding to the small loops. However, we note that the waveform of the large period oscillations resemble that of a single loop (i.e. minima at integer multiples of flux quanta and cusps at integer multiples of half flux quanta) in contrast with the results of the mean-field solution

(Figure 3a), which exhibits a waveform similar to the simple square network shown in Figure 2.

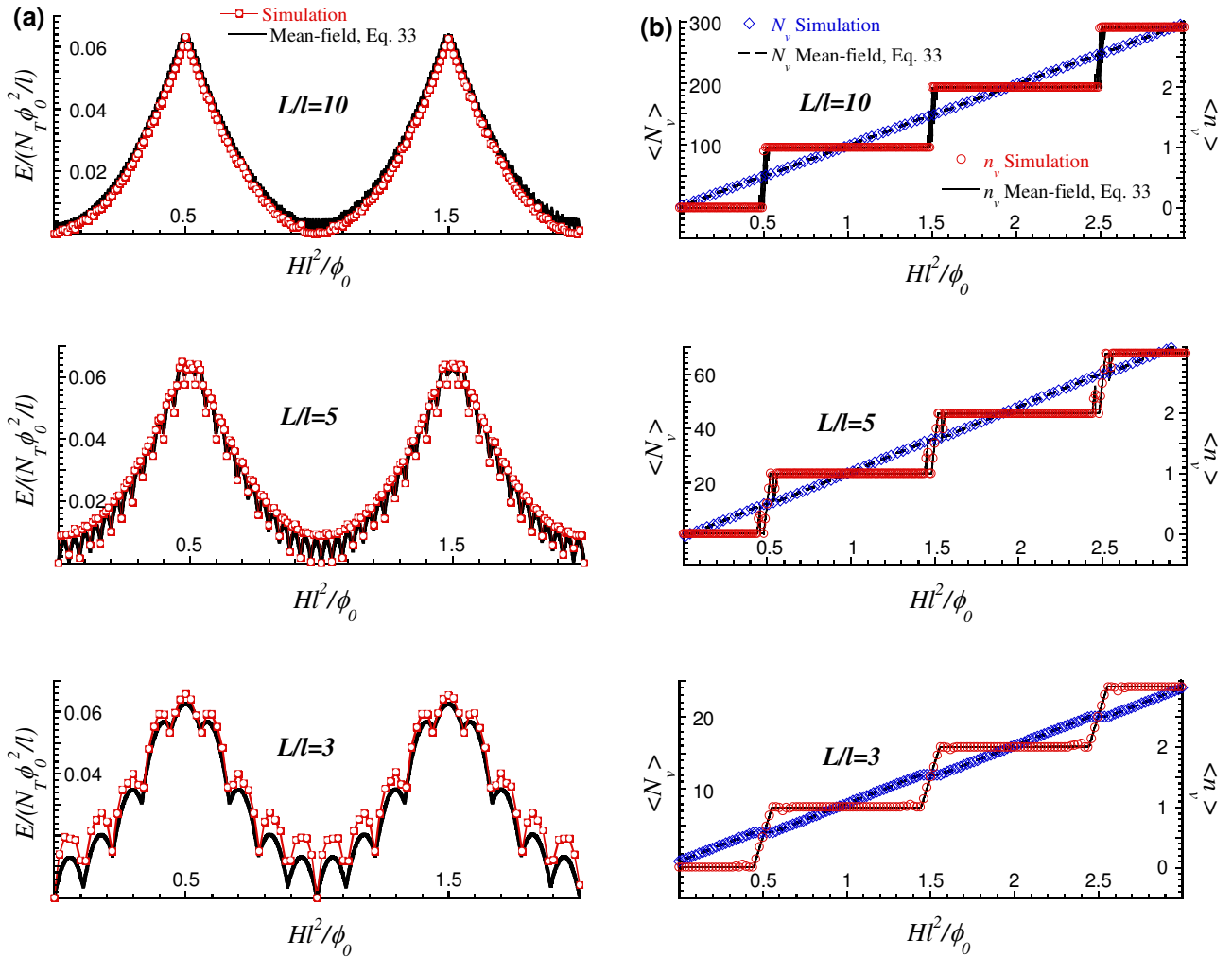


**Figure 4.** (Color online) (a) Normalized energy per unit cell obtained theoretically after minimizing Eq. (37) (bold solid lines) and from simulations (squares connected by thin lines as guide for the eye). (b) Average number of vortices per large loop,  $\langle N_v \rangle$ , and per small loop,  $\langle n_v \rangle$ , obtained theoretically (Eq. (37)), (dashed and solid lines, respectively) and from simulations (diamonds and circles, respectively). The different panels relate to double networks with size ratios  $L/\ell = 10, 5$  and 3 (from top to bottom). Both numerical and analytical solutions show breaks around the middle of the steps resulting from competition in occupation of large and small loops. This competition occurs in the field range where the energy cost to insert a vortex into a small loop or a large loop is similar. The field increment (in units of  $Hl^2/\phi_0$ ) in the simulations is 0.02 for  $L/\ell = 3$ , and 0.01 for  $L/\ell = 5$  and 10. The step in the  $\langle n_v \rangle$  plot for  $L/\ell = 10$  is relatively sharp ( $< 0.01$ ) and hence points on this step are absent.

The diamonds and circles in Figure 4b show the average number of vortices per loop calculated for the large and small loops respectively, as a function of the magnetic flux normalized to the area of the small loops. Results are shown for three ratios  $L/\ell = 3, 5, 10$ . The large loops are filled with vortices approximately linearly as the magnetic field increases. In contrast, the small loops are filled in a step-wise manner that becomes sharper as the ratio  $L/\ell$  increases. This indicates that the system prefers to distribute vortices between the large loops and to expel vortices from the small loops. Only when the normalized magnetic field is close to  $0.5+m$ , the system may accept vortices into the small loops. This behavior is not predicted in the framework of the mean-field solution as described in the previous section. The step-wise occupation and the energy waveform both imply that the sub-lattice of the small loops behaves as an ensemble of decoupled single loops<sup>27</sup>. In the next section we show how these results may be obtained theoretically from a modified mean-field model, assuming decoupling of the small loops.

### **Modified mean-field model**

As mentioned above, the mean-field analysis of the double network described in the beginning of this section shows that the two sub-lattices of the double network are populated as two separate square lattices. This is in contrast with the results of the simulations presented in this section that show stepwise occupation of the small loops. We will now show how an assumption on the decoupling between the small loops may be introduced into the mean-field description, and that this hybrid framework explains the numerical findings.

We incorporate the decoupling of the small loops by ignoring the requirement that the currents around them should match with the currents on their neighboring large loops. Namely, for the large loops we assume the square-lattice mean-field description with Eq. (11) replaced by:

$$\begin{aligned}\beta_L[FJ_{++} + (1-F)J_{+-}] &= (N+1)\phi_0 - \alpha_L H \\ \beta_L[FJ_{+-} + (1-F)J_{--}] &= N\phi_0 - \alpha_L H\end{aligned}\quad (35)$$

Here, the total area  $N_T L^2$  is covered by a square lattice of  $N_T$  large loops, each with area  $\alpha_L = L^2 - \ell^2$  and perimeter  $\beta_L = 4(x + \ell) = 4(L + (1 - \sqrt{2})\ell)$ , and with  $N_T$  disconnected small loops, each with area  $\alpha_s = \ell^2$  and perimeter  $\beta_s = 4\ell$ . We use the convention  $N$ ,  $F$ ,  $n$  and  $f$ , from the beginning of this section to describe the population of these loops, and as in the mean-field solution, compliance of the total magnetic flux with the external field leads to Eq. (19).

For each small loop, we assume that the current is distributed uniformly around its perimeter; for a small loop carrying  $k$  vortices, this current is thus  $j = (k\phi_0 - \alpha_s H) / \beta_s$ , resulting in an energy  $E = j^2 \beta_s = (k\phi_0 - \alpha_s H)^2 / \beta_s$ . From (35), we express  $J_{++}$  and  $J_{--}$  in terms of  $J_{+-}$ , and substitute the result in the expression for the energy:

$$\begin{aligned}\frac{E}{N_T} &= \frac{\beta_L}{4} [F^2 J_{++}^2 + 2F(1-F)J_{+-}^2 + (1-F)^2 J_{--}^2] + \\ &+ \frac{f}{\beta_s} [(n+1)\phi_0 - \alpha_s H]^2 + \frac{1-f}{\beta_s} [n\phi_0 - \alpha_s H]^2\end{aligned}\quad (36)$$

where the first term is the mean-field expression for the contribution to the energy from the large loops (see Eq. (12)),

and the last two terms average the contributions from populated and vacant small loops according to their abundance. By minimizing  $E$  with respect to  $J_{+-}$  we eventually obtain:

$$\frac{E}{N_T} = \frac{[(N+F)\phi_0 - \alpha_L H]^2 + 2F(1-F)\phi_0^2}{4\beta_L} + \frac{[(n+f)\phi_0 - \alpha_S H]^2 + f(1-f)\phi_0^2}{\beta_S} \quad (37)$$

Note that we are still free to choose the ratio  $(N+F)/(n+f)$  such that Eq. (37) is minimized.

The bold solid lines in Figure 4a show the normalized energy per unit cell obtained after minimizing Eq. (37) for  $L/\ell=10, 5$  and  $3$  (from top to bottom). Impressive agreement with the results of the simulations (circles in Figure 4a) is evident. The dashed and solid lines in Figure 4b show the average number of vortices per large loop,  $N_v$ , and per small loop,  $n_v$ , respectively, as calculated from Eq. (37). These results are in perfect agreement with the results of the simulations described by diamonds and circles in Figure 4b. Note that our hybrid model treats the large loops by mean-field interactions and the small loops as disconnected. Yet, the behavior of the small loops is not identical to that of loops without network, since the presence of the large loops affect the distribution of vortices in the small ones. For example, as shown in Figure 4b, for small  $L/\ell$  the steps in  $n_v$  are not sharp as expected for loops without network. These steps become sharper as the ratio  $L/\ell$  increases.

### ***Spatial configuration of vortices***

Our numerical simulation allows mapping the occupation of the small and large loops in the double network in the state of minimum energy, for different external fields. Figure 5 shows the distribution of vortices in a double network with  $L/\ell=5$  at low normalized fields. In this field range the large loops are occupied in the same way as a simple square network: For  $H\ell^2/\phi_0=0.01$  vortices are located far away from each other; at  $H\ell^2/\phi_0=0.02$  corresponding to half filling of the large loops,  $H(L^2 - \ell^2)/\phi_0 \approx 0.5$ , a checkerboard distribution<sup>3, 12, 14</sup> is observed in the large loops, while all small loops are empty; at  $H\ell^2/\phi_0=0.03$  most of the large loops are occupied with one vortex. The small loops, however, are empty at all these fields and, therefore, a plateau in  $n_v(H)$  is observed in Figure 4b.

Figure 6 shows the vortex distribution in a double network with  $L/\ell=5$  at relatively high fields of  $H\ell^2/\phi_0=0.48, 0.50$  and  $0.52$ . In this narrow field range the number vortices in the small loops increases sharply from zero at  $0.48$  to one at  $0.52$ . The  $n_v(H)$  curve at these fields (Figure 4b) corresponds to the transition from one plateau to another. As the field is further increased, the number of vortices in the large loops increases linearly, while the number of vortices in the small remains constant.

### **Summary**

We have theoretically studied the recently realized superconducting double network consisting of two interlaced sub-networks of small and large loops. Our

numerical simulations show that the vortex occupation of the large and small loops is completely different. Vortices prefer to occupy the large loops, even in large numbers, before the occupation of the small loops begins. The population of the sub-network of the large loops increases linearly with the field, while the occupation of the sub-network of the small loops grows in steps. The energies of both sub-networks oscillate with the field with different periodicities determined by the areas of the large and small loops. The energy oscillations of the sub-network of the large loops are of low amplitude and short period and resemble that of a simple square network, exhibiting cusps at the beginning and at the end of each period. These oscillations are superimposed on the high amplitude and long period energy oscillations of the sub-network of the small loops, which resemble the energy oscillations of isolated loops exhibiting cusps at the middle of each period. The low amplitude of the energy oscillations of the large loops is a result of the relatively small screening current induced in the large loops. At the end of the first short period each of the large loops is occupied with one vortex, in the next period with two vortices, *etc.* In contrast, the sub-network of the small loops remains empty up to fields of approximately half of the long period, i.e.  $\phi_0/2\ell^2$ . Up to this field the screening current in the small loops increases linearly and consequently the contribution to the energy increases quadratically with the field. Around  $\phi_0/2\ell^2$ , in a relatively narrow field range defined by the ratio  $L/\ell$ , all the small loops are filled with one vortex. In the next long period, at  $3\phi_0/(2\ell^2)$ , each of the small loops is occupied with two vortices, *etc.* Thus the

behavior of the small loops resembles that of a single loop.

The above physical picture is explained by a modified mean-field analysis in which we treat the large loops by mean-field interactions and the small loops as disconnected. This hybrid framework yields the stepwise population and energy oscillations in excellent agreement with the numerical simulations. We therefore conclude that the sub-network of the small loops behaves as a large ensemble of decoupled loops. As demonstrated in Figure 4b, the degree of decoupling improves as the size ratio  $L/\ell$  between the two networks increases.

The numerical simulations have the advantage in providing the actual vortex distribution in the network as a function of the external field as demonstrated in Figs. 5 and 6. Experimental imaging of vortex distribution in simple networks of micron size squares has been previously performed using Hall probe technique<sup>28, 29</sup>, scanning SQUID microscopy<sup>30</sup> and Bitter decoration<sup>31-33</sup>. Extension of these works to imaging of vortex distribution in nano-loops of the double network may be realized by exploiting Magnetic Force and SQUID microscopy. This study may lead to novel designs of network and methods of controlling the position of a single vortex, with implications to future nano-scale superconducting devices. Our work may also be applicable to the recent activity on arrays of single-domain ferromagnetic islands<sup>34-36</sup>.

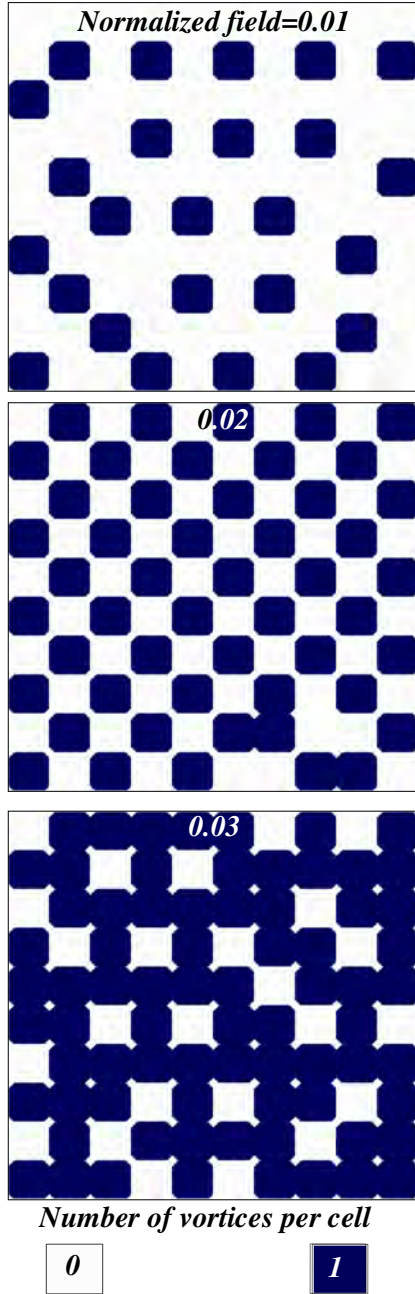


**Figure 5.** (Color online) Vortex configuration in the double network at low normalized fields,  $H\ell^2/\phi_0 = 0.01, 0.02$  and  $0.03$ , for  $L/\ell = 5$ . The large loops are continuously occupied in the same way as in a simple square network while the small loops remain empty. Note the checkerboard distribution at  $H\ell^2/\phi_0 = 0.02$  corresponding to half filling of the large loops,  $H(L^2 - \ell^2)/\phi_0 \approx 0.5$ .

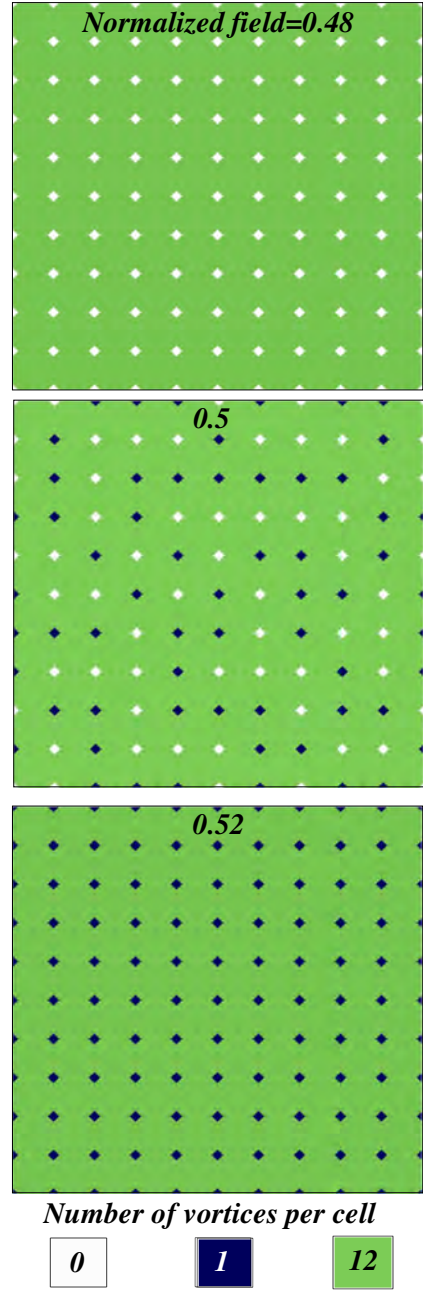


**Figure 6.** (Color online) Vortex configuration in the double network at relatively high fields  $H\ell^2/\phi_0 = 0.48, 0.5$  and  $0.52$  for  $L/\ell = 5$ . Note that in this narrow field range the number of vortices in the small loops increases sharply from zero to one.

## Appendix A – Kirchoff-law's matrices for the simple square network

The four  $M^2 \times M^2$  matrices  $\mathbf{K}^0$ ,  $\mathbf{K}^1$ ,  $\mathbf{K}^2$  and  $\mathbf{K}^3$  with periodic boundary conditions have the form

$$K_{\alpha\beta}^0 = \begin{cases} 1 & \text{if } \alpha = \beta \\ -1 & \text{if } \alpha = \beta + 1 \quad \text{and } \alpha \neq 0, M, 2M \dots M^2 - M \\ -1 & \text{if } \alpha = \beta - M + 1 \quad \text{and } \alpha = 0, M, 2M \dots M^2 - M \\ 0 & \text{otherwise} \end{cases};$$

$$K_{\alpha\beta}^1 = \begin{cases} 1 & \text{if } \alpha = \beta \\ -1 & \text{if } \alpha = \beta + M \quad \text{and } \alpha \geq M \\ -1 & \text{if } \alpha = \beta - M^2 + M \quad \text{and } \alpha < M \\ 0 & \text{otherwise} \end{cases};$$

$$K_{\alpha\beta}^2 = \begin{cases} 1 & \text{if } \alpha = \beta \\ -1 & \text{if } \alpha = \beta - 1 \quad \text{and } \alpha \neq M - 1, 2M - 1 \dots M^2 - 1 \\ -1 & \text{if } \alpha = \beta + M - 1 \quad \text{and } \alpha \neq M - 1, 2M - 1 \dots M^2 - 1 \\ 0 & \text{otherwise} \end{cases};$$

$$K_{\alpha\beta}^3 = \begin{cases} 1 & \text{if } \alpha = \beta \\ -1 & \text{if } \alpha = \beta - M \quad \text{and } \alpha < M^2 - M \\ -1 & \text{if } \alpha = \beta + M^2 - M \quad \text{and } \alpha \geq M^2 - M \\ 0 & \text{otherwise} \end{cases}.$$

This matrix uses Kirchoff's law to express the total current in a specific wire in a square network using the circular currents in two adjacent loops sharing the same wire. Using Eq. (15) one can get for example  $J_{0,M+1} = \tilde{J}_{M+1} - \tilde{J}_M$ ,  $J_{1,M+1} = \tilde{J}_{M+1} - \tilde{J}_1$ ,  $J_{1,M+1} = \tilde{J}_{M+1} - \tilde{J}_{M+2}$  and  $J_{1,M+1} = \tilde{J}_{M+1} - \tilde{J}_{2M+1}$ .

## Appendix B - Kirchoff-law's matrices for the double network

The matrices  $\mathbf{A}^\delta$ ,  $\mathbf{B}^\delta$ ,  $\mathbf{C}^\gamma$  and  $\mathbf{D}^\gamma$  with periodic boundary condition are evaluated as

$$A_{\alpha\beta}^1 = K_{\alpha\beta}^0; A_{\alpha\beta}^3 = K_{\alpha\beta}^1; A_{\alpha\beta}^5 = K_{\alpha\beta}^2; A_{\alpha\beta}^7 = K_{\alpha\beta}^3;$$

$$A_{\alpha\beta}^0 = A_{\alpha\beta}^2 = A_{\alpha\beta}^4 = A_{\alpha\beta}^6 = \begin{cases} 1 & \text{if } \alpha = \beta \\ 0 & \text{otherwise} \end{cases};$$

$$B_{\alpha\beta}^1 = B_{\alpha\beta}^3 = B_{\alpha\beta}^5 = B_{\alpha\beta}^7 = 0;$$

$$B_{\alpha\beta}^0 = \begin{cases} -1 & \text{if } \alpha = \beta - M & \text{and } \alpha < M^2 - M \\ -1 & \text{if } \alpha = \beta + M^2 - M & \text{and } \alpha \geq M^2 - M; \\ 0 & \text{otherwise} \end{cases};$$

$$B_{\alpha\beta}^2 = \begin{cases} -1 & \text{if } \alpha = \beta; \\ 0 & \text{otherwise} \end{cases};$$

$$B_{\alpha\beta}^4 = \begin{cases} -1 & \text{if } \alpha = \beta - 1 & \text{and } \alpha \neq M - 1, 2M - 1 \dots M^2 - 1 \\ -1 & \text{if } \alpha = \beta + M - 1 & \text{and } \alpha = M - 1, 2M - 1 \dots M^2 - 1; \\ 0 & \text{otherwise} \end{cases};$$

$$B_{\alpha\beta}^6 = \begin{cases} 0 & \text{if } \alpha = M^2 - 1 & \text{and } \beta = 0 \\ -1 & \text{if } \alpha = \beta - M - 1 & \text{and } \alpha < M^2 - M & \text{and } \alpha \neq M - 1, 2M - 1 \dots M^2 - M - 1 \\ -1 & \text{if } \alpha = \beta - 1 & \text{and } \alpha = M - 1, 2M - 1 \dots M^2 - M - 1 \\ -1 & \text{if } \alpha = \beta + M^2 - M - 1 & \text{and } \alpha \neq M^2 - 1 & \text{and } \alpha \neq M - 1, 2M - 1 \dots M^2 - M - 1 \\ 0 & \text{otherwise} \end{cases};$$

$$C_{\alpha\beta}^0 = \begin{cases} 0 & \text{if } \alpha = 0 & \text{and } \beta = M^2 - 1 \\ -1 & \text{if } \alpha = \beta - M^2 + M + 1 & \text{and } 0 < \alpha < M \\ -1 & \text{if } \alpha = \beta + 1 & \text{and } \alpha = M, 2M \dots M^2 - M & \text{and } \alpha \neq 0 \\ -1 & \text{if } \alpha = \beta + M + 1 & \text{and } \alpha > M - 1 & \text{and } \alpha \neq M, 2M \dots M^2 - M \\ 0 & \text{otherwise} \end{cases};$$

$$C_{\alpha\beta}^1 = \begin{cases} -1 & \text{if } \alpha = \beta - M^2 + M & \text{and } \alpha < M \\ -1 & \text{if } \alpha = \beta + M & \text{and } \alpha \geq M; \\ 0 & \text{otherwise} \end{cases};$$

$$C_{\alpha\beta}^2 = \begin{cases} -1 & \text{if } \alpha = \beta; \\ 0 & \text{otherwise} \end{cases};$$

$$C_{\alpha\beta}^3 = \begin{cases} -1 & \text{if } \alpha = \beta - M + 1 & \text{and } \alpha = 0, M \dots M^2 - M \\ -1 & \text{if } \alpha = \beta + 1 & \text{and } \alpha \neq \alpha = 0, M \dots M^2 - M; \\ 0 & \text{otherwise} \end{cases};$$

$$D_{\alpha\beta}^0 = D_{\alpha\beta}^1 = D_{\alpha\beta}^2 = D_{\alpha\beta}^3 = \begin{cases} 1 & \text{if } \alpha = \beta \\ 0 & \text{otherwise} \end{cases}.$$

These matrices use Kirchoff's law to express the total current in a specific wire in the double network using the circular currents in two adjacent loops sharing the same wire. Using Eq. (31) one can get, for example,

$$J_{1,M+1} = \tilde{J}_{M+1} - \tilde{J}_M \quad \text{and}$$

$$j_{2,M+1} = \tilde{j}_{M+1} - \tilde{j}_{M+1}.$$

**Acknowledgements** This work was supported by the Deutsche Forschungsgemeinschaft through the Deutsch Israelische Projektkooperation (DIP – Grant no. 563363). Y.Y. acknowledges support from the Israel Science Foundation. I.S. thanks the Israeli Ministry of Science and Technology for Eshkol scholarship.

## References

- 1 F. London, Phys. Rev. **74**, 562 (1948).
- 2 W. A. Little and R. D. Parks, Phys. Rev. Lett. **9**, 9 (1962).
- 3 An extensive literature on the superconducting networks made of Low- $T_c$  materials can be found in Proceedings of the NATO Workshop on Conference in Superconducting Networks, Delft, The Netherlands, 1987, ed. by Mooij, J. E. and Schon, G. B. J. [*Phys. B* **152**, No. 1&2 (1988)].
- 4 S. Alexander, Phys. Rev. B **27**, 1541 (1983).
- 5 P. G. de Gennes, C. R. Acad. Sci. Ser. B **292**, 9 (1981).
- 6 P. G. de Gennes, C. R. Acad. Sci. Ser. B **292**, 279 (1981).
- 7 H. J. Fink, A. Lopez, and R. Maynard, Phys. Rev. B **26**, 5237 (1982).
- 8 B. Pannetier, J. Chaussy, and R. Rammal, J. Phys. (Paris) Lett. **44**, L853 (1983).
- 9 B. Pannetier, J. Chaussy, R. Rammal, and J. C. Villegier, Phys. Rev. Lett. **53**, 1845 (1984).
- 10 R. Rammal, T. C. Lubensky, and G. Toulouse, Phys. Rev. B **27**, 2820 (1983).
- 11 J. Simonin, D. Rodrigues, and A. Lopez, Phys. Rev. Lett. **49**, 944 (1982).
- 12 A. Behrooz, M. J. Burns, D. Levine, B. Whitehead, and P. M. Chaikin, Phys. Rev. B **35**, 8396 (1987).
- 13 P. M. Chaikin, A. Behrooz, M. A. Itzler, C. Wilks, B. Whitehead, G. Grest, and D. Levine, Physica B **152**, 113 (1988).
- 14 M. A. Itzler, A. M. Behrooz, C. W. Wilks, R. Bojko, and P. M. Chaikin, Phys. Rev. B **42**, 8319 (1990).
- 15 H. Yoshino, T. Nogawa, and B. Kim, New J. Phys. **11**, 013010 (2009).
- 16 E. Granato, Phys. Rev. Lett. **101**, 027004 (2008).
- 17 S. J. Lee, B. Kim, and J. Lee, Physica A **315**, 314 (2002).
- 18 I. Sochnikov, A. Shaulov, Y. Yeshurun, G. Logvenov, and I. Bozovic, Nature Nanotech. **5**, 516 (2010).
- 19 I. Sochnikov, A. Shaulov, Y. Yeshurun, G. Logvenov, and I. Bozovic, Phys. Rev. B **82**, 094513 (2010).
- 20 C. Reichhardt, C. J. O. Reichhardt, and A. R. Bishop, Physica C **460**, 1178 (2007).
- 21 M. Tinkham, *Introduction to Superconductivity* (McGraw-Hill, New York, 1996).
- 22 V. G. Kogan, J. R. Clem, and R. G. Mints, Phys. Rev. B **69**, 064516 (2004).
- 23 E. H. Brandt and J. R. Clem, Phys. Rev. B **69**, 184509 (2004).
- 24 S. Teitel and C. Jayaprakash, Phys. Rev. Lett. **51**, 1999 (1983).
- 25 T. C. Halsey, Phys. Rev. B **31**, 5728 (1985).
- 26 Note that in the analytical solution, due to its mean-field nature, we require that the average current in the network vanishes, while in the numerical simulations we require current conservation at every node.
- 27 The breaks around the middle of the steps result from competition in

occupation of large and small loops. This competition occurs in the field range where the energy cost to insert a vortex into a small loop or a large loop is similar.

28 A. M. Chang, H. D. Hallen, L. Harriott, H. F. Hess, H. L. Kao, J. Kwo, R. E. Miller, R. Wolfe, J. van der Ziel, and T. Y. Chang, *Appl. Phys. Lett.* **61**, 1974 (1992).

29 H. D. Hallen, R. Seshadri, A. M. Chang, R. E. Miller, L. N. Pfeiffer, K. W. West, C. A. Murray, and H. F. Hess, *Phys. Rev. Lett.* **71**, 3007 (1993).

30 L. N. Vu, M. S. Wistrom, and D. J. Van Harlingen, *Appl. Phys. Lett.* **63**, 1693 (1993).

31 K. Runge and B. Pannetier, *Europhys. Lett.* **24**, 737 (1993).

32 E. Serret, P. Butaud, and B. Pannetier, *Europhys. Lett.* **59**, 225 (2002).

33 A. Bezryadin, Y. N. Ovchinnikov, and B. Pannetier, *Phys. Rev. B* **53**, 8553 (1996).

34 C. Nisoli, J. Li, X. Ke, D. Garand, P. Schiffer, and V. H. Crespi, *Phys. Rev. Lett.* **105**, 047205 (2010).

35 C. Nisoli, R. Wang, J. Li, W. F. McConville, P. E. Lammert, P. Schiffer, and V. H. Crespi, *Phys. Rev. Lett.* **98**, 217203 (2007).

36 R. F. Wang, C. Nisoli, R. S. Freitas, J. Li, W. McConville, B. J. Cooley, M. S. Lund, N. Samarth, C. Leighton, V. H. Crespi, and P. Schiffer, *Nature* **439**, 303 (2006).

### 3.2 UNCORRELATED BEHAVIOR OF FLUXOIDS IN SUPERCONDUCTING DOUBLE NETWORKS



# Uncorrelated behavior of fluxoids in superconducting double networks

I. Sochnikov<sup>1</sup>, I. Božović<sup>2</sup>, A. Shaulov<sup>1</sup> and Y. Yeshurun<sup>1</sup>

<sup>1</sup>*Department of Physics, Institute of Superconductivity and Institute of Nanotechnology and Advanced Materials, Bar-Ilan University, Ramat-Gan 52900, Israel*

<sup>2</sup>*Brookhaven National Laboratory, Upton, New York 11973-5000, USA*

We study the effect of magnetic fields on the resistance,  $R$ , of a superconducting  $\text{La}_{1.84}\text{Sr}_{0.16}\text{CuO}_4$  film patterned into a 'double' network comprising nano-size square loops having their vertexes linked by relatively long wires. The results are compared with those obtained in a regular network of square loops of the same size. Both networks exhibit periodic dependence of  $R$  on the ratio  $\Phi/\Phi_0$  between the flux penetrating a loop and the superconducting flux quantum. However, while the regular network exhibit features characteristic of collective behavior of the loops, the double network exhibits a single loop behavior. This observation indicates uncorrelated arrangements of fluxoids in the double network, in agreement with a recent theoretical prediction.

A variety of superconducting networks have been studied, both theoretically and experimentally, aiming at revealing correlated behavior of fluxoids in such networks<sup>1-14</sup>. The foundation of these studies traces back to the fluxoid quantization work of Little and Parks<sup>15-17</sup> who demonstrated in magnetoresistance measurements the theoretical prediction of F. London<sup>18</sup> showing that the deviation of the magnetic flux through a superconducting loop from an integral number of flux quanta must be compensated by a circulating current, satisfying the equation

$$\frac{2\lambda^2}{c\Phi_0} \oint j \cdot d\ell = n - \frac{\Phi}{\Phi_0},$$

where the line integral is taken around the loop,  $\lambda$  is the penetration depth,  $\Phi$  is the magnetic flux penetrating the loop, and  $\Phi_0$  is the superconducting flux quantum. In a network, the above equation must be satisfied for any and every loop. In addition, the arrangements of fluxoids on the underlying network must fulfill the

requirement of minimum energy. These two requirements give rise to correlated arrangements of fluxoids in periodic networks, the most famous one being the checkerboard arrangement of fluxoids in a regular square network<sup>8, 11, 14, 19</sup>, manifested by secondary dips of the magneto-resistance at half integer values of  $\Phi/\Phi_0$ .

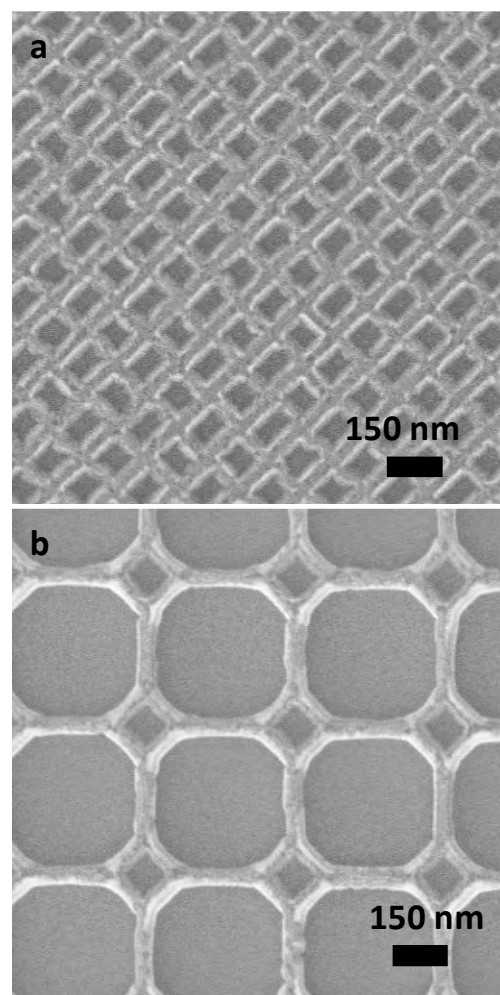
Recently, we fabricated a novel type of superconducting network<sup>20, 21</sup> made by connecting the vertexes of small square loops with relatively long wires, forming two interlaced sub-networks of small and large loops. The motivation for designing such a network was to create an array of decoupled small loops that behave like isolated loops. In a previous manuscript<sup>22</sup> we theoretically simulated the behavior of this unique network in a perpendicular magnetic field. The simulations showed that as the field increases, the vortex population in the small loops grows in steps, resembling the behavior of an ensemble of nearly decoupled loops. In

addition, the loop energy  $E$  was found to be a periodic function of the ratio  $\Phi/\Phi_0$ , with a waveform similar to that of a single isolated loop. Features indicative of collective behavior of the loops, e.g. finite slope  $dE/dH$  at  $H=0$ , downward cusps in  $E(H)$  and pronounced secondary dips at half integer values of  $\Phi/\Phi_0$ , which are found in a regular square network, are all absent in the case of a double network. The purpose of the present work was to confirm experimentally the predictions of these simulations. For this purpose we fabricated a regular square network and a double network having square loops of the same size, and compared their magnetoresistance behavior.

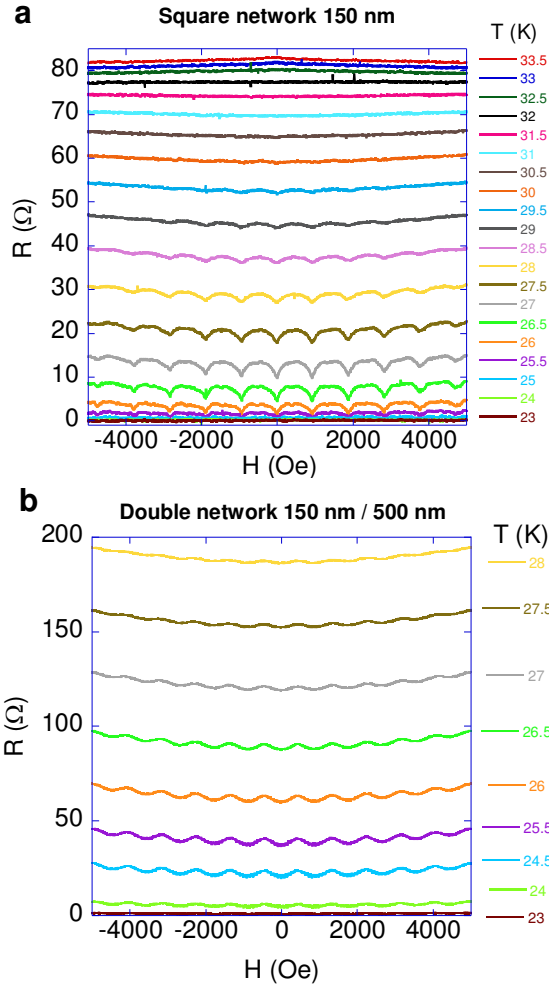
Molecular Beam Epitaxially grown  $\text{La}_{1.84}\text{Sr}_{0.16}\text{CuO}_4$  high- $T_c$  superconducting films (nominally 26 nm thick) were patterned into a regular square network of  $150 \times 150 \text{ nm}^2$  loops, and a double network consisting of square loops of the same size having their vertexes connected by  $\sim 300 \text{ nm}$  long wires, as shown in Figure 1. The wire width in both networks was  $\sim 45 \text{ nm}$ . Resistance measurements were performed using a Quantum Design PPMS<sup>®</sup> with bias current of 100 nA. Magnetic fields were applied normal to the film surface (a-b crystallographic plane), keeping a constant temperature in the range 20–40 K with stability of few mK.

Figure 2 shows the magnetoresistance per unit cell,  $R(H)$ , for the square network (left panel) and for the double network (right panel) as a function of the applied magnetic field  $H$ , measured at the indicated temperatures. Both networks exhibit periodic oscillations of  $R$  vs.  $H$  with the same period of  $\sim 900 \text{ Oe}$ ,

corresponding approximately to  $\Phi_0/A$  where  $A = 150 \times 150 \text{ nm}^2$  is the area of a single square loop. However, the oscillations waveform,  $R(H)$ , for the two networks is evidently different. While the regular network exhibits features characteristic of collective behavior of the loops, e.g. finite slope  $dR/dH$  at  $H=0$  and downward cusps, the double network behavior resembles that of a single loop, exhibiting zero slope  $dR/dH$  at  $H=0$  and upward cusps.



**Figure 1.** Scanning electron microscopy image of the square (a) and the double (b) networks patterned in  $\text{La}_{1.84}\text{Sr}_{0.16}\text{CuO}_4$  high temperature film. The brighter elements are the superconducting wires composing the networks.



**Figure 2.** (Color on line) Resistance per network unit cell as a function of magnetic field measured at different temperatures in the square (a) and the double (b) networks.

A closer look at the magnetoresistance oscillations reveals fine structures in the magnetoresistance of the both networks. In Figure 3 we zoom on the magnetoresistance data of each network at a temperature  $T/T_c \sim 0.85$ . The square network (Figure 3a) exhibits pronounced secondary dips at half integer values of  $\Phi/\Phi_0$  (see inset), corresponding to the checkerboard arrangement of vortices in this network<sup>8, 11, 14, 19</sup>. In the double network these secondary dips are absent; however, as shown in the inset to Figure 3b, oscillations of a period  $\sim 80$  Oe, corresponding to the sub-network of the

large loops, are superimposed on the longer period oscillations, shown as a parabolic-like 'envelope' in the inset to Figure 3b, originating from the sub-network of the small square loops. These small oscillations, which are more pronounced at the minima of  $R(H)$ , exhibit downwards cusps characteristics of the square network behavior originating from the large loops.

Figure 2 shows that in both networks the oscillatory behavior of  $R$  is limited to a temperature range roughly between  $\sim 22$  and  $\sim 31$  K, resulting in non-monotonic variation of the oscillations amplitude  $\Delta R$  with the temperature, as summarized by the squares in Figure 4. This figure also shows the temperature dependence of the network resistance per unit cell  $R(T)$  (circles), as well as  $dR/dT$  (diamonds), for the regular and the double networks. Evidently,  $R(T)$  of the double network is significantly larger as it includes the resistance of the long wires composing the large loops. Nevertheless, the unit cell amplitude of the oscillations,  $\Delta R$ , for both networks are similar, indicating that it cannot distinguish between correlated and uncorrelated behavior of fluxoids in networks of loops of the same size.

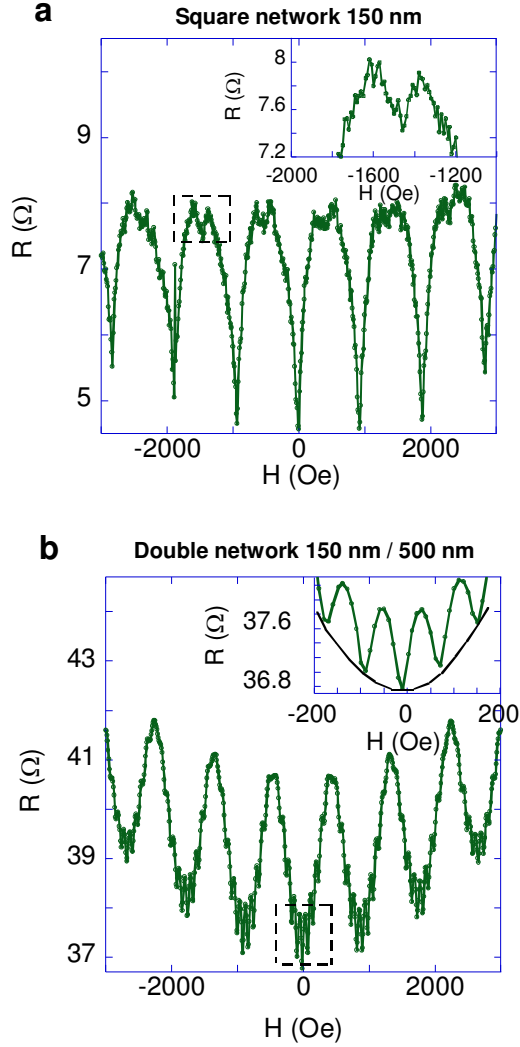


**Figure 3.** (Color on line) Resistance per network unit cell as a function of magnetic field measured in the square (a) and the double (b) networks at 26.5 and 25.5 K respectively. The insets zoom on the regions marked by dashed lines. Inset (a) shows a secondary dip at half period corresponding to checkerboard arrangement of vortices in the square network. Inset (b) shows the magnetoresistance oscillations corresponding to the large loops of the double network. The solid line in inset (b) is a guide for the eye showing parabolic-like 'envelope' corresponding to the small loops.

By passing we note that no correspondence is found between  $\Delta R$  and  $dR/dT$ , see Figure 4. Such a

correspondence should follow if we assume that  $\Delta R$  results from periodic changes in the critical temperature  $T_c$ , as in the analysis of the Little-Parks experiment<sup>15-17</sup>. More remarkable deviation from this analysis is found in the magnitude of  $\Delta R$ . Contrary to classical superconductors, the predicted changes in the critical temperature,  $\Delta T_c \propto T_c (\xi_0 / r)^2$ , in high- $T_c$  materials are extremely small because of the short coherence length  $\xi_0$ , failing to explain the large amplitude of the oscillations<sup>23, 24</sup>. In previous papers<sup>20, 21</sup> we developed a model for a single, isolated loop which explains the details of the double network magnetoresistance, including the large oscillations amplitude and its temperature dependence. This model ascribes the magnetoresistance oscillations in high- $T_c$  superconductors to the periodic changes in the interaction between thermally-excited moving vortices and the oscillating persistent current induced in the loops. The model explains well the magnitude of  $\Delta R$  as well as its temperature dependence<sup>20, 21</sup>.

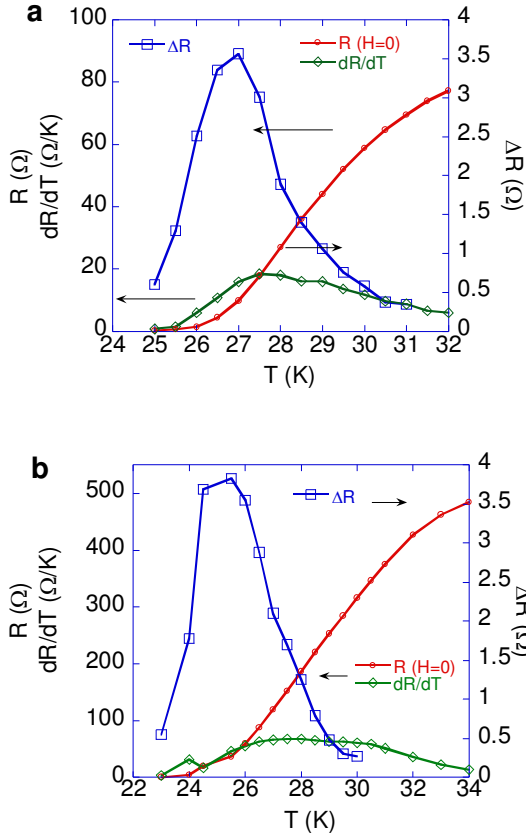


**Figure 4.** (Color on line) Resistance,  $R$ , measured at zero magnetic field (circles), amplitude of the magnetoresistance oscillations (squares), and the derivative  $dR/dT$  (diamonds) as a function of temperature in the square (a) and the double networks (b). Solid lines are guide to the eye.

In summary, we observed different fluxoid quantization effects in a superconducting double network as compared to a regular, square network. The regular network exhibit correlated behavior of the fluxoids, which is manifested by e.g. finite slope  $dR/dH$  at  $H=0$ , downward cusps and secondary dips at half integer values of  $\Phi/\Phi_0$ . In contrast, the sub-network of the small square loops in the double network exhibits a single loop behavior lacking all these features. This observation indicates uncorrelated arrangements of fluxoids in

the sub-network of the small loops, in agreement with our recent theoretical prediction. Experimentally, the double network has an advantage over a single loop as it allows application of larger currents, thus improving the signal to noise ratio. In addition, measurements on large number of loops in the network average effects of inhomogeneity and size distribution, allowing more precise studies of e.g. recent theoretical predictions of 'exotic' flux periodicity in unconventional superconductors<sup>25-32</sup>.

**Acknowledgements** We thank A. Sharoni for providing access to the measurement system. The work at Bar-Ilan University was supported by the Deutsche Forschungsgemeinschaft through the Deutsch Israelische Projektkooperation (grant no. 563363). Y.Y. acknowledges support of the Israel Science Foundation. I.S. thanks the Israeli Ministry of Science and Technology for Eshkol scholarship. The work at BNL was supported by US DOE contract MA-509-MACA.

## References

- 1 P. G. de Gennes, C. R. Acad. Sci. Ser. B **292**, 9 (1981).
- 2 P. G. de Gennes, C. R. Acad. Sci. Ser. B **292**, 279 (1981).
- 3 J. Simonin, D. Rodrigues, and A. Lopez, Phys. Rev. Lett. **49**, 944 (1982).
- 4 S. Alexander, Phys. Rev. B **27**, 1541 (1983).
- 5 B. Pannetier, J. Chaussy, and R. Rammal, J. Phys. (Paris) Lett. **44**, L853 (1983).
- 6 R. Rammal, T. C. Lubensky, and G. Toulouse, Phys. Rev. B **27**, 2820 (1983).
- 7 B. Pannetier, J. Chaussy, R. Rammal, and J. C. Villegier, Phys. Rev. Lett. **53**, 1845 (1984).

- 8 A. Behrooz, M. J. Burns, D. Levine, B. Whitehead, and P. M. Chaikin, Phys. Rev. B **35**, 8396 (1987).
- 9 F. Nori, Q. Niu, E. Fradkin, and S.-J. Chang, Phys. Rev. B **36**, 8338 (1987).
- 10 P. M. Chaikin, A. Behrooz, M. A. Itzler, C. Wilks, B. Whitehead, G. Grest, and D. Levine, Physica B **152**, 113 (1988).
- 11 M. A. Itzler, A. M. Behrooz, C. W. Wilks, R. Bojko, and P. M. Chaikin, Phys. Rev. B **42**, 8319 (1990).
- 12 E. Granato, Phys. Rev. Lett. **101**, 027004 (2008).
- 13 H. Yoshino, T. Nogawa, and B. Kim, New J. Phys. **11**, 013010 (2009).
- 14 An extensive literature on the superconducting networks made of Low- $T_c$  materials can be found in Proceedings of the NATO Workshop on Conference in Superconducting Networks, Delft, The Netherlands, 1987, ed. by Mooij, J. E. and Schon, G. B. J. [*Phys. B* **152**, No. 1&2 (1988)].
- 15 W. A. Little and R. D. Parks, Phys. Rev. Lett. **9**, 9 (1962).
- 16 R. D. Parks and W. A. Little, Phys. Rev. **133**, A97 (1964).
- 17 M. Tinkham, *Introduction to Superconductivity* (McGraw-Hill, New York, 1996).
- 18 F. London, Phys. Rev. **74**, 562 (1948).
- 19 C. Reichhardt, C. J. O. Reichhardt, and A. R. Bishop, Physica C **460**, 1178 (2007).
- 20 I. Sochnikov, A. Shaulov, Y. Yeshurun, G. Logvenov, and I. Bozovic, Nature Nanotech. **5**, 516 (2010).
- 21 I. Sochnikov, A. Shaulov, Y. Yeshurun, G. Logvenov, and I. Bozovic, Phys. Rev. B **82**, 094513 (2010).
- 22 I. Sochnikov, Y. Shokef, A. Shaulov, and Y. Yeshurun, unpublished.
- 23 F. Carillo, G. Papari, D. Stornaiuolo, D. Born, D. Montemurro, P. Pingue, F. Beltram, and F. Tafuri, Phys. Rev. B **81**, 054505.
- 24 P. L. Gammel, P. A. Polakos, C. E. Rice, L. R. Harriott, and D. J. Bishop, Phys. Rev. B **41**, 2593 (1990).
- 25 Y. S. Barash, Phys. Rev. Lett. **100**, 177003 (2008).
- 26 V. Juricic, I. F. Herbut, and Z. Tesanovic, Phys. Rev. Lett. **100**, 187006 (2008).
- 27 F. Loder, A. P. Kampf, T. Kopp, J. Mannhart, C. W. Schneider, and Y. S. Barash, Nat. Phys. **4**, 112 (2008).
- 28 C. Qiu and T. Qian, Phys. Rev. B **77**, 174517 (2008).
- 29 V. Vakaryuk, Phys. Rev. Lett. **101**, 167002 (2008).
- 30 T.-C. Wei and P. M. Goldbart, Phys. Rev. B **77**, 224512 (2008).
- 31 J.-X. Zhu and H. T. Quan, Phys. Rev. B **81**, 054521 (2010).
- 32 E. Berg, E. Fradkin, and S. A. Kivelson, Nature Phys. **5**, 830 (2009).

### 3.3 LARGE OSCILLATIONS OF THE MAGNETORESISTANCE IN NANO-PATTERNED HIGH-TEMPERATURE SUPERCONDUCTING FILMS: EXPERIMENTAL RESULTS AND THEORETICAL MODEL



# Large oscillations of the magnetoresistance in nanopatterned high-temperature superconducting films

Ilya Sochnikov<sup>1\*</sup>, Avner Shaulov<sup>1</sup>, Yosef Yeshurun<sup>1</sup>, Gennady Logvenov<sup>2</sup> and Ivan Božović<sup>2</sup>

Measurements on nanoscale structures constructed from high-temperature superconductors are expected to shed light on the origin of superconductivity in these materials<sup>1–7</sup>. To date, loops made from these compounds have had sizes of the order of hundreds of nanometres<sup>8–11</sup>. Here, we report the results of measurements on loops of  $\text{La}_{1.84}\text{Sr}_{0.16}\text{CuO}_4$ , a high-temperature superconductor that loses its resistance to electric currents when cooled below  $\sim 38$  K, with dimensions down to tens of nanometres. We observe oscillations in the resistance of the loops as a function of the magnetic flux through the loops. The oscillations have a period of  $h/2e$ , and their amplitude is much larger than the amplitude of the resistance oscillations expected from the Little–Parks effect<sup>12,13</sup>. Moreover, unlike Little–Parks oscillations, which are caused by periodic changes in the superconducting transition temperature, the oscillations we observe are caused by periodic changes in the interaction between thermally excited moving vortices and the oscillating persistent current induced in the loops. However, despite the enhanced amplitude of these oscillations, we have not detected oscillations with a period of  $h/e$ , as recently predicted for nanoscale loops of superconductors with *d*-wave symmetry<sup>1–6</sup>, or with a period of  $h/4e$ , as predicted for superconductors that exhibit stripes<sup>7</sup>.

Molecular beam epitaxy (MBE) was used to synthesize 26-nm-thick films of optimally doped  $\text{La}_{1.84}\text{Sr}_{0.16}\text{CuO}_4$  on single-crystal  $\text{LaSrAlO}_4$  substrates polished perpendicular to the (001) direction<sup>10,11</sup>. The films were characterized *in situ* by reflection high-energy electron diffraction (RHEED), and *ex situ* by X-ray diffraction, atomic force microscopy and mutual inductance measurements. Subsequently, as detailed in the Methods, the films were patterned into a network of ‘small’ square loops, the sides of which were between 75 and 150 nm long, separated by ‘large’ square loops with sides of length 500 nm; the width of all features was  $\sim 25$  nm. A typical network of small and large loops is shown in Fig. 1. The length and width of the small squares were almost an order of magnitude smaller than those in previously studied high- $T_c$  networks and rings<sup>8–11</sup>.

Figure 2 shows the magnetoresistance of the 150/500-nm network measured at  $T = 28.4$  K in a magnetic field applied normal to the film surface (and to the *a*–*b* crystallographic plane). The measured magnetoresistance exhibits large oscillations superimposed on a parabolic-like background. The period of these oscillations,  $H_0 \approx 950$  Oe, corresponds to the magnetic flux quantum,  $\Phi_0 = h/2e = AH_0$ , where  $h$  is Planck’s constant,  $e$  the electron charge and  $A$  the area of the small loop. Oscillations with a period of  $\sim 80$  Oe, which correspond to the large loops, are also observed, but their amplitude is too small to be noticed on the scale of Fig. 2.

The measured magnetoresistance, normalized to the normal-state resistance at  $T = 30.2$  K,  $R_n = 36 \Omega$ , is presented in Fig. 3a as a function of the temperature  $T$  and the applied magnetic field  $H$ . Periodic oscillations of  $R$  are observed for temperatures between 26 and 30.2 K. The temperature dependence of the amplitude of these oscillations is described by the diamonds in the inset to Fig. 2. Note that the field range in Fig. 3 is limited to low fields where the parabolic-like background is insignificant.

It is tempting to interpret these data as Little–Parks oscillations<sup>8,12–17</sup> originating from the periodic dependence of the critical temperature  $T_c$  on the magnetic field. However, the amplitude of the oscillations seen in Fig. 2 is much too large. Taking a typical value<sup>18</sup> for the coherence length in  $\text{La}_{1.84}\text{Sr}_{0.16}\text{CuO}_4$

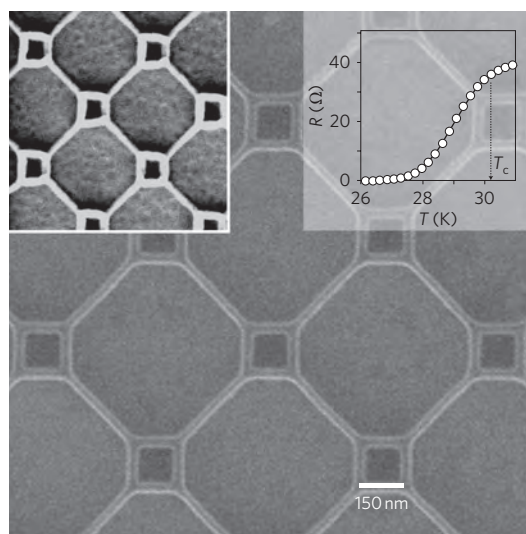


**Figure 1 | Patterned superconducting film.** Main panel: scanning electron microscope (SEM) image of a  $\text{La}_{1.84}\text{Sr}_{0.16}\text{CuO}_4$  superconducting film covered with a patterned layer of poly(methyl methacrylate) (PMMA) resist (thin lines with bright edges). The left inset shows an SEM image of a part of the resulting superconducting network ( $150 \times 150\text{-nm}^2$  loops separated by  $500 \times 500\text{-nm}^2$  loops) after the uncovered parts of the film were removed by ion milling. The right inset shows the measured (white circles) temperature dependence of the network ( $30 \times 30 \mu\text{m}^2$ ) resistance in zero magnetic field near the superconducting transition; the current is  $1 \mu\text{A}$ . In the patterned film the onset temperature for superconductivity is 30.2 K and the transition width is  $\sim 2$  K (compared with 38 K and  $\sim 0.5$  K for the as-grown film).

<sup>1</sup>Department of Physics, Institute of Superconductivity and Institute of Nanotechnology and Advanced Materials, Bar-Ilan University, Ramat-Gan 52900, Israel, <sup>2</sup>Brookhaven National Laboratory, Upton, New York 11973-5000, USA. \*e-mail: ph89@mail.biu.ac.il

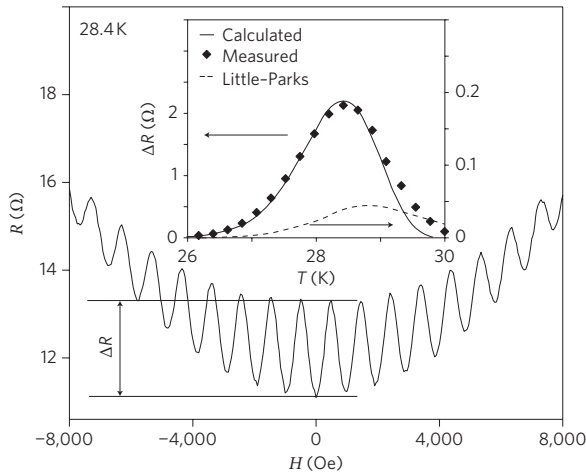


**Figure 2 | Magnetoresistance oscillations.** Resistance of the  $\text{La}_{1.84}\text{Sr}_{0.16}\text{CuO}_4$  network shown in Fig. 1 as a function of applied magnetic field, measured at 28.4 K. The oscillations are superimposed on a parabolic-like background. The amplitude of the oscillations,  $\Delta R$ , is well defined at low fields. Inset:  $\Delta R$  as a function of temperature; the solid line is a theoretical fit based on equation (5). The dashed line is an upper limit for the amplitude of resistance oscillations calculated for the Little-Parks effect (right axis; note that the scale on this axis is expanded tenfold).

of  $\xi_0 = 2$  nm, the measured critical temperature at zero field  $T_c^{\text{onset}} = 30.2$  K, and the loop effective radius  $r = a/\sqrt{\pi} = 83.5$  nm ( $a = 150$  nm is the loop side length), one would expect to find oscillations in  $T_c$  with an amplitude  $\Delta T_c = 0.14 T_c (\xi_0/r)^2 \approx 2.4$  mK (refs 8,12,13,15,16). This value of  $\Delta T_c$  yields an upper limit to the resistance amplitude,  $\Delta R = \Delta T_c (dR/dT)$ , depicted by the dashed line in the inset to Fig. 2, the maximum value of which is a factor of  $\sim 50$  smaller than the measurement from our experiment.

Given that the Little-Parks effect cannot explain the observed large magnetoresistance oscillations, we suggest that the origin of this phenomenon is the drastically modified vortex dynamics in the patterned film. Although in continuous films the activation energy for vortex creep usually decreases monotonically with the applied magnetic field<sup>19–21</sup>, in nanopatterned films this activation energy becomes oscillatory, as moving vortices interact with the current induced in the nanoloops, which is a periodic function of the field strength. Periodicity of the induced current results directly from the fluxoid quantization<sup>12,13,15,22</sup>, which is also the source of the Little-Parks effect. The fluxoid, consisting of the flux induced by the supercurrent in the loop and by the external magnetic field, is characterized by the quantum vorticity number  $N$ , which defines the energy state of the superconducting loop. In the lowest energy state,  $N$  is equal to  $H/H_0$  rounded to the nearest integer<sup>15,16</sup>.

Thermal excitation of vortices causes fluxoid transitions from the equilibrium quantum state  $N$  to a higher energy state. Other groups<sup>23,24</sup>, in their analysis of magnetic scanning microscope measurements of a mesoscopic superconducting ring, have calculated the energies  $\Delta E_{\text{in}}^{\pm}$  and  $\Delta E_{\text{out}}^{\pm}$  required to create a vortex (+) or an antivortex (–) and carry it into or outside of the superconducting loop, respectively:

$$\Delta E_{\text{in}}^{\pm} = \Delta E_{\text{out}}^{\pm} = E_v + E_0 [\pm(N - H/H_0) + 1/4] \quad (1)$$

The first term in equation (1),  $E_v = (\Phi_0^2/(8\pi^2 \Lambda(T))) \ln(2w/(\pi\xi(T)))$ , is field-independent and represents the energy needed for the creation of the vortex/antivortex in the superconducting wire. Here,  $w$  is the wire width,  $\xi(T) = 0.74\xi_0(1-T/T_c)^{-1/2}$  is the Ginzburg-Landau coherence length<sup>16</sup>, and  $\Lambda(T) = 2\lambda(T)^2/d$  is the Pearl

penetration depth<sup>16,25</sup> in a film of thickness  $d$  and with a London penetration depth  $\lambda(T) = \lambda_0(1-T/T_c)^{-1/2}$ . The second term in equation (1) is periodic with the field, expressing the interaction of a vortex or an antivortex with the current associated with the fluxoid in terms of the energy,  $E_0 = (\Phi_0^2/(8\pi^2 \Lambda(T)))(w/a)$ . Note that equation (1) is valid in the limit of large penetration depth,  $\Lambda \gg w$ , and for narrow rings with widths much smaller than the radius of the loops,  $r$ . Nevertheless, the width has to be sufficiently large to accommodate a vortex<sup>26</sup>. The quantized values of  $N$  lead to periodically oscillating values of  $(N - H/H_0)$ .

In the following we consider fluxoid transitions accomplished by only one vortex or antivortex entry and exit. Thermodynamic averaging of these four types of excitation energies,  $\Delta E_i$ , yields an effective potential barrier  $\Delta E_{\text{eff}}$ :

$$\Delta E_{\text{eff}} = \sum \Delta E_i e^{-\Delta E_i/k_B T} / \sum e^{-\Delta E_i/k_B T} \quad (2)$$

By inserting equation (1) for  $\Delta E_i$ , one obtains

$$\Delta E_{\text{eff}} \approx (E_v + E_0/4) - E_0^2(N - H/H_0)^2/k_B T \quad (3)$$

which includes a field-independent term and a term periodic with the field.

We derive the magnetoresistance by applying Tinkham's approach in analysing the broadening of the resistive transition in high- $T_c$  superconductors<sup>20</sup>. Replacing the activation energy in his equations with  $\Delta E_{\text{eff}}$  given in equation (3), yields

$$\frac{R}{R_n} = \left[ I_0 \left( \frac{\Delta E_{\text{eff}}}{2k_B T} \right) \right]^{-2} \quad (4)$$

where  $I_0$  is the zero-order modified Bessel function of the first kind. Equation (4) describes a periodic function with period  $H_0 = \Phi_0/A$  and temperature-dependent amplitude

$$\Delta R \approx R_n \left( \frac{E_0}{2k_B T} \right)^2 \frac{I_1(\alpha)}{(I_0(\alpha))^3} \quad (5)$$

where  $\alpha = (E_v + E_0/4)/(2k_B T)$ , and  $I_1$  is the first-order modified Bessel function of the first kind. Note that  $E_v$  and  $E_0$  are a function of the two length scales,  $\lambda_0$  and  $\xi_0$ , which can be used as fitting parameters for the measured temperature dependence of the amplitude of the oscillations. The fit shown by the solid line in the inset to Fig. 2 yields  $\lambda_0 = 750$  nm and  $\xi_0 = 2.4$  nm. Note that these values of  $\lambda_0$  and  $\xi_0$  may be influenced by the lithographic process, which may cause damage in regions near the surfaces, thus making the effective thickness and width significantly smaller than the nominal values.

Figure 3b presents calculation of  $R(H,T)/R_n$  based on equation (4) and using the above values for  $\lambda_0$  and  $\xi_0$ . The calculated  $R(H,T)$  is similar to the experimental results (Fig. 3a) in low magnetic fields where the parabolic-like background on which the oscillations are superimposed is negligible (see Fig. 2). Extension of this analysis to also describe the background arising at higher fields requires modification of equation (1) to include field-dependent terms of higher order<sup>24</sup>. Comparing the details of the experimental and calculated waveforms shown in Fig. 3a and b, one notices that the experimental resistance oscillations look rather sinusoidal, whereas the calculated results exhibit a 'scallop' shape with sharper curvature at the top than at the bottom. This difference is most likely related to the distribution of the size of the fabricated loops.

We note that equation (4) can also explain the broadening of  $R(H=0,T)$  in the patterned film as shown in the inset to Fig. 1. In zero field,  $R$  depends only on the non-periodic part,  $E_v$ , in

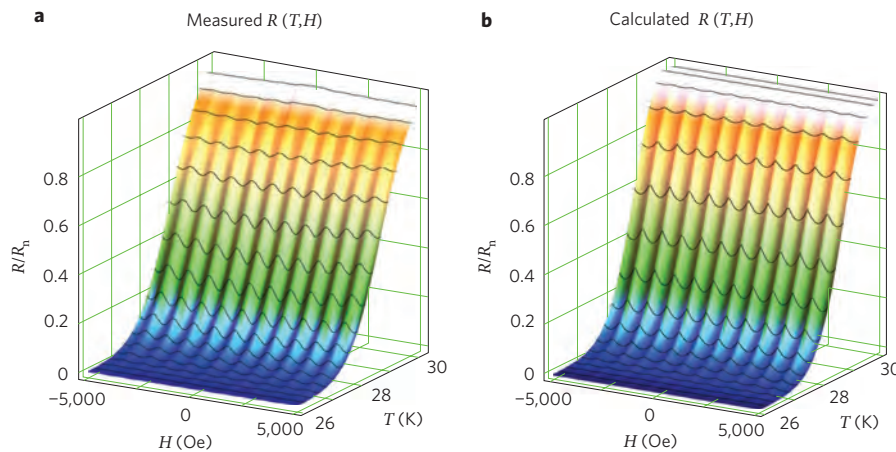


**Figure 3 | Comparison of measured and calculated magnetoresistance oscillations.** **a**, Measured normalized resistance of the network shown in Fig. 1 as a function of the applied magnetic field and temperature. **b**, Normalized resistance calculated using equation (4) for wire width  $w = 25$  nm, film thickness  $d = 26$  nm, zero-temperature penetration depth  $\lambda_0 = 750$  nm and coherence length  $\xi_0 = 2.4$  nm. The calculation was made for circular loops of the same area as the square loops: that is, with an effective radius  $r = a/\sqrt{\pi} = 83.5$  nm ( $a = 150$  nm is the actual loop side length). The values for  $\lambda_0$  and  $\xi_0$  are obtained from the fit of equation (5) to the temperature dependence of the amplitude shown in the inset to Fig. 2. The colour changes from blue to green to orange to white as the resistance increases from zero to the normal-state value.

equation (3), which decreases as the wire width  $w$  is reduced. This allows for easier excitations of vortices and antivortices at lower temperatures, giving rise to non-zero resistance.

In general, magnetoresistance oscillations originate from both the Little–Parks effect and the modified vortex dynamics reported here. However, in high- $T_c$  superconductors, the contribution of the Little–Parks effect is relatively small because of the short coherence length<sup>21</sup>, and the contribution of the vortex dynamics is large because of strong thermal fluctuations<sup>27</sup>. It should be mentioned that large-amplitude magnetoresistance oscillations have previously been observed in a different nanostructure made of two low- $T_c$  superconducting nanowires. These oscillations were attributed to the field-driven modulation of barrier heights for phase slips<sup>28,29</sup>.

As that interpretation relates to the one-dimensional superconducting wires ( $w < \xi$ ), it may not be directly applicable to our high- $T_c$  loops in which the wire width is an order of magnitude larger than the coherence length.

Recent theoretical studies<sup>1–6</sup> predicted that the magnetoresistance in high- $T_c$  superconducting nanorings with a  $d$ -wave order-parameter should show an additional component with flux periodicity  $h/e$ . This component is expected even for loops of length scales larger than the coherence length. Figure 4 shows the Fourier transform analysis of magnetoresistance oscillations for both the 75- and 150-nm loops. Evidently, despite the enhanced magnetoresistance oscillations observed in our experiment, a periodicity of  $h/e$  is not observed, even in the 75-nm loops (which are the smallest prepared so far with high- $T_c$  superconductors).

More recently, a periodicity of  $h/4e$  (corresponding to half a quantum of flux) was predicted for striped high- $T_c$  superconductors, replacing the usual periodicity of  $h/2e$  (which corresponds to a quantum of flux<sup>7</sup>). As is evident from Fig. 4, in our optimally doped  $\text{La}_{1.84}\text{Sr}_{0.16}\text{CuO}_4$  films, the  $h/4e$  flux periodicity does not replace the  $h/2e$  periodicity, but only appears as its second harmonic.

In summary, the resistance of a network of nanoscale loops of  $\text{La}_{1.84}\text{Sr}_{0.16}\text{CuO}_4$  oscillates as a function of the magnetic flux through the loops in a way that cannot be explained by the classic Little–Parks effect. These oscillations are rather attributed to the field-driven modulation of the height of the energy barrier to vortex motion. The absence of  $h/e$  and  $h/4e$  periodicities in these oscillations is at variance with some recent theoretical predictions<sup>1–7</sup> for this type of system. However, efforts to discover such periodicities should continue by extending this work to higher and lower doping across the entire phase diagram.

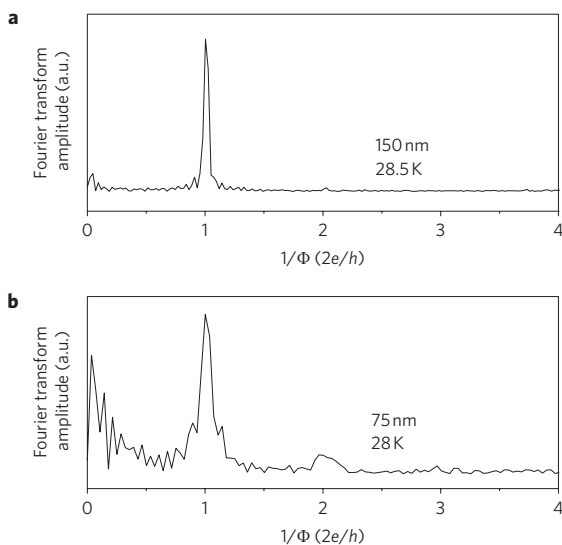


**Figure 4 | Periodicity of the magnetoresistance oscillations.** **a, b**, Amplitude of the Fourier transform of the magnetoresistance oscillations versus inverse magnetic flux in the 150-nm loops at 28.5 K (**a**) and the 75-nm loops at 28 K (**b**). The  $h/2e$  periodicity is apparent, but the  $h/e$  periodicity is absent, and the  $h/4e$  periodicity appears as the second harmonic of the  $h/2e$  fundamental component.

### Methods

The  $\text{La}_{1.84}\text{Sr}_{0.16}\text{CuO}_4$  films were synthesized by MBE and spin-coated with poly(methyl methacrylate) (PMMA) electron-beam resist with a molecular weight of 495,000, diluted with anisole, providing a thickness of 180 nm after 1 min of spinning at 4,000 rpm. The samples coated with PMMA were subsequently baked for 90 s on a hotplate at 100 °C. The desired network pattern was exposed in the PMMA layer using a CRESTEC CABLE-9000C high-resolution electron-beam lithography system. The PMMA was used as a negative electron-beam resist; note that when PMMA is exposed to a sufficiently high electron dose it crosslinks<sup>30</sup> and becomes insoluble in most organic solvents. After removing the unexposed PMMA using methyl isobutyl ketone (MIBK), a mask was formed that defined the desired

network pattern (Fig. 1, main panel). This pattern was then transferred to the superconducting film by removing the uncovered parts of film using a standard argon ion milling process. The result of this last step is shown in the left inset to Fig. 1.

The network resistance was measured using a Quantum Design Physical Properties System over temperatures from 2 to 300 K with a stability of about  $\pm 0.001$  K, and in magnetic fields of up to 9 T. A four-point contact resistance configuration was used, in which a d.c. current of 1  $\mu$ A was fed through two relatively large current leads placed on opposite sides of the network and the d.c. voltage was measured across an additional two leads. All four leads were made from the same  $\text{La}_{1.84}\text{Sr}_{0.16}\text{CuO}_4$  superconducting film as a continuous part of the network to avoid undesirable metal/superconductor contact effects.

Received 1 March 2010; accepted 10 May 2010;  
published online 13 June 2010

## References

- Barash, Y. S. Low-energy subgap states and the magnetic flux periodicity in  $d$ -wave superconducting rings. *Phys. Rev. Lett.* **100**, 177003 (2008).
- Juricic, V., Herbut, I. F. & Tesanovic, Z. Restoration of the magnetic  $hc/e$ -periodicity in unconventional superconductors. *Phys. Rev. Lett.* **100**, 187006 (2008).
- Loder, F. *et al.* Magnetic flux periodicity of  $h/e$  in superconducting loops. *Nature Phys.* **4**, 112–115 (2008).
- Vakaryuk, V. Universal mechanism for breaking the  $hc/2e$  periodicity of flux-induced oscillations in small superconducting rings. *Phys. Rev. Lett.* **101**, 167002 (2008).
- Wei, T.-C. & Goldbart, P. M. Emergence of  $h/e$ -period oscillations in the critical temperature of small superconducting rings threaded by magnetic flux. *Phys. Rev. B* **77**, 224512 (2008).
- Zhu, J.-X. & Quan, H. T. Magnetic flux periodicity in a hollow  $d$ -wave superconducting cylinder. *Phys. Rev. B* **81**, 054521 (2010).
- Berg, E., Fradkin, E. & Kivelson, S. A. Charge- $4e$  superconductivity from pair-density-wave order in certain high-temperature superconductors. *Nature Phys.* **5**, 830–833 (2009).
- Gammel, P. L., Polakos, P. A., Rice, C. E., Harriott, L. R. & Bishop, D. J. Little–Parks oscillations of  $T_c$  in patterned microstructures of the oxide superconductor  $\text{YBa}_2\text{Cu}_3\text{O}_7$ : experimental limits on fractional-statistics-particle theories. *Phys. Rev. B* **41**, 2593–2596 (1990).
- Castellanos, A., Wordenweber, R., Ockenfuss, G., Hart, A. v. d. & Keck, K. Preparation of regular arrays of antidots in  $\text{YBa}_2\text{Cu}_3\text{O}_7$  thin films and observation of vortex lattice matching effects. *Appl. Phys. Lett.* **71**, 962–964 (1997).
- Crisan, A. *et al.* Anisotropic vortex channeling in  $\text{YBa}_2\text{Cu}_3\text{O}_{7+\delta}$  thin films with ordered antidot arrays. *Phys. Rev. B* **71**, 144504 (2005).
- Ooi, S., Mochiku, T., Yu, S., Sadki, E. S. & Hirata, K. Matching effect of vortex lattice in  $\text{Bi}_2\text{Sr}_2\text{CaCu}_2\text{O}_{8+\gamma}$  with artificial periodic defects. *Physica C* **426–431**, 113–117 (2005).
- Little, W. A. & Parks, R. D. Observation of quantum periodicity in the transition temperature of a superconducting cylinder. *Phys. Rev. Lett.* **9**, 9–12 (1962).
- Parks, R. D. & Little, W. A. Fluxoid quantization in a multiply-connected superconductor. *Phys. Rev. A* **133**, 97–103 (1964).
- Mooij, J. E. & Schön, G. B. J. (eds) Proc. NATO Workshop on Coherence in Superconducting Networks. *Physica B* **152**, 1–302 (1988).
- Tinkham, M. Consequences of fluxoid quantization in the transitions of superconducting films. *Rev. Mod. Phys.* **36**, 268–276 (1964).
- Tinkham, M. *Introduction to Superconductivity* (McGraw-Hill, 1996).
- Koshnick, N. C., Bluhm, H., Huber, M. E. & Moler, K. A. Fluctuation superconductivity in mesoscopic aluminum rings. *Science* **318**, 1440–1443 (2007).
- Wen, H. H. *et al.* Hole doping dependence of the coherence length in  $\text{La}_{2-x}\text{Sr}_x\text{CuO}_4$  thin films. *Europhys. Lett.* **64**, 790–796 (2003).
- Yeshurun, Y., Malozemoff, A. P. & Shaulov, A. Magnetic relaxation in high-temperature superconductors. *Rev. Mod. Phys.* **68**, 911–949 (1996).
- Tinkham, M. Resistive transition of high-temperature superconductors. *Phys. Rev. Lett.* **61**, 1658–1661 (1988).
- Blatter, G., Feigel'man, M. V., Geshkenbein, V. B., Larkin, A. I. & Vinokur, V. M. Vortices in high-temperature superconductors. *Rev. Mod. Phys.* **66**, 1125–1388 (1994).
- London, F. On the problem of the molecular theory of superconductivity. *Phys. Rev.* **74**, 562–573 (1948).
- Kirtley, J. R. *et al.* Fluxoid dynamics in superconducting thin film rings. *Phys. Rev. B* **68**, 214505 (2003).
- Kogan, V. G., Clem, J. R. & Mints, R. G. Properties of mesoscopic superconducting thin-film rings: London approach. *Phys. Rev. B* **69**, 064516 (2004).
- Pearl, J. Current distribution in superconducting films carrying quantized fluxoids. *Appl. Phys. Lett.* **5**, 65–66 (1964).
- Qiu, C. & Qian, T. Numerical study of the phase slip in two-dimensional superconducting strips. *Phys. Rev. B* **77**, 174517 (2008).
- Yeshurun, Y. & Malozemoff, A. P. Giant flux creep and irreversibility in an Y-Ba-Cu-O crystal: an alternative to the superconducting-glass model. *Phys. Rev. Lett.* **60**, 2202–2205 (1988).
- Hopkins, D. S., Pekker, D., Goldbart, P. M. & Bezryadin, A. Quantum interference device made by DNA templating of superconducting nanowires. *Science* **308**, 1762–1765 (2005).
- Pekker, D., Bezryadin, A., Hopkins, D. S. & Goldbart, P. M. Operation of a superconducting nanowire quantum interference device with mesoscopic leads. *Phys. Rev. B* **72**, 104517 (2005).
- Hoole, A. C. F., Welland, M. E. & Broers, A. N. Negative PMMA as a high-resolution resist—the limits and possibilities. *Semicond. Sci. Technol.* **12**, 1166–1170 (1997).

## Acknowledgements

The authors thank A. Frydman, B. Ya. Shapira, B. Rosenstein, E. Zeldov, Y. Oreg, O. Pelleg, A. Bollinger, A. Gozar, Z. Radović and V. Vinokur for helpful discussions. Y.Y. and A.S. acknowledge support of the Deutsche Forschungsgemeinschaft through the Deutsch–Israelische Projektkooperation (grant no. 563363). I.S. thanks the Israeli Ministry of Science and Technology for an Eshkol scholarship. The work at BNL was supported by the US Department of Energy (contract no. MA-509-MACA).

## Author contributions

G.L. and I.B. synthesized and characterized the superconducting films. I.S. designed and made the patterns, performed the magnetoresistance measurements and analysed the data. All authors contributed to the theoretical interpretation and were involved in the completion of the manuscript.

## Additional information

The authors declare no competing financial interests. Reprints and permission information is available online at <http://npg.nature.com/reprintsandpermissions/>. Correspondence and requests for materials should be addressed to I.S.

3.4 CONTRIBUTION OF THERMALLY EXCITED VORTICES AND ANTIVORTICES TO THE  
MAGNETORESISTANCE OF  $\text{La}_{1.84}\text{Sr}_{0.16}\text{CuO}_4$  NANOLOOPS: POSSIBILITY OF  
BEREZINSKII-KOSTERLITZ-THOULESS TRANSITION



**Oscillatory magnetoresistance in nanopatterned superconducting  $\text{La}_{1.84}\text{Sr}_{0.16}\text{CuO}_4$  films**I. Sochnikov,<sup>1</sup> A. Shaulov,<sup>1</sup> Y. Yeshurun,<sup>1</sup> G. Logvenov,<sup>2</sup> and I. Božović<sup>2</sup><sup>1</sup>*Department of Physics, Institute of Superconductivity and Institute of Nanotechnology and Advanced Materials, Bar-Ilan University, Ramat-Gan 52900, Israel*<sup>2</sup>*Brookhaven National Laboratory, Upton, New York 11973-5000, USA*

(Received 17 June 2010; revised manuscript received 27 August 2010; published 21 September 2010)

A superconducting  $\text{La}_{1.84}\text{Sr}_{0.16}\text{CuO}_4$  film patterned into a network of  $100 \times 100 \text{ nm}^2$  noninteracting square loops exhibits large magnetoresistance oscillations superimposed on a background which increases monotonically with the applied magnetic field. Neither the oscillations amplitude nor its temperature dependence can be explained by the Little-Parks effect. Conversely, a good quantitative agreement is obtained with a recently proposed model ascribing the oscillations to the interaction between thermally excited moving vortices and the oscillating persistent currents induced in the loops. Extension of this model, allowing for direct interaction of the vortices and antivortices magnetic moment with the applied field, accounts quantitatively for the monotonic background as well. Analysis of the background indicates that in the patterned film both vortices and antivortices are present at comparable densities. This finding is consistent with the occurrence of Berezinskii-Kosterlitz-Thouless transition in  $\text{La}_{1.84}\text{Sr}_{0.16}\text{CuO}_4$  films.

DOI: [10.1103/PhysRevB.82.094513](https://doi.org/10.1103/PhysRevB.82.094513)

PACS number(s): 74.78.Na, 74.25.Uv, 74.25.Wx

**I. INTRODUCTION**

Quantization of the fluxoid in multiply connected superconductors was first predicted by Fritz London in the early days of superconductivity.<sup>1</sup> This prediction was later confirmed experimentally by Little and Parks<sup>2-4</sup> who demonstrated that a thin-walled superconducting cylinder pierced by a magnetic flux shows magnetoresistance oscillations with the period equal to the superconducting flux quantum  $\Phi_0 = h/2e$ . The explanation provided by Little and Parks was that the resistance oscillations  $\Delta R(H)$  reflect periodic changes in the superconducting transition temperature  $T_c$  given by  $\Delta T_c = \Delta R(H)(dT/dR)$ . Subsequent studies have demonstrated periodic changes in the magnetoresistance also in two-dimensional (2D) networks of superconducting wires (see Refs. 5 and 6, and references therein). These studies were focused on determining the arrangements of vortices in the network and the effects of size and symmetry of the network on the periodic oscillations.

Magnetoresistance oscillations in a high- $T_c$  superconducting network were first reported by Gammel *et al.*,<sup>7</sup> who ascribed them to the Little-Parks effect. However, the amplitude of the oscillations and its temperature dependence could not be accounted for while no attempt was made to analyze the monotonic background on which the magnetoresistance oscillations were superimposed.

We have recently demonstrated<sup>8</sup> large magnetoresistance oscillations in a network of decoupled  $150 \times 150 \text{ nm}^2$   $\text{La}_{1.84}\text{Sr}_{0.16}\text{CuO}_4$  loops and showed that the oscillations amplitude is much larger than what one would expect from the periodic changes in the critical temperature associated with the Little-Parks effect. We ascribed these oscillations to a dynamic effect: thermally excited vortices move and interact with the persistent current induced in the loops by the magnetic field. As the induced current oscillates periodically with the magnetic flux piercing the loops, due to fluxoid quantization, this interaction is periodic with the applied magnetic field; this gives rise to the magnetoresistance oscillations.

This effect is especially important in high- $T_c$  superconductors, where the Little-Parks effect is suppressed because of the relatively small coherence length, while the vortex dynamics is enhanced due to relatively large thermal fluctuations. As the size of the loops decreases down to the nanoscale, the dynamic effect becomes even more significant, because of an increase in the persistent current induced in the loops. We have also outlined a theoretical analysis<sup>8</sup> based on the fluxoid dynamics model,<sup>9,10</sup> that successfully accounts for the amplitude of the observed magnetoresistance oscillations and its temperature dependence.

In this paper we present data on smaller  $\text{La}_{1.84}\text{Sr}_{0.16}\text{CuO}_4$  loops of size  $100 \times 100 \text{ nm}^2$ , almost an order of magnitude smaller than what has been reported previously for other high- $T_c$  materials. In addition, we extend our theoretical analysis to include description of the monotonic background on which the magnetoresistance oscillations are superimposed. The analysis of the magnetoresistance background provides evidence for the presence of both vortices and antivortices in  $\text{La}_{1.84}\text{Sr}_{0.16}\text{CuO}_4$  films at elevated temperatures. This is consistent with thermal generation of vortex-antivortex pairs that dissociate above a certain temperature, the so-called Berezinskii-Kosterlitz-Thouless (BKT) transition point.<sup>11</sup> The occurrence of a BKT transition has been predicted in thin high- $T_c$  superconducting films with the lateral dimensions smaller than the perpendicular penetration depth.<sup>12</sup> However, the experimental efforts to observe such a phase transition in superconductors have so far yielded inconclusive results.

**II. EXPERIMENTAL**

An advanced molecular-beam epitaxy system was employed to synthesize optimally doped  $\text{La}_{1.84}\text{Sr}_{0.16}\text{CuO}_4$  films, 26 nm thick, epitaxially on  $\text{LaSrAlO}_4$  substrates polished perpendicular to the (001) direction.<sup>13,14</sup> The films were characterized *in situ* by reflection high-energy electron diffraction, and *ex situ* by x-ray diffraction, atomic force micros-

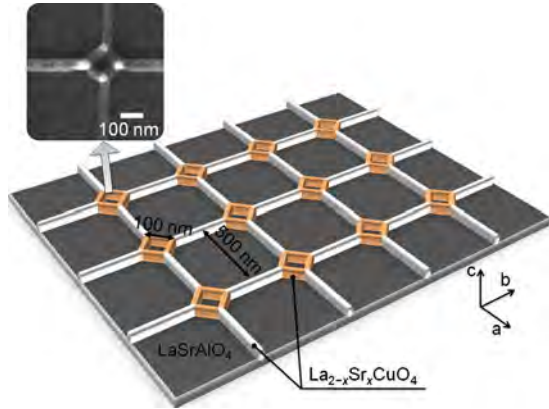


FIG. 1. (Color online) Main panel: schematic description of a sample consisting of  $100 \times 100 \text{ nm}^2$  loops (orange color) interconnected by  $500 \text{ nm}$  long wires (bright bars). Inset: SEM image of a single loop patterned by electron-beam lithography in a  $\text{La}_{1.84}\text{Sr}_{0.16}\text{CuO}_4$  film. The whole sample contains  $60 \times 60$  small loops.

copy and mutual inductance measurements. Subsequently, the films were patterned into a  $30 \times 30 \mu\text{m}^2$  network consisting of  $100 \times 100 \text{ nm}^2$  square loops with  $\sim 25 \text{ nm}$  wire width, separated by  $500 \times 500 \text{ nm}^2$  loops, as shown schematically in Fig. 1. We note that the size of the loops and the wire width in the present experiment are nearly an order of magnitude smaller than previously studied in high- $T_c$  networks and rings.<sup>7,15–19</sup> In this specially designed network the small loops do not share sides, thus eliminating complications that may arise in simple networks (e.g., a square network), such as vortex interaction and frustration or interstitial vortices trapped in the wires.<sup>5–7,15–18</sup> Simulations<sup>20</sup> show that the decoupling of the small loops improves as the ratio between the sides of the large and the small loops increases. In the present network we achieved a ratio of 5:1 as compared to about 3:1 in our previous published work.<sup>8</sup> In such a network, the behavior of the small loops approximates that of an ensemble of isolated loops, thus reflecting the behavior of a single loop. Nevertheless, this decoupled network has an advantage over a single loop as it allows application of larger currents, thus improving the signal-to-noise ratio. In addition, measurements on large number of loops in the network average effects of inhomogeneities and size distribution.

The network pattern of Fig. 1 was created using a CRESTEC Cable-9000C high resolution e-beam lithography system in a layer of poly(methyl methacrylate) (PMMA) resist spun-off on top of a superconducting  $\text{La}_{1.84}\text{Sr}_{0.16}\text{CuO}_4$  film. This PMMA pattern served as a mask for transferring the pattern to the superconducting film by Ar-ion milling. The scanning electron microscope (SEM) image in the inset shows a detail (a single loop) of the resulting superconducting network. The network magnetoresistance was measured using a Quantum Design physical properties measurement system. The magnetic field was applied normal to the film surface (the  $a$ - $b$  crystallographic plane) and the bias current was  $1 \mu\text{A}$ .

Figure 2 shows measurements of the network resistance  $R(T)$  at zero field as a function of temperature before (closed circles) and after (open circles) patterning. Evidently, pat-

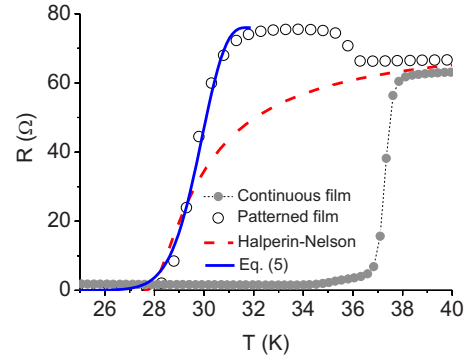


FIG. 2. (Color online) Measured temperature dependence of the resistance in a continuous film (solid circles, the dotted line is a guide to the eyes) and the patterned film (open circles) at zero applied field. The solid blue line is calculated using Eq. (5) with  $T_c=32 \text{ K}$  and  $R_n=76 \Omega$  yielding fit values  $\lambda_0=750 \text{ nm}$ ,  $\xi_0=2.5 \text{ nm}$ ,  $d=23.4 \text{ nm}$ , and  $w=21 \text{ nm}$ . The red dashed line is based on the Halperin-Nelson formula for a 2D superconductor (Ref. 21) using the Berezinski-Kosterlitz-Thouless transition temperature,  $T_{\text{BKT}}=27.6 \text{ K}$ , the fluctuation-corrected BCS critical temperature,  $T_{\text{BCS}}=32 \text{ K}$ , and  $R_n=76 \Omega$ .

tering of the film into narrow wires causes broadening of the resistive transition. In the following we show that this broadening can be interpreted as the result of a decrease in energy required to create a vortex/antivortex pair as the wire width decreases. Figure 2 also shows an anomalous peak in  $R(T)$  of the patterned film near  $T_c$ . A similar peak was observed previously in superconducting nanostructures and its origin is still debated.<sup>22–24</sup>

Figure 3 shows the network magnetoresistance measured at different temperatures between 27 and 32 K. The measured magnetoresistance exhibits large oscillations superimposed on a monotonic background. The temperature up to which the oscillations persist, which in what follows we define as the transition temperature,  $T_c$ , is  $\sim 32 \text{ K}$ . The oscillation amplitude decreases as the field increases. At temperatures above  $\sim 32 \text{ K}$ ,  $R(H)$  exhibits an anomalous shape, the magnetoresistance is decreasing with the field (negative magnetoresistance).<sup>25</sup> The period of the oscillations,  $H_0 \approx 2300 \text{ Oe}$ , corresponds to the magnetic flux quantum,  $H_0 = \Phi_0 / \pi r^2$ , where  $r \approx 52.8 \text{ nm}$  is the effective radius of the

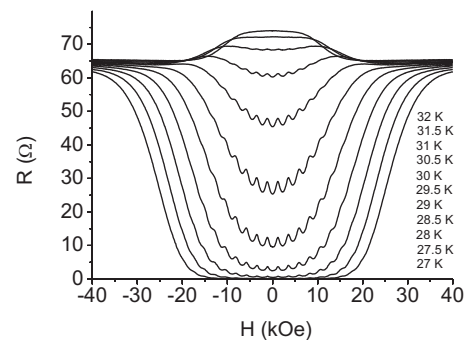


FIG. 3. Resistance of the patterned film as a function of magnetic field perpendicular to the sample plane (i.e., parallel to the  $c$ -crystallographic axis) at different temperatures. The lowest and the uppermost curves correspond to 27 K and 32 K, respectively.

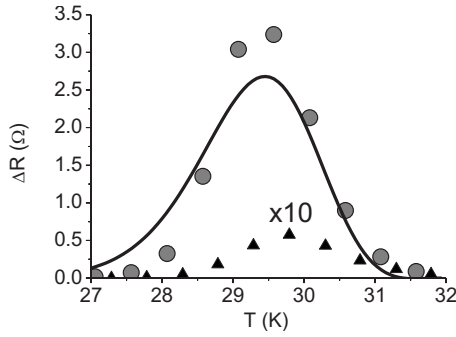


FIG. 4. Temperature dependence of the measured oscillation amplitude (circles). The solid line is calculated using Eq. (7) with the parameters extracted from Fig. 2. The triangles show an upper limit for the resistance oscillations amplitude calculated for the Little-Parks effect; note that this scale is expanded tenfold.

small loop. Oscillations of the period  $\sim 80$  Oe corresponding to the large loops are also observed but on the scale of Fig. 3 their amplitude is too small to be noticed. In Fig. 4, the circles show the measured temperature dependence of the oscillations amplitude. Evidently, the magnetoresistance oscillations are observed only within a limited temperature range around the transition, exhibiting the maximum amplitude around 29.5 K.

### III. THEORETICAL MODEL AND DISCUSSION

The magnetoresistance oscillations shown in Fig. 3 at the first sight resemble the Little-Parks effect<sup>2,3</sup> originating from the periodic dependence of the critical temperature,  $T_c$ , on the applied magnetic field. However, this resemblance is deceptive. For an estimate, let us take as the typical<sup>26</sup> value of the coherence length,  $\xi_0 = 2$  nm, the critical temperature in zero field at the onset of the resistance drop,  $T_c = 32$  K, and the loop effective radius  $r = [\Phi_0 / (\pi H_0)]^{1/2} = 52.8$  nm; using these parameter values for the amplitude of oscillations in  $T_c$  one obtains<sup>11,27</sup>  $\Delta T_c^{LP} = 0.14 T_c (\xi_0 / r)^2 \approx 6.4$  mK. From this  $\Delta T_c^{LP}$  we can calculate an upper limit to the resistance oscillations amplitude,  $\Delta R = \Delta T_c^{LP} (dR/dT)$ , shown by the triangles in Fig. 4. Evidently,  $\Delta R$  expected from the Little-Parks effect exhibits the maximum value which is a factor of  $\sim 50$  smaller than the maximum value measured in our experiment. Moreover, attributing the data shown in Fig. 3 to the Little-Parks effect leads to the illogical conclusion that  $\Delta T_c^{LP}$  would be temperature dependent. This is shown in Fig. 5, where the solid points were calculated from the experimentally measured oscillation amplitude,  $\Delta R$ , and the temperature derivative  $dR/dT$ , using  $\Delta T_c = \Delta R / (dR/dT)$ . Note that the extracted  $\Delta T_c$  exhibits unexpected temperature dependence with values that are two orders of magnitude larger than the constant value of about 6.4 mK (the solid line in Fig. 5).<sup>28</sup>

Given that the Little-Parks effect cannot explain the observed giant magnetoresistance oscillations, one needs to look for alternative explanations. We conjecture that the origin of this phenomenon may be in drastically modified vortex dynamics in nanopatterned films. While in continuous

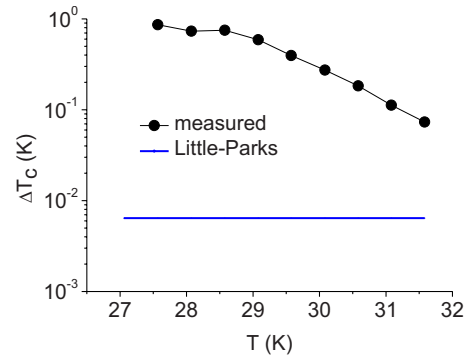


FIG. 5. (Color online) Solid circles: the amplitude of oscillations in  $T_c$ ,  $\Delta T_c = \Delta R(H) (dT/dR)$ , derived from the experimentally measured oscillation amplitude,  $\Delta R$ , and the temperature derivative  $dR/dT$ . The solid black line connecting the experimental points is a guide to the eyes. The solid blue line presents the change in  $T_c$ ,  $\Delta T_c^{LP}$ , that one would expect from the Little-Parks effect. Note that the two scales differ by 2 orders of magnitude.

films the activation energy for vortex creep usually decreases monotonically with the applied magnetic field,<sup>29-31</sup> in nanopatterned films this activation energy becomes oscillatory, since moving vortices interact with the current induced in nanoloops, and this current is a periodic function of the field strength. Periodicity of the induced current results directly from the fluxoid quantization<sup>1-3,27</sup> which is also the cause of the Little-Parks effect. The fluxoid, consisting of the flux induced by the supercurrent in the loop and by the external magnetic field, is characterized by the quantum vorticity number,  $N$ , which defines the energy state of the superconducting loop. In the lowest energy state,  $N$  is equal<sup>11,27</sup> to  $H/H_0$  rounded to the nearest integer. Thermally induced vortices or antivortices cause fluxoid transitions from the equilibrium quantum state,  $N$ , to a higher energy state. Kirtley *et al.*<sup>9</sup> and Kogan *et al.*<sup>10</sup> in their analysis of magnetic scanning microscope measurements of mesoscopic superconducting rings, calculated the energies  $\Delta E_{in}^{\pm}$  and  $\Delta E_{out}^{\pm}$  that are required to create a vortex (+) or an antivortex (-) in a superconducting wire forming a loop and to carry it into or outside of the loop hole, respectively,

$$\Delta E_{in}^{\pm} = E_v(T) + E_0(T)(N - H/H_0 + 1/2) \mp \mu H,$$

$$\Delta E_{out}^{\pm} = E_v(T) + E_0(T)(N - H/H_0 - 1/2) \mp \mu H. \quad (1)$$

The first term in Eq. (1),  $E_v$ , is field independent and represents the energy needed for creation of the vortex/antivortex in a ring with annulus width  $w$ . For our rings with  $r/w > 1/2$  we can use  $E_v = \Phi_0^2 \ln[2w/\pi\xi(T)]/8\pi^2\Lambda(T)$ . Here,  $\xi(T) = 0.74\xi_0(1 - T/T_c)^{-1/2}$  is the Ginzburg-Landau coherence length<sup>11</sup> and  $\Lambda(T) = 2\lambda(T)^2/d$  the Pearl penetration depth<sup>11,32</sup> in a film of thickness  $d$  and with the London penetration depth<sup>11</sup>  $\lambda(T) = \lambda_0[1 - (T/T_c)^2]^{-1/2}$ .

The second term in Eq. (1) is periodic with the field, expressing the interaction of a vortex or an antivortex with the current associated with the fluxoid in terms of the energy  $E_0$ . For our rings we use  $E_0 = \Phi_0^2 \ln[(r+w/2)/(r-w/2)]/8\pi^2\Lambda(T)$ . The quantized values of  $N$  lead to periodi-

cally oscillating values of  $(N-H/H_0)$ . The third term in Eq. (1) is the energy of the magnetic dipole moment,  $\mu(T) = \Phi_0 w^2 / 32 \pi \Lambda(T)$ , associated with a vortex or an antivortex.<sup>33</sup>

As fluxoid transitions of higher order,  $N \rightarrow N+m$  with  $|m| \geq 2$ , are statistically less significant, we consider fluxoid transitions accomplished by only *one* vortex or antivortex entry or exit. Thermodynamic averaging over the above four types of excitation energies,  $\Delta E_i^j$ , yields an effective potential barrier,  $\langle \Delta E \rangle$ ,

$$\langle \Delta E \rangle = \frac{\sum_{\substack{i \in \text{in,out} \\ j \in +,-}} \Delta E_i^j e^{-\Delta E_i^j / k_B T}}{\sum_{\substack{i \in \text{in,out} \\ j \in +,-}} e^{-\Delta E_i^j / k_B T}}. \quad (2)$$

Using Eq. (1) one obtains

$$\begin{aligned} \langle \Delta E(T, H) \rangle &= E_v + E_0/2 - E_0(N-H/H_0) \tanh \left[ \frac{E_0(N-H/H_0)}{k_B T} \right] \\ &\quad - \mu H \tanh \left( \frac{\mu H}{k_B T} \right) \\ &\approx E_v - E_0(N-H/H_0) \tanh \left[ \frac{E_0(N-H/H_0)}{k_B T} \right] \\ &\quad \times \left[ \frac{E_0(N-H/H_0)}{k_B T} \right] - \mu H \tanh \left( \frac{\mu H}{k_B T} \right). \end{aligned} \quad (3)$$

In the approximations made in Eq. (3) we assumed that  $E_v \gg E_0$ , which is especially valid for narrow rings,  $r \gg w$ . The first term in Eq. (3),  $E_v(T)$ , describes the zero-field excitation energy as a function of temperature, since the other two terms vanish at zero magnetic field. The second term describes the periodic part and the third term is responsible for the monotonic field-dependent ‘‘background’’ (see Fig. 3). Note that in this model  $E_v$ ,  $E_0$ , and  $\mu$  depend only on temperature.

In the next step, we derive the magnetoresistance following Tinkham’s approach in his analysis<sup>29</sup> of the resistive transition in high- $T_c$  superconductors. Replacing the activation energy in his equations with  $\langle \Delta E \rangle$  as given in Eq. (3) yields

$$\frac{R}{R_n} = \left[ I_0 \left( \frac{\langle \Delta E \rangle}{2k_B T} \right) \right]^{-2}, \quad (4)$$

where  $I_0$  is the zero-order modified Bessel function of the first kind. In the following, we show that Eq. (4) in conjunction with Eq. (3) can explain a rich variety of phenomena, including the observed transition broadening, the oscillations of magnetoresistance, the temperature dependence of the oscillation amplitude, and the shape of the monotonic background on which the magnetoresistance oscillations are superimposed.

Equations (1)–(4) are applicable to a single loop of radius  $r$  and can also apply to a wire for which  $r \rightarrow \infty$ . In applying these equations to a network of decoupled loops interconnected by relatively long wires (see Fig. 1), we note that the total resistance of such a network is  $R = R^{\text{loop}} + R^{\text{wire}}$ , where  $R^{\text{loop}}$  and  $R^{\text{wire}}$  are the resistances of a small loop and of a single interconnecting wire, respectively. Expressions for  $R^{\text{loop}}$  and  $R^{\text{wire}}$  can be obtained on the basis of Eq. (4),

$$R = R_n^{\text{loop}} \left[ I_0 \left( \frac{\langle \Delta E^{\text{loop}} \rangle}{2k_B T} \right) \right]^{-2} + R_n^{\text{wire}} \left[ I_0 \left( \frac{\langle \Delta E^{\text{wire}} \rangle}{2k_B T} \right) \right]^{-2}, \quad (5)$$

where  $\langle \Delta E^{\text{loop}} \rangle$  and  $\langle \Delta E^{\text{wire}} \rangle$  are given in Eq. (3) by including and omitting the  $E_0$  term, respectively. (The term  $E_0$  is responsible for the oscillations that are absent in the wires.) For the network described in Fig. 1,  $R^{\text{loop}}$  and  $R^{\text{wire}}$  are 22% and 78%, respectively, of the measured  $R_n = 76 \, \Omega$  at  $T_c = 32 \, \text{K}$ , reflecting the relative lengths of the short and the long wires in the network.

### A. Transition broadening at zero field

The solid blue line in Fig. 2 shows a fit to the data points of the resistance in a patterned film in the transition region, using Eq. (5) in the zero-field limit. Note that in this limit  $\langle \Delta E^{\text{loop}} \rangle$  and  $\langle \Delta E^{\text{wire}} \rangle$  reduce to  $E_v(T)$ . This fit yields  $d = 23.4 \, \text{nm}$ ,  $w = 21 \, \text{nm}$ ,  $T_c = 32 \, \text{K}$ ,  $R_n = 76 \, \Omega$ ,  $\lambda_0 = 750 \, \text{nm}$ , and  $\xi_0 = 2.5 \, \text{nm}$ . The calculated resistance is in a reasonably good agreement with the experimental data, indicating that the transition broadening is primarily due to enhanced vortex motion across narrow wires due to reduced  $E_v$ . Equation (5) does not account for the anomalous resistive peak observed at elevated temperatures. A similar peak was observed in other superconducting nanostructures<sup>22–24</sup> but its origin is still controversial.

The dashed line in Fig. 2 shows an attempt to fit the resistance data of the patterned film to the Halperin-Nelson formula for 2D superconductors, based on vortex-antivortex unbinding.<sup>21</sup> In the calculation of this curve we assumed a BKT transition temperature,  $T_{\text{BKT}} = 27.5 \, \text{K}$ , and the ‘‘fluctuation-corrected BCS critical temperature,’’  $T_{\text{BCS}} = 32 \, \text{K}$ . Apparently, this model does not account for the temperature dependence of the magnetoresistance measured in our nanoloops except for a limited temperature range in the immediate vicinity of  $\sim 27.5 \, \text{K}$ . At higher temperatures the Halperin-Nelson formula describes ‘‘fluctuation-corrected BCS behavior,’’ which does not explain our results.

### B. Oscillations amplitude—temperature dependence

As the origin of the oscillations is in the small loops, in the following we derive an expression for the oscillations amplitude based on Eq. (3). We apply this equation for low fields such that the term  $-\mu H \tanh(\mu H / k_B T)$  in the excitation energy [Eq. (3)] is small compared to  $E_v$ . Using the approximation  $\tanh[E_0(N-H/H_0)/k_B T] \approx E_0(N-H/H_0)/k_B T$  in the periodic term, one obtains

$$\frac{R}{R_n} \approx [I_0 \{ E_v / 2k_B T - [E_0(N-H/H_0)/k_B T]^2 / 2 \}]^{-2}, \quad (6)$$

which is an oscillating function of the magnetic field.

One can approximate the amplitude of the oscillations,  $\Delta R(T)$ , as the difference between the zero-field curve,  $R(T, H=0)$ , and the shifted resistance curve  $R(T, H=H_0/2)$ . If the difference is relatively small,  $\Delta R$  can be approximated as

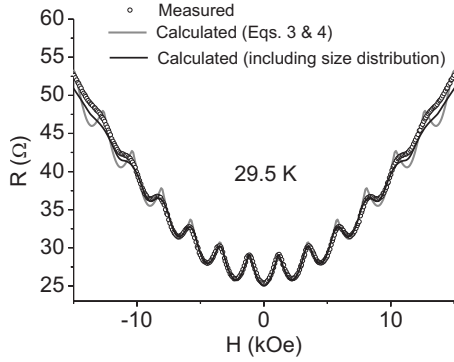


FIG. 6. Magnetoresistance oscillations at 29.5 K: measured (open circles) and calculated using Eq. (5) (the solid gray line). The solid black line is calculated with the same equations but assuming a size distribution of the loops, resulting in the spread of  $\pm 8\%$  in  $H_0$  around the mean value of  $\sim 2300$  Oe.

$$\Delta R \approx \left. \frac{dR}{d\langle E \rangle} \right|_{H=0} \Delta E = R_n \frac{I_1(E_v/2k_B T)}{I_0[E_v/2k_B T]^3} \left[ \frac{E_0}{2k_B T} \right]^2, \quad (7)$$

where  $\Delta E$  is the amplitude of periodic change in the excitation energy with the field and  $I_1$  is the first-order modified Bessel function of the first kind. This equation, which was derived for a single loop, is also valid for the network if we replace  $R_n$  with  $R_n^{loop}$ , because the origin of oscillations is in the small loops.

We note that  $E_v$  and  $E_0$  are functions of two length scales,  $\lambda_0$  and  $\xi_0$ . The calculated amplitude, using Eq. (7) with  $\lambda_0 = 750$  nm,  $\xi_0 = 2.5$  nm,  $r = 52.8$  nm,  $d = 23.4$  nm, and  $w = 21$  nm, is shown as the solid line in Fig. 4. A fairly good agreement between the experimental data and the theoretical curve is obtained. We note that the values of the parameters  $\lambda_0$  and  $\xi_0$  may be influenced by the lithography process, which may cause damage in regions near the surface and sides and make the effective thickness and width significantly smaller than the nominal values.

It should be mentioned that an earlier work has found large-amplitude magnetoresistance oscillations in a different nanostructure made of two low- $T_c$  superconducting nanowires.<sup>34,35</sup> These oscillations were attributed to the field-driven modulation of barrier heights for phase slips. As that interpretation relates to one-dimensional superconducting wires ( $w < \xi$ ), it may not be directly applicable to our high- $T_c$  loops in which the wire width is an order of magnitude larger than the coherence length.

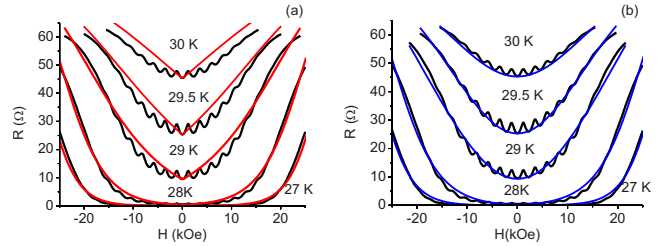


FIG. 7. (Color online) Theoretical fits of the nonoscillating background (the line connecting the *minima* of the oscillatory magnetoresistance) to the experimental data (black lines) taking into account (a) only vortices (left panel, red lines) and (b) both vortices and antivortices (right panel, blue lines).

### C. Magnetoresistance oscillations—field dependence

Figure 6 shows a comparison of the field dependence of magnetoresistance measured at 29.5 K (open circles) with the one calculated using Eq. (5) (the solid gray line) and taking  $E_v = 94$  and  $E_0 = 72$  in the units of  $k_B$  and  $\mu = 28$  in the units of  $k_B/T$ . A good agreement between the calculated curve and the experimental data is seen only at low fields. As the field increases, the experimentally measured amplitude decreases while the calculated amplitude remains almost constant. The agreement between the theory and the experiment can be extended to high fields if we take into account the distribution of the size of loops in the patterned film. As loops of different size give different period of oscillations, averaging over a size distribution of the small loops causes a decrease in the oscillations amplitude. We can account for this size spread assuming an equal-size distribution of  $\pm 8\%$  around the median value of 52.8 nm and then average over the contributions to  $R(H)$  from loops of different sizes. This procedure yields a good fit (the solid black curve in Fig. 6) over a large field range.

It should be noted that a decay of the magnetoresistance oscillations at high fields was observed not only in networks<sup>5-7</sup> but also in low- $T_c$  cylinders<sup>2-4</sup> and, more recently, in a high- $T_c$  superconducting single ring.<sup>19</sup> The latter observation may be ascribed to variation in the order parameter along the radial direction across the relatively wide ring (270–300 nm), creating a discrete number of concentric independent domains where supercurrent density is different from zero.<sup>19</sup> In low- $T_c$  cylinders<sup>2-4</sup> the oscillations originate from the Little-Parks effect, i.e., from the changes in  $T_c$  with field. The resulting magnetoresistance changes are proportional to  $dR/dT$  which decreases as the field increases.

TABLE I. The values of  $E_v$  and  $\mu$  at different temperatures.

$T$ (K)	$E_v$ (K)	$\mu$ (K/T)	$E_v/2k_B T$	$\mu/2k_B T$ (1/T)	
30	63	21	1.1	0.4	} < 1
29.5	93.5	30	1.6	0.5	
29	134	41	2.3	0.7	
28	243	77	4.3	1.4	} > 1
27	349	104	6.5	1.9	

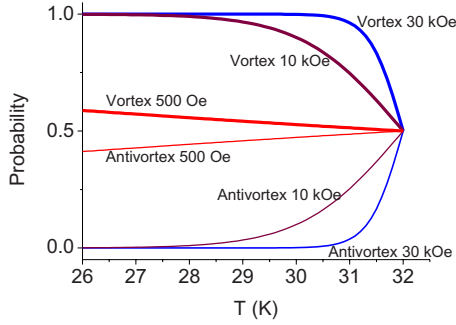


FIG. 8. (Color online) The calculated probabilities of thermally induced creation of a vortex (solid lines) and an antivortex (thin solid lines) as functions of the magnetic field.

#### D. Monotonic field background

We define the background as the line connecting the minima points of the oscillatory magnetoresistance. Thus, in calculating the background, the periodic term included in  $\langle \Delta E^{loop} \rangle$  of Eq. (5) is neglected as it takes zero value at fields  $mH_0$  with integer  $m$ . Assuming that only vortices are present in the system the resistance would be

$$R_{backgr} = R_n^{loop} \{ I_0[(E_0 - \mu|H|)/(2k_B T)] \}^{-2} + R_n^{wire} \{ I_0[-\mu|H|/(2k_B T)] \}^{-2}. \quad (8)$$

In the presence of *both* vortices and antivortices,  $\mu|H|$  in Eq. (8) has to be replaced by  $\mu H \tanh(\mu H/k_B T)$ . Two fits of expression (8) to the experimental data at different temperatures are shown in Figs. 7(a) and 7(b), the first assuming the presence of vortices alone and the second assuming the presence of both vortices and antivortices. It can be seen clearly that taking into account only vortices fails to explain the background at temperatures above  $\sim 28.5$  K while taking into account both vortices and antivortices provides a much better description of the experimental results.

The fits shown in Fig. 7(b) yield the values of  $E_v$  and  $\mu$  at different temperatures listed in Table I. These values decrease with temperature as predicted in Ref. 33 and are of same order of magnitude as the calculated values of  $E_v = \Phi_0^2 \ln[2w/\pi\xi(T)]/8\pi^2\Lambda(T)$  and  $\mu(T) = \Phi_0 w^2/32\pi\Lambda(T)$ .

The need to account for antivortices in explaining the magnetoresistance background at high temperatures becomes apparent by considering the probabilities  $P_V$  and  $P_{AV}$  of thermally excited vortex and antivortex in a superconducting wire. These can be expressed as  $P_V(T, H) \propto \exp[-(E_V - \mu|H|)/k_B T]$  and  $P_{AV}(T, H) \propto \exp[-(E_V + \mu|H|)/k_B T]$ , respectively. In Fig. 8 we show the calculated  $P_V$  and  $P_{AV}$  as a

function of temperature for different fields. From these curves it is clear that at high magnetic fields the probability of antivortices is highly suppressed. However, at sufficiently high temperatures antivortices occur with a relatively high probability even at high fields.

#### IV. SUMMARY AND CONCLUSIONS

In uniform (unpatterned) films the activation energy for vortex creep usually decreases monotonically with the applied magnetic field.<sup>29–31</sup> In contrast, in films nanopatterned into a network of loops, this activation energy becomes oscillatory, because moving vortices interact with the periodically oscillating current induced in the loops. The activation energy also includes a term that varies monotonically with the applied field because of magnetic interaction of vortices and antivortices with the applied field. The combination of monotonic and oscillatory terms of the activation energy gives rise to magnetoresistance oscillations superimposed on a monotonically increasing background. On the basis of this model, we have derived analytical expressions for the magnetoresistance oscillations and for the background and showed good quantitative agreement with the experimental results obtained from an array of noninteracting nanosized loops in a  $\text{La}_{1.84}\text{Sr}_{0.16}\text{CuO}_4$  film.

In analyzing the monotonic background of magnetoresistance we showed that it is necessary to account for the presence in the film of antivortices alongside with vortices, especially at elevated temperatures. This finding may have an implication on the debated BKT transition, which predicts dissociation of vortex-antivortex pairs above the transition temperature in thin superconducting films. Further study of the possibility of manifestation of Berezinskii-Kosterlitz-Thouless transition in our experiment requires an extension of our analysis to include the contribution of vortex-(anti)vortex interactions to the activation energy.

#### ACKNOWLEDGMENTS

We thank A. Bollinger, A. Frydman, A. Gozar, L. Klein, V. V. Kogan, J. Mannhart, Y. Oreg, O. Pelleg, Z. Radović, B. Rosenstein, B. Ya. Shapiro, E. Shimshoni, V. Vinokur, and E. Zeldov for helpful discussions. The work at Bar-Ilan University was supported by the Deutsche Forschungsgemeinschaft through the Deutsch Israelische Projektkooperation (Grant No. 563363). Y.Y. acknowledges support of the Israel Science Foundation. I.S. thanks the Israeli Ministry of Science and Technology. The work at BNL was supported by US DOE under Contract No. MA-509-MACA.

<sup>1</sup>F. London, *Phys. Rev.* **74**, 562 (1948).

<sup>2</sup>W. A. Little and R. D. Parks, *Phys. Rev. Lett.* **9**, 9 (1962).

<sup>3</sup>R. D. Parks and W. A. Little, *Phys. Rev.* **133**, A97 (1964).

<sup>4</sup>R. P. Groff and R. D. Parks, *Phys. Rev.* **176**, 567 (1968).

<sup>5</sup>An extensive literature on the Little-Parks effect in low- $T_c$  materials can be found in Proceedings of the NATO Workshop on

Conference in Superconducting Networks, Delft, The Netherlands, edited by J. E. Mooij and G. B. J. Schon, 1987 [*Physica B* **152**(1-2) (1988)].

<sup>6</sup>A. Behrooz, M. J. Burns, D. Levine, B. Whitehead, and P. M. Chaikin, *Phys. Rev. B* **35**, 8396 (1987).

<sup>7</sup>P. L. Gammel, P. A. Polakos, C. E. Rice, L. R. Harriott, and D. J.

- Bishop, *Phys. Rev. B* **41**, 2593 (1990).
- <sup>8</sup>I. Sochnikov, A. Shaulov, Y. Yeshurun, G. Logvenov, and I. Bozovic, *Nat. Nanotechnol.* **5**, 516 (2010).
- <sup>9</sup>J. R. Kirtley, C. C. Tsuei, V. G. Kogan, J. R. Clem, H. Raffy, and Z. Z. Li, *Phys. Rev. B* **68**, 214505 (2003).
- <sup>10</sup>V. G. Kogan, J. R. Clem, and R. G. Mints, *Phys. Rev. B* **69**, 064516 (2004).
- <sup>11</sup>M. Tinkham, *Introduction to Superconductivity* (McGraw-Hill, New York, 1996).
- <sup>12</sup>D. R. Strachan, C. J. Lobb, and R. S. Newrock, *Phys. Rev. B* **67**, 174517 (2003).
- <sup>13</sup>I. Bozovic, *IEEE Trans. Appl. Supercond.* **11**, 2686 (2001).
- <sup>14</sup>I. Bozovic, G. Logvenov, I. Belca, B. Narimbetov, and I. Sveklo, *Phys. Rev. Lett.* **89**, 107001 (2002).
- <sup>15</sup>A. Castellanos, R. Wordenweber, G. Ockenfuss, A. d. Hart, and K. Keck, *Appl. Phys. Lett.* **71**, 962 (1997).
- <sup>16</sup>A. Crisan, A. Pross, D. Cole, S. J. Bending, R. Wordenweber, P. Lahl, and E. H. Brandt, *Phys. Rev. B* **71**, 144504 (2005).
- <sup>17</sup>S. Ooi, T. Mochiku, S. Yu, E. S. Sadki, and K. Hirata, *Physica C* **426-431**, 113 (2005).
- <sup>18</sup>S. Goldberg, Y. Segev, Y. Myasoedov, I. Gutman, N. Avraham, M. Rappaport, E. Zeldov, T. Tamegai, C. W. Hicks, and K. A. Moler, *Phys. Rev. B* **79**, 064523 (2009).
- <sup>19</sup>F. Carillo, G. Papari, D. Stornaiuolo, D. Born, D. Montemurro, P. Pingue, F. Beltram, and F. Tafuri, *Phys. Rev. B* **81**, 054505 (2010).
- <sup>20</sup>I. Sochnikov (unpublished).
- <sup>21</sup>B. I. Halperin and D. R. Nelson, *J. Low Temp. Phys.* **36**, 599 (1979).
- <sup>22</sup>I. L. Landau and L. Rinderer, *Phys. Rev. B* **56**, 6348 (1997).
- <sup>23</sup>P. Santhanam, C. C. Chi, S. J. Wind, M. J. Brady, and J. J. Bucchignano, *Phys. Rev. Lett.* **66**, 2254 (1991).
- <sup>24</sup>C. Strunk, V. Bruyndoncx, C. Van Haesendonck, V. V. Moshchalkov, Y. Bruynseraede, C. J. Chien, B. Burk, and V. Chandrasekhar, *Phys. Rev. B* **57**, 10854 (1998).
- <sup>25</sup>The sensitivity of the resistance to the magnetic field above 32 K may suggest that some parts of the array are superconducting already below 35 K, see Refs. 22–24 and 36.
- <sup>26</sup>H. H. Wen, H. P. Yang, S. L. Li, X. H. Zeng, A. A. Soukiassian, W. D. Si, and X. X. Xi, *Europhys. Lett.* **64**, 790 (2003).
- <sup>27</sup>M. Tinkham, *Rev. Mod. Phys.* **36**, 268 (1964).
- <sup>28</sup>Discrepancies between the Little-Parks model and the experimental results, namely, the magnitude of magnetoresistance oscillations and their anomalous temperature dependence, were already observed in low- $T_c$  superconductors (e.g., in Refs. 2 and 3). In our case, however, the discrepancies amount to 2 orders of magnitude, much larger than observed in low- $T_c$  materials, indicating a different underlying physics.
- <sup>29</sup>M. Tinkham, *Phys. Rev. Lett.* **61**, 1658 (1988).
- <sup>30</sup>G. Blatter, M. V. Feigel'man, V. B. Geshkenbein, A. I. Larkin, and V. M. Vinokur, *Rev. Mod. Phys.* **66**, 1125 (1994).
- <sup>31</sup>Y. Yeshurun, A. P. Malozemoff, and A. Shaulov, *Rev. Mod. Phys.* **68**, 911 (1996).
- <sup>32</sup>J. Pearl, *Appl. Phys. Lett.* **5**, 65 (1964).
- <sup>33</sup>V. G. Kogan, *Phys. Rev. B* **49**, 15874 (1994).
- <sup>34</sup>D. S. Hopkins, D. Pekker, P. M. Goldbart, and A. Bezryadin, *Science* **308**, 1762 (2005).
- <sup>35</sup>D. Pekker, A. Bezryadin, D. S. Hopkins, and P. M. Goldbart, *Phys. Rev. B* **72**, 104517 (2005).
- <sup>36</sup>D. Y. Vodolazov, D. S. Golubović, F. M. Peeters, and V. V. Moshchalkov, *Phys. Rev. B* **76**, 134505 (2007).



## 4 SUMMARY AND CONCLUSIONS

In this work, we designed and fabricated a new type of a network – the double network – consisting of two interlaced sub-networks of small and large loops. We demonstrated, both theoretically and experimentally, uncorrelated behavior of fluxoids in the sub-network of the small loops. Namely, the vortex occupation of the small loops increases in steps, resembling the behavior of an ensemble of nearly decoupled loops. In addition, the loop energy is a periodic function of the ratio between the flux penetrating a loop and a superconducting flux quantum, with a waveform identical to that of a single isolated loop.

Measurements of the magnetoresistance of double networks made of MBE grown  $\text{La}_{1.84}\text{Sr}_{0.16}\text{CuO}_4$  film, with a small loop side ranging typically from 150 to 75 nm, revealed large oscillations with flux periodicity  $hc/2e$  and amplitude much larger than expected from the Little-Parks effect. Also, the temperature dependence of the oscillations' amplitude was inconsistent with the Little-Parks prediction.

To explain our experimental results, we developed a new model which ascribes the magnetoresistance oscillations in high- $T_c$  superconductors to the periodic changes in the interaction between thermally excited moving vortices and the oscillating persistent current induced in the loops. We found a good agreement between the experimental results and the predictions of this fluxoid dynamic model for both the size of oscillations' amplitude and its temperature dependence. We note that although, in general, magnetoresistance oscillations originate from both the Little-Parks effect and the fluxoid dynamics, in high- $T_c$  superconductors the contribution of the Little-Parks effect is relatively small because of the short coherence length. On the other hand, the contribution of the vortex dynamics is large in high- $T_c$  superconductors due to the strong thermal fluctuations.

We extended our dynamic model to include the interaction between the external field and the magnetic moment of the vortices and antivortices. The extended model accounts quantitatively for the monotonic background on which the magnetoresistance oscillations are superimposed. Moreover, an analysis of the background indicates that in the patterned film both vortices

and antivortices are present, consistent with the superconducting phase transition scenario proposed by Berezinskii, Kosterlitz, and Thouless.

The double network may serve as an efficient tool in the search for the recently predicted  $hc/4e$  and  $hc/e$  periodicities [34-39]. The absence of such periodicities in the present work is at variance with these theoretical predictions. However, efforts to discover these periodicities should continue by extending this work to higher and lower doping across the entire phase diagram, in  $\text{La}_{2-x}\text{Sr}_x\text{CuO}_4$  and  $\text{La}_{2-x}\text{Ba}_x\text{CuO}_4$  [52].

## APPENDIX: PUBLICATIONS, PRESENTATIONS, AND AWARDS

### Publications

[1] I. Sochnikov, A. Shaulov, Y. Yeshurun, G. Logvenov and I. Bozovic, "*Large oscillations of the magnetoresistance in nano-patterned high-temperature superconducting films*",

**Nature Nanotechnology** **5**, 516 - 519 (2010).

[2] I. Sochnikov, Y. Shokef, A. Shaulov, Y. Yeshurun, "*Single-loop like energy oscillations and staircase vortex occupation in superconducting double networks*",

submitted to **Physical Review B** (2010).

[3] I. Sochnikov, A. Shaulov, Y. Yeshurun, G. Logvenov and I. Bozovic, "*Oscillatory magnetoresistance in nano-patterned superconducting  $La_{1.84}Sr_{0.16}CuO_4$  films*",

**Physical Review B** **82**, 094513 (2010).

[4] I Sochnikov, A Shaulov, T. Tamegai and Y Yeshurun, "*Vortex phase transitions in  $Bi_2Sr_2CaCu_2O_{8+x}$  probed by nonlinear AC magnetic response*",

**Journal of Physics** **150** 052244 (2009).

[5] I. Sochnikov, A. Shaulov, and Y. Yeshurun, "*Investigation of the vortex order-disorder phase transition line in  $Bi_2Sr_2CaCu_2O_{8+d}$  using AC techniques*",

**Journal of Applied Physics** **103**, 07C705 (2008).

[6] D. Barness, I. Sochnikov, B.Kalisky, A. Shaulov, Y. Yeshurun, "*Oscillatory magnetic relaxation in  $Bi_2Sr_2CaCu_2O_{8+\delta}$* ",

**Physica C** **468**, 280 (2008).

[7] A. Friedman, Y. Wolfus, F. Kopansky, I. Soshnikov, V. Roitberg, S. Asulay, B. Kalisky, and Y. Yeshurun, "*I-V Curves of BSCCO Tape Carrying DC Current Exposed to Perpendicular and Parallel AC Fields*",

**IEEE Transactions on Applied Superconductivity**, **15**, No. 2 (2005).

## **Awards and Scholarships**

- 2009- Eshkol Scholarship, Israeli Ministry of Science and Technology  
2011
- 2011 Publications Award, Institute for Nanotechnology and Advanced  
Materials, Bar-Ilan University
- 2006- Bar-Ilan University President's Scholarship for Ph.D. students  
2010
- 2010 Award for Best Poster, Nanolsrael Conference
- 2010 Award for Research Excellence, Department of Physics, Bar-Ilan  
University
- 2010 Publications Award, Institute for Nanotechnology and Advanced  
Materials, Bar-Ilan University
- 2008- Excellence Scholarship, Institute for Nanotechnology and Advanced  
2009 Materials, Bar-Ilan University
- 2007 David Barkovski Award, Faculty of Exact Sciences, Bar-Ilan  
University
- 2006 Salim Benin Award, Jewish Agency
- 2004 Haim Ben-Noah Fund Award, Ministry of Justice, Israel
- 2004 Rachel and Reuben Jacobs Award, Faculty of Exact Sciences, Bar-  
Ilan University
- 2004 Municipality of Ramat-Gan, the Mayor's Award
- 2003 Award for Excellence, Department of Physics, Bar-Ilan University

## Presentations & talks

- 2011 "Large oscillations of the magnetoresistance in nano-patterned high-temperature superconducting films", **contributed talk** at the March Meeting 2011, American Physical Society Conference, Dallas, USA
- 2011 "Large oscillations ...", **seminar**, MIT, USA
- 2011 "Large oscillations ...", **seminar**, Stanford University, USA
- 2010 "Large oscillations of the magnetoresistance in nano-patterned high-temperature superconducting films", **invited talk**, The sixth International Conference on Mathematical Modeling and Computer Simulation of Materials Technologies, Israel
- 2010 "Large oscillations ...", **seminar**, Brookhaven National Laboratory, USA
- 2010 "Large oscillations ...", **seminar**, Harvard University, USA
- 2010 "Large oscillations ...", **contributed talk**, Annual Israeli Physics Society Meeting
- 2010 "Oscillatory magnetoresistance in nano-patterned superconducting  $La_{1.84}Sr_{0.16}CuO_4$  films", **poster (Award for Best Poster)**, Nanolsrael Conference, Israel
- 2010 "Large oscillations ...", **poster**, Nanostructure Fabrication, Gordon Research Conference, Tilton, New Hampshire, USA.
- 2010 "Large oscillations ...", Hagoshrim Internal Conference, **contributed talk**, Institute for Nanotechnology and Advanced Materials, Bar-Ilan University, Israel.
- 2010 "Large oscillations ...", **poster**, Russell Berrie Nanotechnology Institute Winter School, Dead Sea, Israel.
- 2008 "Vortex phase transitions in  $Bi_2Sr_2CaCu_2O_{8+x}$  probed by nonlinear AC magnetic response", **poster**, Low Temperature Physics Conference (LT25), Amsterdam, The Netherlands.

- 2007 “Investigation of the vortex order-disorder phase transition line in  $\text{Bi}_2\text{Sr}_2\text{CaCu}_2\text{O}_{8+x}$  using ac techniques”, **contributed talk**, 52nd Annual Conference on Magnetism and Magnetic Materials, Tampa, USA.
- 2005 “Investigation of the vortex phase diagram of  $\text{Bi}_2\text{Sr}_2\text{CaCu}_2\text{O}_{8+x}$  using ac techniques”, **poster**, Israel Physics Society Conference, Jerusalem.

## REFERENCES

- [1] F. London, "*On the problem of the molecular theory of superconductivity*," Phys. Rev. **74**, 562 (1948).
- [2] M. Tinkham, *Introduction to Superconductivity*. (McGraw-Hill, New York, 1996), p.454.
- [3] An extensive literature on the superconducting networks made of Low- $T_c$  materials can be found in Proceedings of the NATO Workshop on Conference in Superconducting Networks, Delft, The Netherlands, 1987, ed. by Mooij, J. E. and Schon, G. B. J. [*Phys. B* **152**, No. 1&2 (1988)].
- [4] A. Behrooz, M. J. Burns, D. Levine, B. Whitehead, and P. M. Chaikin, "*Superconducting phase boundary of aperiodic networks in a magnetic field*," Phys. Rev. B **35**, 8396 (1987).
- [5] P. M. Chaikin, A. Behrooz, M. A. Itzler, C. Wilks, B. Whitehead, G. Grest, and D. Levine, "*Studies of quasicrystalline superconducting networks*," Physica B **152**, 113 (1988).
- [6] M. A. Itzler, A. M. Behrooz, C. W. Wilks, R. Bojko, and P. M. Chaikin, "*Commensurate states in disordered networks*," Phys. Rev. B **42**, 8319 (1990).
- [7] W. A. Little and R. D. Parks, "*Observation of quantum periodicity in the transition temperature of a superconducting cylinder*," Phys. Rev. Lett. **9**, 9 (1962).
- [8] R. D. Parks and W. A. Little, "*Fluxoid quantization in a multiply-connected superconductor*," Phys. Rev. **133**, A97 (1964).
- [9] R. P. Groff and R. D. Parks, "*Fluxoid Quantization and Field-Induced Depairing in a Hollow Superconducting Microcylinder*," Phys. Rev. **176**, 567 (1968).
- [10] V. V. Moshchalkov, H. Vloeberghs, M. Dhallé, G. Neuttiens, C. van Haesendonck, Y. Bruynseraede, and R. Jonckheere, "*Anomalous Little-Parks oscillations and field enhanced superconductivity in mesoscopic loops*," Physica Scripta **1992**, 226 (1992).
- [11] D. Davidovic, S. Kumar, D. H. Reich, J. Siegel, S. B. Field, R. C. Tiberio, R. Hey, and K. Ploog, "*Correlations and Disorder in Arrays of Magnetically Coupled Superconducting Rings*," Phys. Rev. Lett. **76**, 815 (1996).
- [12] X. Zhang and J. C. Price, "*Susceptibility of a mesoscopic superconducting ring*," Phys. Rev. B **55**, 3128 (1997).
- [13] S. Pedersen, G. R. Kofod, J. C. Hollingbery, C. B. Sorensen, and P. E. Lindelof, "*Dilation of the giant vortex state in a mesoscopic superconducting loop*," Phys. Rev. B **64**, 104522 (2001).
- [14] D. Y. Vodolazov, F. M. Peeters, S. V. Dubonos, and A. K. Geim, "*Multiple flux jumps and irreversible behavior of thin Al superconducting rings*," Phys. Rev. B **67**, 054506 (2003).

- [15] A. A. Burlakov, V. L. Gurtovoi, S. V. Dubonos, A. V. Nikulov, and V. A. Tulin, "*Observation of the Little-Parks Oscillations in a System of Asymmetric Superconducting Rings*," JETP Letters **86**, 517 (2007).
- [16] A. Kanda, B. J. Baelus, D. Y. Vodolazov, J. Berger, R. Furugen, Y. Ootuka, and F. M. Peeters, "*Evidence for a different type of vortex that mediates a continuous fluxoid-state transition in a mesoscopic superconducting ring*," Phys. Rev. B **76**, 094519 (2007).
- [17] N. C. Koshnick, H. Bluhm, M. E. Huber, and K. A. Moler, "*Fluctuation Superconductivity in Mesoscopic Aluminum Rings*," Science **318**, 1440 (2007).
- [18] G. R. Berdiyrov, S. H. Yu, Z. L. Xiao, F. M. Peeters, J. Hua, A. Imre, and W. K. Kwok, "*Effect of sample geometry on the phase boundary of a mesoscopic superconducting loop*," Phys. Rev. B **80**, 064511 (2009).
- [19] J. A. Bert, N. C. Koshnick, H. Bluhm, and K. A. Moler, "*Fluxoid fluctuations in mesoscopic superconducting rings*," cond-mat arXiv:1008.4821v1 (2010).
- [20] B. Pannetier, J. Chaussy, R. Rammal, and J. C. Villegier, "*Experimental Fine Tuning of Frustration: Two-Dimensional Superconducting Network in a Magnetic Field*," Phys. Rev. Lett. **53**, 1845 (1984).
- [21] J. M. Gordon and A. M. Goldman, "*Magnetoresistance measurements on fractal wire networks*," Phys. Rev. B **35**, 4909 (1987).
- [22] M. Tinkham, D. W. Abraham, and C. J. Lobb, "*Periodic flux dependence of the resistive transition in two-dimensional superconducting arrays*," Phys. Rev. B **28**, 6578 (1983).
- [23] V. M. Vinokur, T. I. Baturina, M. V. Fistul, A. Y. Mironov, M. R. Baklanov, and C. Strunk, "*Superinsulator and quantum synchronization*," Nature **452**, 613 (2008).
- [24] T. I. Baturina, V. M. Vinokur, A. Y. Mironov, N. M. Chtchelkatchev, D. A. Nasimov, and A. V. Latyshev, "*Nanopattern-stimulated superconductor-insulator transition in thin TiN films*," Europhys. Lett. **93**, 47002 (2011).
- [25] D. S. Hopkins, D. Pekker, P. M. Goldbart, and A. Bezryadin, "*Quantum Interference Device Made by DNA Templating of Superconducting Nanowires*," Science **308**, 1762 (2005).
- [26] D. Pekker, A. Bezryadin, D. S. Hopkins, and P. M. Goldbart, "*Operation of a superconducting nanowire quantum interference device with mesoscopic leads*," Phys. Rev. B **72**, 104517 (2005).
- [27] P. L. Gammel, P. A. Polakos, C. E. Rice, L. R. Harriott, and D. J. Bishop, "*Little-Parks oscillations of  $T_c$  in patterned microstructures of the oxide superconductor  $YBa_2Cu_3O_7$ : Experimental limits on fractional-statistics-particle theories*," Phys. Rev. B **41**, 2593 (1990).
- [28] J. R. Kirtley, C. C. Tsuei, V. G. Kogan, J. R. Clem, H. Raffy, and Z. Z. Li, "*Fluxoid dynamics in superconducting thin film rings*," Phys. Rev. B **68**, 214505 (2003).

- [29] F. Carillo, G. Papari, D. Stornaiuolo, D. Born, D. Montemurro, P. Pingue, F. Beltram, and F. Tafuri, "*Little-Parks effect in single nanoscale  $YBa_2Cu_3O_{6+x}$  rings,*" Phys. Rev. B **81**, 054505 (2010).
- [30] D. J. Van Harlingen, "*Phase-sensitive tests of the symmetry of the pairing state in the high-temperature superconductors—Evidence for  $d_{x^2-y^2}$  symmetry,*" Rev. of Mod. Phys. **67**, 515 (1995).
- [31] C. C. Tsuei and J. R. Kirtley, "*Pairing symmetry in cuprate superconductors,*" Rev. of Mod. Phys. **72**, 969 (2000).
- [32] T. Timusk and B. Statt, "*The pseudogap in high-temperature superconductors: an experimental survey,*" Rep. Prog. Phys. **62**, 61 (1999).
- [33] M. R. Norman, "*High-temperature superconductivity in the iron pnictides,*" Physics **1**, 21 (2008).
- [34] Y. S. Barash, "*Low-energy subgap states and the magnetic flux periodicity in d-wave superconducting rings,*" Phys. Rev. Lett. **100**, 177003 (2008).
- [35] V. Juricic, I. F. Herbut, and Z. Tesanovic, "*Restoration of the magnetic  $hc/e$ -periodicity in unconventional superconductors,*" Phys. Rev. Lett. **100**, 187006 (2008).
- [36] F. Loder, A. P. Kampf, T. Kopp, J. Mannhart, C. W. Schneider, and Y. S. Barash, "*Magnetic flux periodicity of  $h/e$  in superconducting loops,*" Nature Phys. **4**, 112 (2008).
- [37] V. Vakaryuk, "*Universal mechanism for breaking the  $hc/2e$  periodicity of flux-induced oscillations in small superconducting rings,*" Phys. Rev. Lett. **101**, 167002 (2008).
- [38] T.-C. Wei and P. M. Goldbart, "*Emergence of  $h/e$ -period oscillations in the critical temperature of small superconducting rings threaded by magnetic flux,*" Phys. Rev. B **77**, 224512 (2008).
- [39] E. Berg, E. Fradkin, and S. A. Kivelson, "*Charge-4e superconductivity from pair-density-wave order in certain high-temperature superconductors,*" Nature Phys. **5**, 830 (2009).
- [40] A. W. Hunt, P. M. Singer, K. R. Thurber, and T. Imai, " *$^{63}\text{Cu}$  NQR Measurement of Stripe Order Parameter in  $La_{2-x}Sr_xCuO_4$ ,*" Physical Review Letters **82**, 4300 (1999).
- [41] V. L. Berezinskii, "*Destruction of long-range order in one-dimensional and two-dimensional systems with a continuous symmetry group. II. Quantum systems (in Russian),*" ZhETF **61**, 1144 (1971).
- [42] V. L. Berezinskii, "*Destruction of long-range order in one-dimensional and two-dimensional systems with a continuous symmetry group. II. Quantum systems (in Russian),*" Sov. Phys. JETP **34**, 610 (1972).
- [43] J. M. Kosterlitz and D. J. Thouless, "*Ordering, Metastability and Phase-Transitions in 2 Dimensional Systems,*" J. Phys. C **6**, 1181 (1973).

- [44] M. R. Beasley, J. E. Mooij, and T. P. Orlando, "*Possibility of Vortex-Antivortex Pair Dissociation in Two-Dimensional Superconductors*," Phys. Rev. Lett. **42**, 1165 (1979).
- [45] A. F. Hebard and A. T. Fiory, "*Evidence for the Kosterlitz-Thouless Transition in Thin Superconducting Aluminum Films*," Phys. Rev. Lett. **44**, 291 (1980).
- [46] A. T. Fiory, A. F. Hebard, P. M. Mankiewich, and R. E. Howard, "*Renormalization of the Mean-Field Superconducting Penetration Depth in Epitaxial  $YBa_2Cu_3O_{7-\delta}$  Films*," Phys. Rev. Lett. **61**, 1419 (1988).
- [47] L. C. Davis, M. R. Beasley, and D. J. Scalapino, "*Kosterlitz-Thouless transition in high- $T_c$  superconductor films*," Phys. Rev. B **42**, 99 (1990).
- [48] J. M. Repaci, C. Kwon, Q. Li, X. Jiang, T. Venkatessan, R. E. Glover, C. J. Lobb, and R. S. Newrock, "*Absence of a Kosterlitz-Thouless transition in ultrathin  $YBa_2Cu_3O_{7-\delta}$  films*," Phys. Rev. B **54**, R9674 (1996).
- [49] D. R. Strachan, C. J. Lobb, and R. S. Newrock, "*Dynamic scaling and two-dimensional high- $T_c$  superconductors*," Phys. Rev. B **67**, 174517 (2003).
- [50] L. Miu, D. Miu, G. Jakob, and H. Adrian, "*Vortex-antivortex unbinding in oxygen-deficient  $YBa_2Cu_3O_{7-\delta}$  films*," Physica C **463-465**, 236 (2007).
- [51] A. C. F. Hoole, M. E. Welland, and A. N. Broers, "*Negative PMMA as a high-resolution resist - the limits and possibilities*," Semiconductor Science and Technology **12**, 1166 (1997).
- [52] M. Hucker, M. v. Zimmermann, G. D. Gu, Z. J. Xu, J. S. Wen, G. Xu, H. J. Kang, A. Zheludev, and J. M. Tranquada, "*Stripe order in superconducting  $La_{2-x}Ba_xCuO_4$  ( $0.095 \leq x \leq 0.155$ )*," Phys. Rev. B **83**, 104506 (2011).

## תקציר

בעבודה זו חקרנו תופעות דינמיות של פלקסואידים בסוג חדש של רשת מוליכת-על המשלבת שתי תת-רשתות המורכבות מלולאות גדולות וקטנות. המוטיבציה לתכנון רשת זו הייתה ליצור מערך של לולאות קטנות לא מצומדות אשר מתנהגות כלולאות בודדות. יצרנו רשתות 'כפולות' כאלה משכבות דקות של מוליך על  $\text{La}_{1.84}\text{Sr}_{0.16}\text{CuO}_4$  עם פני שטח חלקים ברמה של אטומים בודדים. השתמשנו בלייתוגרפית קרן אלקטרונים עם רזולוציה גבוהה כדי להכין אלפי לולאות בגדלים של 150 עד 75 ננומטר אשר מורכבות מחוטם ברוחב של כ-30 ננומטר. אלו הן הלולאות הקטנות ביותר שהוכנו עד כה ממוליכי-על בטמפרטורות גבוהות.

אפיינו תיאורטית את ההתנהגות הסטטית של הרשת הכפולה בהתבסס על סימולאציות מחשב וחישובי 'שדה ממוצע'. מחקר תיאורטי זה הראה התנהגות דיכטומית של שתי תתי-הרשת המרכיבות את הרשת הכפולה. בפרט, החישובים מראים כי בעוד האכלוס של הטבעות הגדולות גדל באופן ליניארי עם השדה המגנטי החיצוני, האכלוס של הלולאות הקטנות גדל באופן מדרגתי כפי שמצופה עבור אכלוס של לולאה בודדת. יתרה מזו, התלות של האנרגיה בשדה המגנטי החיצוני עבור תת-הרשת של הלולאות הקטנות דומה לזו של טבעת בודדת, בעוד שהאנרגיה של תת-הרשת של הטבעות הגדולות דומה לזו של ריבועית רגילה. תכונות אופייניות לטבעת בודדת נצפו גם כן באופן ניסיוני במדידות של מגנטו-התנגדות של רשתות כפולות שיצרנו מ- $\text{La}_{1.84}\text{Sr}_{0.16}\text{CuO}_4$ .

מדידות של מגנטו-התנגדות ברשתות הנ"ל הראו תנודות מחזוריות עם מחזור שמתאים ליחידה קוונטית של שטף מגנטי,  $\Phi_0 = hc/2e$  ( $h$  - קבוע של פלאנק,  $c$  - מהירות האור בריק,  $e$  - המטען של אלקטרון), כפי שמצופה מאפקט Little-Parks. אולם, משרעת התנודות שנמדדה הייתה גדולה בשני סדרי גודל מהמצופה מאפקט זה. יתר על כן, התלות בטמפרטורה של משרעת התנודות לא התאימה לציפיות של אפקט Little-Parks. סתירות אלה הובילו אותנו לחיפוש של מנגנון אחר אשר אחראי לתנודות של המגנטו-התנגדות בלולאות של מוליכי-על בטמפרטורות גבוהות. בניגוד למנגנון הסטטי של Parks-Little (תלות של  $T_c$  בשדה החיצוני), המנגנון שהצענו הוא דינמי שמקורו אף הוא בקוונטיזציה של הפלקסואיד בלולאות.

במודל שפיתחנו ההתנגדות נובעת מניתור של וורטקסים דרך הלולאות אשר מונע ע"י אקטיוואציות תרמיות, והתנודות בהתנגדות נובעות משינויים מחזוריים באנרגית האקטיוואציה הדרושה למעבר של וורטקס. השינויים המחזוריים באנרגית האקטיוואציה נגרמים ע"י אינטראקציה של הוורטקסים עם זרמי פלקסואיד בלולאה אשר משתנים באופן

מחזורי עם השדה. מצאנו התאמה טובה מאוד בין תוצאות הניסוי לבין המודל הדינאמי הן עבור משרעת התנודות והן עבור התלות שלה בטמפרטורה.

כדי להסביר את הרקע המונוטוני עליו מורכבות התנודות, הרחבנו את המודל הדינאמי ע"י הכללה של אינטראקציה של וורטקסים ואנטי-וורטקסים עם השדה החיצוני. התאמת המודל לרקע הנמדד הראתה התאמה טובה מאד וחשפה את קיומם של וורטקסים ואנטי-וורטקסים בהסתברות דומה. ממצאים אלו עומדים בהתאמה עם התרחשות אפשרית של מעבר Berezinskii-Kosterlitz-Thouless בשכבות דקות של  $\text{La}_{1.84}\text{Sr}_{0.16}\text{CuO}_4$ .

התנודות הגדולות במגנטו-התנגדות המאפיינות לולאות של מוליכי-על בטמפרטורות גבוהות, והיחסים הגבוהים בין סיגנל לרעש אשר מתקבלים ברשתות, מציעים את הרשתות הכפולות העשויות ממוליכי-על בטמפרטורות גבוהות ככלי יעיל לחיפוש אחרי מחזוריות בלתי רגילה של שטף מגנטי במוליכי-על לא קונוונציונליים. במיוחד, ניתן ליישם רשתות כפולות כאלה בחיפוש אחר מחזוריות של שטף מגנטי של  $\Phi_0/2 = hc/4e$  ושל  $2\Phi_0 = hc/e$  אשר לאחרונה נובאו תיאורטית במוליכי-על עם stripes ועם סימטרית  $d$ -wave בפונקצית הגל של זוגות Cooper, בהתאמה. מאמצים לגלות מחזוריות זו צריכים להמשך ע"י הרחבה של עבודה זו למדידות בתרכובות של  $\text{La}_{2-x}\text{Sr}_x\text{CuO}_4$  ושל  $\text{La}_{2-x}\text{Ba}_x\text{CuO}_4$  עם ריכוזי Ba ו-Sr משתנים.

## תוכן עניינים

א.....	תקציר	
1.....	מבוא	1
1.1	קוונטיזציה של פלקסואיד וניסויים קודמים המראים תנודות במגנטו-התנגדות בלולאות של מוליכי-על בטמפרטורות נמוכות	1
1.2	תנודות של מגנטו-התנגדות בלולאות של מוליכי-על בטמפרטורות גבוהות	5
1.3	ניבויים תיאורטיים של מחזוריות המתאימה למחצית ולכפולה של שתיים של היחידה	8
1.4	מעבר של BEREZINSKII-KOSTERLITZ-THOULESS	10
11.....	שיטות נסיוניות	2
2.1	הכנת שכבות של $LA_{2-x}SR_xCUO_4$ דקות באמצעות MOLECULAR BEAM EPITAXY (MBE)	12
2.2	יצירה של תבניות ננומטריות	14
2.3	מדידות של מגנטו-התנגדות	17
19.....	תוצאות	3
3.1	סימולציות וחישובי 'שדה ממוצע' של האיכלוס והתנודות באנרגיה ברשת כפולה	21
3.2	התנהגות לא מתואמת של פלקסואידים ברשת כפולה	41
3.3	תנודות גדולות במגנטו-התנגדות של לולאות ננומטריות עשויות ממוליכי-על בטמפרטורות גבוהות: תוצאות נסיוניות ומודל תיאורטי	49
3.4	תרומה של וורטקסים ואנטי-וורטקסים למגנטו-התנגדות של לולאות $LA_{1.84}SR_{0.16}CUO_4$ : אפשרות למעבר BEREZINSKII-KOSTERLITZ-THOULESS	55
65.....	סיכום ומסקנות	4
67.....	נספח: רשימות פרסומים, הרצאות בכנסים ופרסים	
71.....	רשימת מקורות	



עבודה זו נעשתה בהדרכתם של

פרופ' יוסף ישורון ופרופ' אבנר שאולוב

מן המחלקה לפיזיקה של אוניברסיטת בר-אילן.



**אפקטים של קוונטיזציה של פלקסואיד  
בלולאות ננו-מטריות של**



חיבור לשם קבלת התואר "דוקטור לפילוסופיה"

מאת

**איליה סושניקוב**

המחלקה לפיזיקה

הוגש לסנט של אוניברסיטת בר-אילן

אייר, תשע"א

רמת גן